Numerical and Experimental Investigations of Ultrasonic Assisted Magnetic Abrasive Finishing process on Hastelloy C-276

Submitted in partial fulfilment of the requirements

For the award of the degree of

DOCTOR OF PHILOSOPHY

in

MECHANICAL ENGINEERING

by

KAMEPALLI ANJANEYULU

(Roll No. 718028)

Under the supervision of

Dr. G. Venkatesh

(Assistant Professor, MED)

DEPARTMENT OF MECHANICAL ENGINEERING

NATIONAL INSTITUTE OF TECHNOLOGY WARANGAL

WARANGAL– 506 004, TELANGANA, INDIA.

JUNE 2023

THESIS APPROVAL FOR PH.D.

This thesis entitled **"Numerical and Experimental Investigations of Ultrasonic Assisted Magnetic Abrasive Finishing process on Hastelloy C-276"** by **Mr. Kamepalli Anjaneyulu** is approved for the degree of Doctor of Philosophy.

_____

_____

_____

Examiner

Dr. G. Venkatesh

Assistant Professor, Department of Mechanical Engineering, NIT Warangal

Supervisor

Prof. V. Suresh Babu

Head, Department of Mechanical Engineering, NIT Warangal

Chairman

NATIONAL INSTITUTE OF TECHNOLOGY

WARANGAL – 506 004, Telangana State, INDIA

CERTIFICATE

This is to certify that the thesis entitled **"Numerical and Experimental Investigations of Ultrasonic Assisted Magnetic Abrasive Finishing process on Hastelloy C-276"** being submitted by **Mr. Kamepalli Anjaneyulu** for the award of the degree of Doctor of Philosophy in Mechanical Engineering to the National Institute of Technology, Warangal, India is a record of the bonafide research work carried out by him under my supervision. The thesis has fulfilled the requirements according to the regulations of this Institute and in my opinion has reached the standards for submission. The results embodied in the thesis have not been submitted to any other University or Institute for the award of any degree.

Place: Warangal,

Date:

Dr. G. Venkatesh
Supervisor
Assistant Professor,
Department of Mechanical Engineering
National Institute of Technology, Warangal.

NATIONAL INSTITUTE OF TECHNOLOGY
WARANGAL – 506 004, Telangana State, INDIA

DECLARATION

This is to certify that the work presented in the thesis entitled **"Numerical and Experimental Investigations of Ultrasonic Assisted Magnetic Abrasive Finishing process on Hastelloy C-276"** is a bonafide work done by me under the supervision of **Dr. G. Venkatesh**, Assistant Professor, Department of Mechanical Engineering and was not submitted elsewhere for award of any degree.

I declare that this written submission represents my ideas in my own words and where others ideas or words have not been included. I have adequately cited and referenced the sources. I also declare that I have adhered to all principles of academic honesty and integrity and have not misrepresented or fabricated or falsified any idea/data/fact/source in my submission. I understand that any violation of the above will be a cause for disciplinary action by the Institute and can also evoke a penal response from the sources which have thus not been appropriately cited or from whom proper permission has not been taken when needed.

Place: Warangal **K. Anjaneyulu**

Date: **Roll no. 718028**

ACKNOWLEDGEMENT

I would like to express my sincere gratitude and profound indebtedness to my supervisor **Dr. G. Venkatesh,** Assistant Professor, Mechanical Engineering Department, NITW because he cultivated a research attitude in my mind for applying learning approach in my research as well as in the individual life. His important thoughts have given me an immense support to complete my research work. His positive and daring attitude in different aspects trained me to handle the situations with enthusiasm. His suggestions helped a lot to make myself stronger in all differing circumstances. His brilliant support made me to sustain and develop knowledge and be close to my home life. I owe a lot to him for making me a part of the continuity of the profession.

I extend my sincere gratitude to university authorities, **Prof. Bidyadhar Subudhi,** Director, National Institute of Technology, Warangal and other top officials who gave me an opportunity to carry out research work and for providing the necessary facilities and encouragement throughout my work.

I sincerely thank **Prof. V. Suresh Babu,** Head, Mechanical Engineering Department, National Institute of Technology, Warangal for his continuous support towards carrying out research work.

I wish to express my sincere and wholehearted thanks and gratitude to my doctoral scrutiny committee (DSC) members **Dr. A. Venu Gopal,** Professor, Department of Mechanical Engineering, **Dr. G. Raghavendra,** Assistant Professor, Department of Mechanical Engineering, **Dr. Ajoy Kumar Pandey,** Associate Professor, Materials and Metallurgy Engineering Department, National Institute of Technology, Warangal for their kind help, continuous monitoring, encouragement and valuable suggestions for successful completion of research work.

I express my heartfelt thanks and gratitude to my fellow research scholars **Dr. Khirod Kumar. M, Dr. Gurvaiah. P, Dr. T. Sharth Chandra, Dr. Raj Kumar, Mr. M, Amarnath G.B, Mr. K**. **Vijay Bhaskar Reddy**, **Mr. Shobhan. B, Mr. K. Karthik, Mr. M. Raju, M**. **Tech** Scholars – **Mr. Gyan Prakash, Mr. K. V. Hari Shankar** and all the Mechanical engineering faculty members who has directly or indirectly helped me through

their thought-provoking ideas, concepts and for their valuable support in the beautiful journey of my Ph.D.

I would especially want to thank **Dr. M. Ravi Shankar**, the mechanical head of department at IIT Tirupati, for his support and insightful inputs on my Ph.D. I appreciate all of the assistance and technical people at the Department of Mechanical Engineering who supported me with my work, especially **Sri. Yella Swamy** (Technical Officer, Workshop).

Last but not the least, a special debt of deep gratitude to **my parents**, **wife**, **my daughter and son**, who are undoubtedly the happiest to see me complete this endeavour. To them, I owe all my accomplishments.

Finally, I would like to acknowledge the help given by all the persons who have directly or indirectly supported the work.

K. Anjaneyulu

Dedicated

To

My Family

Abstract

Magnetic abrasive finishing (MAF) process is an abrasive based fine finishing process which is used for achieving surface finish in nano-level. In this process, the finishing of surfaces carried out using a flexible magnetic abrasive brush (FMAB) and an external magnetic field is employs to control the finishing forces. The ultrasonic assisted magnetic abrasive finishing (UAMAF) processes is a one of the variants of conventional MAF process. In UAMAF process a relatively high frequency of (30 kHz) vibration is provided to the workpiece externally using a piezo actuator and transducer used to convert frequency into amplitude of maximum 12 µm along with a specially designed fixture. This additional attachment is called ultrasonic assistance. Owing to this, the abrasives present in the FMAB hit the workpiece asperities more rapidly with high finishing forces thereby making them more effective in abrading the targeted asperities. The present work highlights the numerical analysis and experimental investigation on finishing of Hastelloy C-276 using MAF and UAMAF processes.

The modelling and simulation of MAF and UAMAF processes has been developed on flat workpiece with the help of ANSYS Maxwell 16.0 software. The simulation model for MAF and UAMAF is designed according to the dimensions of the experimental setup developed. Studying the effects of parameters such as power intensity, voltage, speed, and working gap was conducted in order to understand how normal force and cutting force are affected by process parameters. It is observed that magnetic flux density is most significant process parameter on finishing forces and it is directly proportional to it. The experimental investigations were planned in two phases.

In phase I - The initial average roughness of the Hastelloy C-276 specimens were maintained to R_a of 1.2 µm to1.4 µm using surface grinding process. Further, the surface finish improvement characteristics of Hastelloy C-276 were carried out by employing a laboratory-developed magnetic abrasive finishing process. Box-Behnken design of response surface methodology (RSM) is used for differing levels of abrasives weight percentages (20%-30%), electromagnet speeds (500-1000rpm), electromagnet supply voltages (35-55V) and working gaps (2-3mm). The measured responses include material removal (MR), change in surface finish ($\%\Delta R_a$), normal force (F_N), and tangential force (F_T).

In Phase II - The UAMAF setup is used to finish the Hastelloy C-276. The experiments were planned according to the Box-Behnken design of response surface

methodology (RSM). The output responses such as change in the surface finish ($\%\Delta R_a$), material removal (MR), Normal force (F_N) and Tangential force (F_T) are measured at various voltage, abrasive amount, speed, working gap, and power intensity levels. Additionally, UAMAF specimens had a chemical coating of yttrium acetate and di-ethanolamine added by physical vapour deposition. The amount of etchant used, the temperature in the chamber, and the number of coatings is factors.

The major observations based on Phase I & II are the average roughness achieved by MAF process is R_a = 0.325 µm, the average roughness achieved by UAMAF is R_a = 0.096 µm, and after chemo based UAMAF, it is reduced to Ra = 0.0224 µm. The maximum MR observed was 22.5 mg. In comparison to MAF process, the normal force and tangential force for UAMAF process are increased by 26.8% and 26.6%, respectively. The experimental results are compared and validated with the numerical results under similar conditions and the results are recorded.

The morphology of the finished samples was characterized using Scanning electronic microscopic analysis and 2-D surface profilometer. Further the Parametric optimization is carried out for MAF and UAMAF processes based on composite desirability approach for multi-objective optimization. The conformational experimentation is carried out at optimum parameters and it is in line with the observed experimental results.

Table of Contents

List of Tables

List of Figures

Nomenclature

MAF	*Magnetic Abrasive Finishing*
UAMAF	*Ultrasonic assisted magnetic abrasive finishing*
Al_2O_3	*Aluminum oxide*
SiC	*Silicon carbide*
FMAB	*Flexible Magnetic Abrasive Brush*
SEM	*Scanning Electron Microscopy*
MS	*Mild Steel*
Al 2024	*Aluminum 2024 alloy*
Hastelloy C-276	*Hastelloy C-276*
AFM	*Abrasive Flow Machining*
MRR	*Material Removal Rate*
R_a	*Surface finish*
$\%\Delta R_a$	*Percentage of change in surface finish*
R_z	*Average of Peak- Vealey height*
R_t	*Total profile height*
R_q	*Mean square root surface finish*
V	*Voltage*
MR	*Material removal*
mg	*Milli grams*
F_N	*Normal force*
F_T	*Tangential force*
N	*Newtons*
RPM	*Revolutions per minute*
mm	*Milli meters*
XRD	*X- ray diffraction*
Mn	*Manganese*
S	*Sulphur*
P	*Phosphorus*
C	*Carbon*
Cu	*Copper*
Mg	*Magnesium*
Si	*Silicon*

Zn	*Zinc*
MPa	*Mega pascal*
BHN	*Brinell hardness number*
^{0}C	*Centigrade*
C_1	*Wt.% of abrasives*
C_2	*Speed of the electromagnet*
C_3	*Voltage*
C_4	*Working gap*
C_5	*Power intensity*
µm	*Micrometer*
A	*Amperes*
T	*Tesla*
DOE	*Design of experiments*
RSM	*Response surface methodology*
BBD	*Box- Behnken design*
CCD	*Central composite design*

1 INTRODUCTION

1.1 Introduction

With a growing demand for improved product performance, industries need a high surface finished product in addition to dimensional accuracy, yet achieving such accuracy with a single simple finishing method is quite challenging. Lapping, honing, grinding, superfinishing, and other conventional finishing methods have existed, but these traditional finishing procedures have limitations in terms of surface finish and dimensional precision. These issues also include the high cost of precise finishing for high strength materials which requires a lot of energy and reduced environmental safety [1]. Furthermore, the workpiece surface is subjected to a lot of pressure, which might damage the finished surface. It is incompatible with processing components in combination with complicated forms, microscopic sizes, or 3-D structures affordably and quickly. The blade of the gas turbine performs the work at a high temperature of 1300 °C. At this high temperature, to perform the work properly and effectively nickel-based alloy has been used [2]. Superalloys based on nickel are mainly utilized in nuclear reactor parts, petrochemical sector check valves, chemical plant parts and aircraft and aviation component parts. It can endure high temperatures due to its mechanical strength, creep resistance, wear resistance, and corrosion resistance. Hastelloy is a nickel-based alloy comprising nickel, chromium, molybdenum, and other alloying elements. Hastelloy C-276 withstands pitting, stress-corrosion cracking and resists oxidizing environments up to 1800 °F [3]. However, these components must be finished at the nanoscale for a variety of applications. As a result, material finishing is depending on how well the finishing process performs.

Abrasive finishing processes can be categorized into conventional finishing processes (grinding, honing, lapping, etc.) and advanced abrasive finishing processes abrasive flow machining (AFM), magnetic abrasive finishing (MAF) and hybrid MAF, etc.). The main advantage of abrasive finishing processes is low force and small cutting edges with random orientation of abrasives. Cutting edges of abrasives can remove the material as a microchip. Because of these micro and nano chip formations lead to better surface finish with stringent tolerances that can achieve even for advanced materials [4]. Conventional finishing processes such as grinding, lapping, honing, etc., cannot produce fine surfaces since the roughness value is around one micron. Even though these are used as tertiary machining processes, sometimes conventional processes are unable to cater for the needs of super finishing

applications. Moreover, advancement in technology requires the necessity of fine-finishing operations. In today's scenario, many engineering applications are needed to produce complex and intricate shapes for advanced parts which are difficult to process using traditional finishing methods [5]. Hence, advanced finishing technics such as magnetic abrasive finishing (MAF), Laser beam machining, hybrid MAF process, etc. have been developed to meet various applications.

1.2 Conventional finishing processes

Grinding, lapping, honing and super finishing processes are commonly named traditional finishing processes. The grinding process (Fig. 1.1) is commonly used for a good finish and close tolerances. Although grinding is more efficient in removing material than other traditional processes, getting a good surface finish is very difficult. It requires dressing off the wheel and skilled worker required. In this process, high stresses and heat generation can decline surface integrity [6].

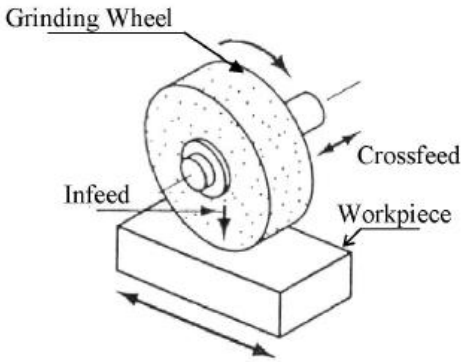

Figure 1.1: Schematic of the grinding process [7]

The lapping process (Fig. 1.2) does not produce a large amount of heat or high stresses. It applies low pressure on the workpiece and removes imperfections between the surfaces. Even though the lapping process is very slow and expensive. In order to avoid micro-cracks on the workpiece, it is essential to apply suitable lap pressure [8].

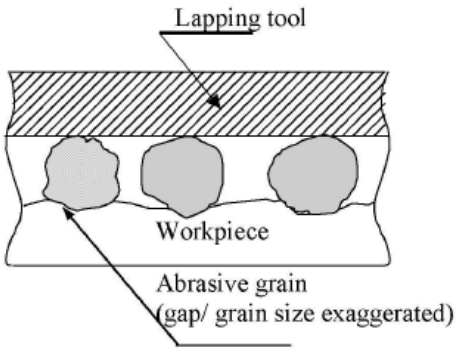

Figure 1.2: Schematic of the lapping process [7]

Honing process (Fig 1.3) is an abrading process carried out at low velocity with the help of abrasive bonded sticks. It is mainly used for finishing round and curved surfaces. The honing gives a smooth finish with a crosshatched pattern appearance [9]. Even though it is very difficult to do the finishing operation of nonmetals can lead to clogging of the voids.

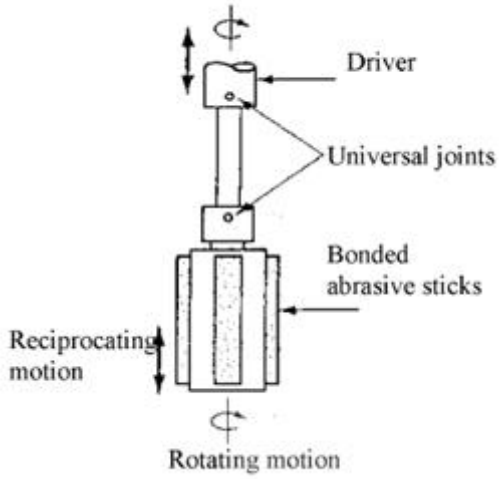

Figure 1.3: Schematic of the honing process [9]

In the case of conventional finishing processes can employ a rigid tool and these processes are not able to finish economically and rapidly for the complex shapes. Super finishing removes the undesirable fragment metal from the finished surface.

The superfinishing methods employ the application of extremely fine abrasive. Because the grit is ultra-fine, super finishing couldn't erase major surface flaws and it can only be utilized after earlier surface modification techniques have been employed to achieve an excellent surface [10].

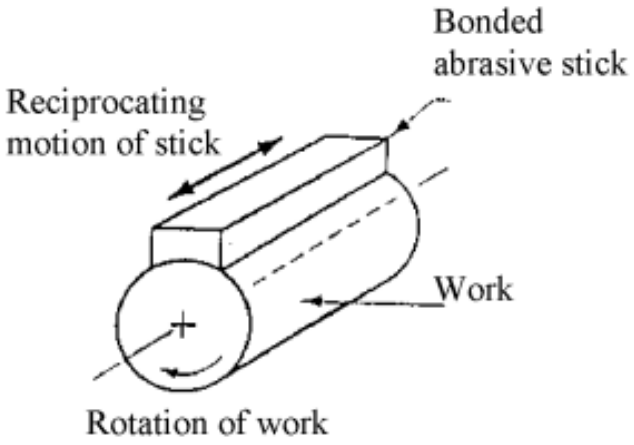

Figure 1.4: Schematic diagram of the superfinishing process [10]

1.3 Non- conventional finishing processes

As technology grows and improves, the demand for high-quality products in terms of texture, fit, and finish is also increasing. Conventional products improve the quality of the product surface only to a certain limit. Therefore, non-conventional methods are employed to get the limits of surface quality to greater accuracy [11].

1.4 Abrasive Flow Machining

In abrasive flow machining, the material is removed when abrasive fluid flows over the workpiece surface to be finished. The particles of the abrasive act as a cutting tool and the medium are composed of abrasive grit semisolid carrier.

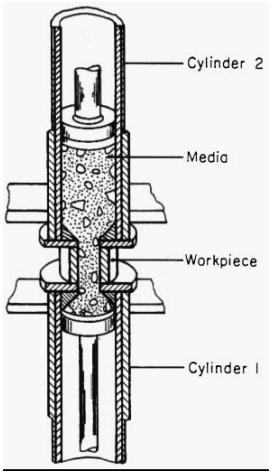

Figure 1.5: Schematic diagram of abrasive flow finishing [12]

The abrasive medium is driven into the workpiece hydraulically or mechanically, where it functions as a flexible file or slug, moldings itself to the geometry of the workpiece accurately.

1.4.1 Magnetic abrasives finishing

Magnetic abrasive finishing (MAF) is a type of micromachining. It is a cutting-edge, non-traditional finishing method designed to deliver a high-quality finished surface quickly and affordably. Its objective is to reduce the incidence of tiny fractures on the workpiece surface, and it may be used to finish the interior and exterior surfaces of cylindrical and flat workpiece. MAF offers improved self-sharpening, flexibility, and controllability, and also it provides a finishing tool that does not require dressing or compensating [13].

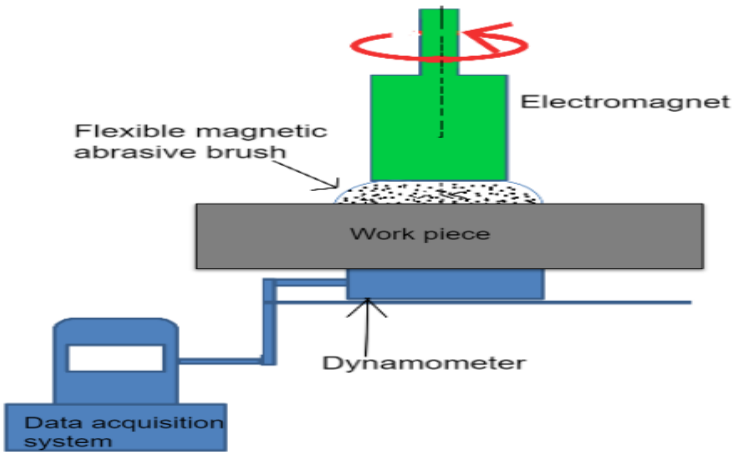

Figure 1.6: Plane magnetic abrasives finishing

In MAF, magnetic abrasive particles (MAPs) are inserted in the gap between the workpiece and magnets, as shown (Fig 1.6). MAPs consist of magnetic particles and abrasive powder; it can be used bonded or unbonded depending on the availability. Usually, the unbonded can be prepared by mixing the iron particles with abrasives and some lubricant such as glycerin but for the preparation of bonded particles sintering is required. By coming together along with the lines of magnetic force between the workpiece and the electromagnets, the magnetic abrasive particles can create a flexible magnetic abrasive brush (FMAB) (Fig 1.7) [14]. This brush is used as a multi-point cutting tool to complete the finishing process. As shown in Fig. 1.7, the FMAB performs a finishing operation and the abrasive particles will form a chain around the end of the electromagnet or N-pole, which acts like a grinding wheel. The finishing forces are controlled by the magnetic field and due to the workpiece and electromagnet relative motion, which can shear the workpiece surface layer. The machining gap and flux density had a substantial impact on the surface roughness and material removal. The size of magnetic abrasive particles influences surface roughness as well. They are increased as the diameter "D_m" of MAPs increases. By decreasing the diameter of abrasive particles "d_s" results in a decrease in the surface roughness of the sample [15].

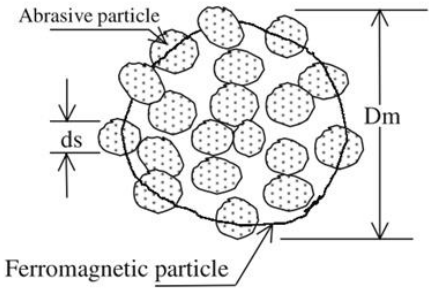

Figure 1.7: Flexible magnetic abrasive particles

1.4.2 Ultrasonic-assisted Magnetic abrasive finishing

The ultrasonic-assisted magnetic abrasive finishing (UAMAF) system comprises an ultrasonic vibration generator unit and a specially built workpiece fixture (Figure 1.8). The ultrasonic vibration producing unit is made up of a power supply, a transducer, and a concentrator or horn. The piezoelectric crystals within the transducer receive high-frequency electrical impulses which can be generated by the ultrasonic power source. The high-frequency electrical impulses of 30 kHz are converted into mechanical vibrations by the transducer. The transducer can reach an amplitude of 8 to 12 um at maximum. As a result, the concentrator or horn amplifies the signal's amplitude before it transmits to the workpiece, which is linked to the horn [16]. The active abrasive particles in FMAB follow a circular route as they revolve with the electromagnet. However, during the UAMAF, the workpiece is also subjected to horizontal ultrasonic vibration. As a result, the path taken by the active abrasive particle in relation to the workpiece surface is somewhat complicated.

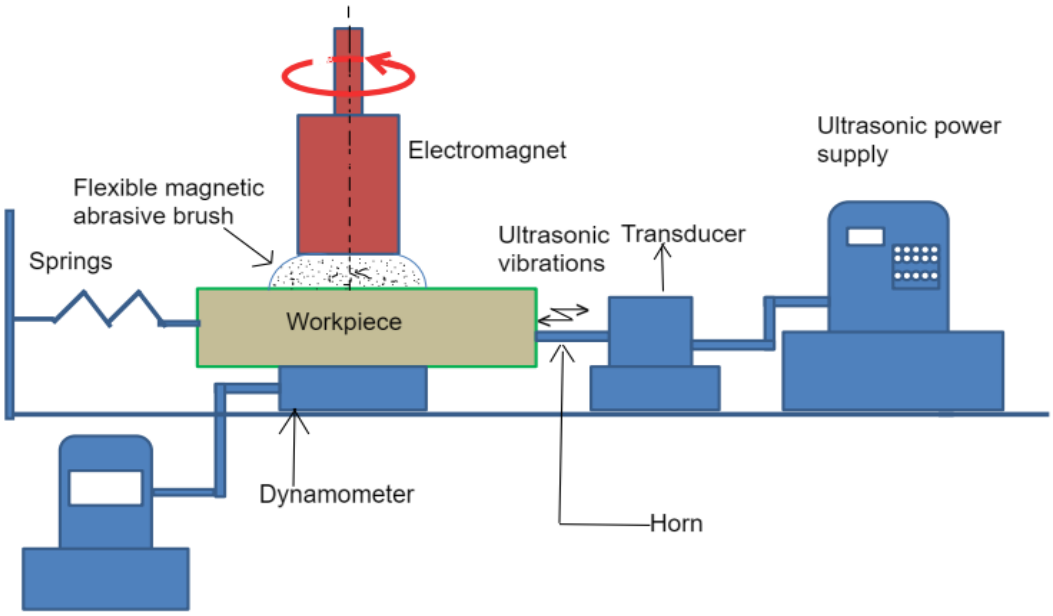

Figure 1.8 : Plane Ultrasonic assisted Magnetic abrasives finishing

Ultrasonic vibration is introduced to the finishing zone of magnetic abrasive finishing processes in UAMAF to finish the workpiece surface more efficiently and in less time than MAF [17]. Because of the vibration action, the flexible magnetic abrasive brush interacts better with workpiece surfaces.

1.5 Principle of MAF and UAMAF process

Because of the cutting action of abrasives particles, the material of the workpiece is removed during the MAF process. Magnetic abrasive particles are magnetized and positioned

along the magnetic field line to generate a flexible magnetic abrasive brush. When the FMAB rotates, two principal forces act on MAPs: indentation force (F_N) toward the workpiece and cutting force along the circular tangential direction. The implanted abrasive particles will generate an indentation depth on the worn surface due to the high indentation force, as shown in Fig. 1.9. The strength of magnetic abrasive particles will affect the indentation depth value. The material removal will occur if the normal force exceeds the workpiece shear strength [18].

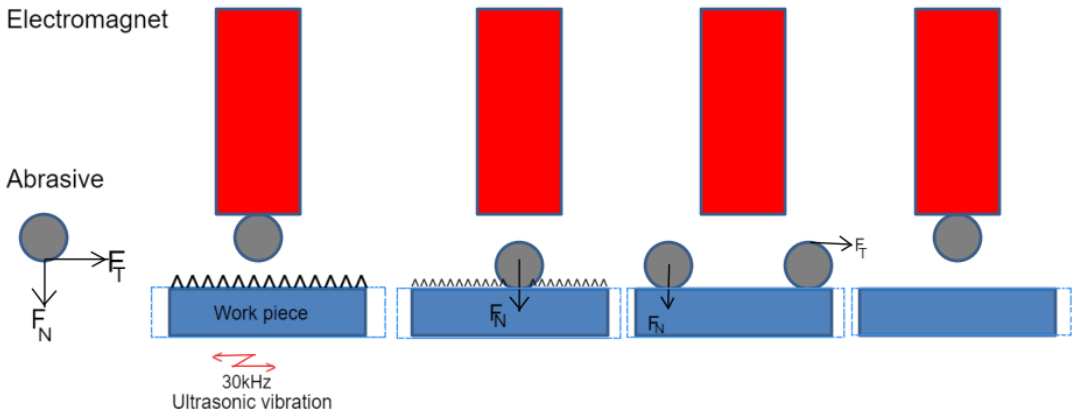

Figure 1.9: Mechanism of UAMAF process

The UAMAF method works similarly to the MAF process with the exception that ultrasonic vibration generates a lot of kinetic energy in the abrasive particles, causing tremendous shear of defects and increasing the surface rate roughness reduction. The percentage change in surface roughness in UAMAF is greater than in MAF for the identical set of parameters.

1.6 Salient features of MAF and UAMAF processes

Because of MAF and UAMAF utilizes at low forces and loose abrasive particles, the surface damage gets minimized. The advantages of MAF and UAMAF over other procedures such as the superfinishing process (lapping process, and honing process) listed below: There are no buns or thermal defects on the material surface.

1. Low power usage.
2. Easy to implement.
3. Environmentally friendly.
4. Self-adaptability.
5. Better control.
6. Nonferrous materials like aluminum and its alloys, as well as brass and its alloys, are similarly simple to finish.

1.7 Application of MAF and UAMAF process

1. Small component polishing, such as printed circuit boards (PCB).
2. The removal of protective coatings and oxide layers.
3. Gear and cam chamfering and deburring
4. Polishing complicated geometry automatically.
5. Polishing of cylindrical and flat surfaces.

1.8 Thesis outline

Chapter 1: Introduction

This chapter briefly overviews the significance of the conventional abrasive finishing process. The importance of magnetic abrasive finishing process and hybrid magnetic abrasive finishing processes, their application and limitations have been outlined.

Chapter 2: Literature Review and objectives

This chapter presents a thorough literature review on developments in the magnetic abrasive finishing method. Both the numerical and experimental studies of the magnetic abrasive finishing process and the ultrasonic-assisted magnetic abrasive finishing process have been detailed. It has been looked into how to identify research gaps in relation to problem identification, present work's goals, and the working approach.

Chapter 3: Experimental Procedure and Design of experiments

The essential component of the experiment's design that was used in this chapter has been investigated. The workpieces, fixtures, components, properties of various materials and different measuring instruments have been discussed in detail in chapter 3. The various models of experimental designs and process parameters levels have been considered for the magnetic abrasive finishing, ultrasonic assisted magnetic abrasive finishing process and spray coating process have been discussed in detail.

Chapter 4: Numerical of MAF and UAMAF processes

This chapter focuses on modelling and simulation of the influence of process parameters on the normal force, cutting force and magnetic flux density in MAF and UAMAF processes with the help of maxwell Ansoft software.

Chapter 5: Finishing of Hastelloy C- 276 using MAF process

This chapter focuses on the experimental investigation of the MAF process to Hastelloy C-276 flat materials. The influence of process parameters is investigated using a full factorial design.

Chapter 6: Finishing of Hastelloy C-276 using UAMAF processes

This chapter focuses on an experimental investigation of MAF and UAMAF processes to finish Hastelloy C-276 for a flat workpiece. Further, spray coating is performed to increase the surface finish. Response surface methodology and full factorial design have been used to study the responses.

Chapter 7: Optimization of process parameters of MAF and UAMAF processes

This chapter focuses on the parametric optimization of the MAF and UAMAF processes. The optimization technique used for the study is response surface methodology (RSM). The confirmation experiments were carried out at optimum process parameters and validated with experimental and simulation results.

Chapter 8: Conclusions and Future Scope

The research work conducted for this study's conclusions is summarised in this chapter, along with suggestions for potential future research in the field. A brief summary of the investigation's major contributions has been provided.

2 LITERATURE REVIEW AND OBJECTIVES

2.1 Introduction

In this section, the literature related to the finishing of magnetic and nonmagnetic materials and other advanced materials using MAF and hybrid MAF finishing operations is described. The simulation studies of MAF, UAMAF processes and the experimental studies of MAF and hybrid MAF processes have been discussed. The optimization of process parameters using advanced algorithms is explored.

2.2 Simulation studies of MAF process

Jayswal et al. [19] investigated the modeling and simulation studies on the finishing of SUS 304 using a magnetic abrasive finishing process. The finishing forces of the simulation are compared with the experimental conditions. The maximum indentation force is observed at the circumference of the electromagnet due to the edge effect.

Amit et al. [20] conducted simulation studies on the prediction of surface finish improvement using magnetic abrasive flow finishing process. A finite elemental analysis technique is applied and the simulation results were compared with experimental results. Also, the influence of magnetic flux density on surface finish and material removal rate are investigated.

Jain et al. [21] investigated the non-uniform surface profiles using theoretical and numerical studies with a magnetic abrasive finishing process. The obtained simulation results were compared with the experimental results of previous literature studies. The most influencing process parameters for better surface finish are flux density, size of magnetic abrasive particle and working gap.

Yuewu et al. [22] studied the modeling of the magnetic abrasive finishing process while finishing SS304 using spherical magnetic abrasive powder. The finite elemental model is designed using a grinding trajectory and the number of active abrasives. The influence of process parameters is also investigated and it is identified that the most influencing parameters are fine abrasives, low working gap and feed rate.

Mohammad et al. [23] investigated the finishing of a silicon wafer with a numerical and experimental study using a magnetic abrasive finishing process. The simulation results were compared with experimental results and also the most influencing process parameters were the machining gap and rotational speed.

Wenhui et al. [24] studied the mechanism of material removal using numerical studies by newly developed abrasive medium. The magnetic poles considered with different angles and it is observed that the maximum magnetic flux observed at the orientation of the south pole and north pole are perpendicular to each other. Also, the optimum abrasive media is observed at 4:3:1 in the combination of polymer, magnetic and abrasive particles**.**

2.3 Simulation studies of UAMAF process

The MAF method was utilized by Zenghua et al. [25] to finish the Ti-6Al-4V alloy's finishing. For the simulation investigations, four permanent magnets with different orientations were employed to finish titanium. The findings showed that at the best magnet orientations, the surface quality improved by 95% over the initial surface finish.

Aviral et al. [26] evaluated the modelling of surface finish improvement when finishing SS 304 using the UAMAF method. In both static and dynamic situations, they looked into how different process parameters affected surface finishing. They also contrasted simulation results with experimental data and discovered a substantial correlation between both.

The UAMAF technique was used by Mulik et al. [27] to model and experimentally investigate the temperature distribution between the workpiece and FMAB. The maximum temperature during experimentation was observed as 46 °C. Due to the low temperature generation, the microstructure features of the finished component will never be changed. Also, the temperature generation increases along with ultrasonic vibration, voltage and abrasive weight.

Harnam et al. [28] investigated the parametric optimization of the electrochemical MAF process using mathematical modeling. The finishing of the AISI 316L workpiece with better MRR was observed compared to the conventional MAF process. Optimization was carried out using TOPSIS method and the maximum MRR value was compared with experimental results at optimum process parameters.

Vipin et al. [29] studied the effect of normal force and finishing torque in UAMAF process using sintered magnetic abrasive particles with mathematical modeling. The removal of surface peaks on the workpiece was explained with the wear mechanism. The three-body wear mechanism was observed at a high working gap and low current with strong FMAB the finishing rate was increased. At a high working gap, the number of active abrasives moves randomly with less wear and a ploughing effect.

Fujjian et al. [30] investigated the FEM analysis of micro cutting of the UAMAF process. The von-Mises stress and area of contact increase with the indentation depth and the

maximum stress value was observed as 1552 MPa. The maximum cutting temperature observed per single UAMAF cycle is 186.4 °C. The maximum chip thickness was observed as 0.16 μm.

Aviral et al. [31] investigated the finishing forces of the UAMAF process using FEM modeling. The individual analysis of the electromagnet and workpiece was carried out. The obtained magnetic flux density was compared with the theoretical magnetic flux density. The magnetic flux density increases with a low working gap and high voltage. The finishing forces increase with the voltage, low working gap, and low concentration of abrasives.

2.4 Experimental studies of MAF process

Jain et al. [32] introduced a new concept of supply of DC power in the form of pulses to the electromagnet and analyzed the effect of FMAB on the surface finish of the workpiece. It was observed that there was an improvement in the surface finish of the material compared to the traditional finishing process.

The effect of process parameters and the influence of force on magnetic and nonmagnetic materials using the MAF process has been investigated by Bhavesh et al. [33]. The authors majorly focus on the influence of current supply, input voltage, machining time, etc., on material removal rate (MRR) and surface finish of samples. They observed that the composition of abrasive magnetic particles and input voltage were the most influential parameters on responses.

Experimental and theoretical studies were investigated by Jiong Z et al. [34] to prepare the internal surface of SS316 using a novel developed magnetic polishing tool. The researchers conducted experiments for different studies such as repeatability and polishing using a single point and along with the varying working gap. They also performed theoretical studies on the mechanism of material removal rate and surface roughness varying working gap.

Payam et al. [35] conducted experiments on AISI321 stainless steel using the MAF process to study the influence of process parameters on surface finish improvement. The researchers observed an improvement in the surface finish of 50% compared to the initial surface finish. The process parameters at the maximum surface finish are a working gap of 1 mm and the speed of the electromagnet of 500 rpm.

The influence of iron particle performance on the flat MAF process was assessed by Girma et al. [36]. It was identified that iron particles achieved high magnetic strength and helped enable a better surface finish of the workpiece. The researchers also studied the effect

of the grain size of iron particles on the surface finish of the workpiece and they observed that the fine size of particles helped in achieving of better surface finish.

Singh et al. [37] investigated the effect of input variables on the surface characteristics of the workpiece using the MAF process. They conducted experiments using the Taguchi orthogonal array and studied the influence of different process variables on surface finish. The authors reported better surface finish improvement on magnetic material compared to nonmagnetic material. The researchers also noted that the process parameters that significantly impacted the surface finish were voltage and working gap.

Jiong Z et al. [38] explored the finishing of laser-melted SS 316L flat surfaces using MAF process. They studied the surface quality before and after finishing and the MRR of seven printed samples. The authors reported that the surface finish improved by 75.7% after MAF finishing and the low amplitude fulses can easily remove in the MAF process. Further, they modeled the mechanism of MRR in the MAF process.

Huijun Xie et al. [39] investigated the mechanism and finishing abilities of the MAF process by an alternating magnetic field on an aluminum alloy plate. They found that the size of the magnetic particles significantly affected the surface finish of the aluminum alloy with varying alternating magnetic fields. As the size of the particle increases, the magnetic force also increases proportionally. The authors also stated that for rough finishing, bigger magnetic particles are better for fine finishing than small magnetic particles giving a better surface finish.

A newly developed media was used to study material removal behavior and finishing performance on the finishing of 6061 aluminum alloy using the MAF process, which had been explored by Wenhui Li et al. [40]. They derived a relationship between simulation and experimental results for better surface finish and material removal rate. They studied the effects of rotational speed, mesh number of the abrasives and the ratio of iron particles and abrasives.

Jiong Zhang et al. [41] investigated the finishing of SS 316 using a novel magnetically driven polishing technique for internal surface finishing using the MAF process. They discovered that the MAF mechanism using abrasive slurry in place of unbound abrasives and iron particles improves the surface finish and MRR. They concluded that with the numerical analysis, tube rotation is an essential factor for getting uniform polishing. Along with process parameters, which include the working gap between the workpiece and electromagnets, the rotational speed of the electromagnet etc.

Atul Babbar et al. [42] investigated finishing and material removal mechanisms while finishing brass plates using the MAF process. The authors conducted experiments using orthogonal arrays and optimized process parameters using the regression equation and found that the most influential input parameters on output responses were surface finish and MRR. Researchers observed that for better surface finish and MRR, the speed of the electromagnet (200rpm) mattered, whereas the abrasive sizes required were different for each response.

Jiong Z et al. [43] investigated the polishing of additively manufactured SS316L using MAF process. The researchers conducted experiments on selective laser melted workpieces at different inclinations from 0^0 to 90^0 and they measured surface roughness and MRR. They reported that the surface roughness value increases up to 45° after which the surface roughness value reduces and MRR observed was maximum at 0^0 and minimum at 15°T.

The effect of abrasive size and different force conditions on finishing Inconel 718 using the MAF process was investigated by Jianguo Guo et al. [44]. These researchers introduced a newly developed dual magnetic roller tool and a 6-axis robot arm to study the interrelations between process parameters and the MAF process mechanism. It was concluded that the surface finish, and surface morphology of the component depend on the type and abrasive size.

2.5 Experimental studies of UAMAF process

Vipin et al. [45] conducted experimental investigations on the creation of various magnetizations utilizing various unbonded and bonded magnetic abrasive particles. The researchers tested sintered magnetic abrasive particles using the orthogonal array L_8. The sintering process was performed at various temperatures, compact loads, and holding times. According to the findings of the experiments, low temperature and a high holding period are the ideal conditions for enhanced magnetization.

Rahul et al. [46] investigation into the effects of unbounded abrasives during the UAMAF process for finishing AISI 52100 steels. They examined the improvement of $\%\Delta R_a$ in the MAF and UAMAF processes using experimental research, and they concluded that the UAMAF process offered a better surface finish of 22 nm with a finishing time of 80 s. The workpiece surface shear grinding marks are significantly removed by the ultrasonic vibrations.

Jinzhoug et al. [47] investigated the effects of ultra-precise finishing SUS304 stainless steel plates using the MAF method and low-frequency alternating currents. The application of amplitude grows as the magnetic particle's diameter and fluctuating finishing force both rises.

The maximum surface polish they were able to observe with this technique was 4.38 nm during studies where they varied the alternating current with the particle diameter.

Yi- Hsun Lee et al. [48] investigation on the two-dimensional vibration-assisted MAF technique for finishing SUS304. They carried out trials using Taguchi orthogonal design and compared the outcomes of the 2DVMAF method with those of the conventional MAF process, noting an improvement of 77% surface finish compared to initial surface finish. Due to the addition of vibrations in two directions, the participation of active abrasives in the finishing process was increased and the polishing efficiency also increased.

Zhou et al. [49] conducted research on the surface integrity of titanium parts produced using the UAMAF process. Using the UAMAF technique, they ran tests on pieces that had been machined using a mill. The surface roughness was decreased from the initial Ra value by 40% based on the experimental investigation, and the residual stresses were decreased from 280 MPa to 20 MPa. Also, after the addition of ultrasonic attachment to the conventional MAF process, the surface texture and microcracks on the titanium were removed uniformly.

A Tungsten substrate's surface quality was improved by Nitesh et al. [50] using a UAMAF approach that had been chemically treated. The effects of MAF process settings and chemical polishing were combined by the researchers to finish tungsten workpieces. The chemical oxidizer functioned with vibrations and it improved the surface finish uniformly with the help of the oxide layer. The improvement in the surface finish was 87% compared to the initial surface.

Using the spray coating method, Wen et al. [51] examined the evaluation of Inconel composite surface coatings on graphene nanoplates. Because the buffer layer prevented excessive deformation, a few microcracks were seen in the IN718-GNPs composites around the indents. They evaluated pure Inconel with Inconel graphene nanoplates in terms of mechanical strength, hardness, and coating effectiveness.

Nitesh et al. [52] investigated the processing of tungsten workpieces using a Chemo-based MAF process. They conducted experiments with different concentrations of H_2O_2 to form an oxide layer on the surface of a workpiece. Based on experimental studies, the surface finish improved by 79% compared to the traditional MAF process.

In a study by Harnam et al. [53] the finishing of SS 316L was investigated utilizing a hybrid finishing technique that combined both UAMAF and electrolytic procedures. Compared to the initial surface finish, experimental research shows that the surface finish of cylindrical SS316L has improved by 82%.

Ankit et al. [54] in order to improve the surface finish employing surface coatings, evaluated the characterization and microstructural investigation of Ti6AlV. Based on geometrical criteria, the researchers investigated the texturing of micro dimples. To investigate how surface roughness varies with width and depth, two micro dimples of varying diameters were taken and extruded.

Sun et al. [55] investigation into SUS304 electrochemical MAF finishing. The purpose of the tests was to test the compatibility of the MAF approach with electrochemical finishing. Additionally, the surface finish was 70% better with the electrochemical MAF process than with the conventional MAF technique.

2.6 Optimization

Rao et al. [56] optimization of abrasive water jet machining using the multi-objective Jaya (MOJA) algorithm. The authors compared the optimum results of MO algorithm with other well-known optimization techniques and concluded that the results obtained using MOJ algorithm are better regarding the number of generations and the optimum values. The researchers also used the PROMETHEE method to find the best solution with the Pareto-optimum solutions.

Optimization of Inconel 800 was carried out using the Taguchi approach for the electrical discharge machining process investigated by Dharmendra et al. [57]. The authors used Minitab software for higher MRR and low Ra at optimum pulse on as well as pulse off times and peak current. The researchers also used a modified Taguchi approach to assign weights based on the requirement.

Yang et al. [58] investigated the multi-objective parametric optimization of the laser welding process using Non-dominated Sorting Genetic Algorithm -II (NSGA-II). The authors analyzed variances to identify the most significant process parameters on welding reinforcement, tensile strength, and the depth-to-width ratio of the weld. They also identified that the laser power and welding speed were optimum process parameters after NSGA-II.

Multi-objective parametric optimization of the turning process in the finishing of titanium alloy was investigated by Ramana et al. [59]. The authors used grey relational analysis to identify the optimum process parameters for higher MRR and low Ra value. The researchers identified that the influential process parameters are feed, cutting speed and depth of cut in decreasing order of importance.

Ajith et al. [60] investigated the multi-objective parametric optimization of the friction stir welding process using response surface methodology and GA. The authors conducted

optimization studies using GA to get optimum input process parameters for maximum welding strength and hardness. Based on the Pareto- optimum solutions, the most influencing process parameters are upset pressure, friction pressure and rotation speed.

Nevzat et al. studied the use of grey relational analysis for multi-objective parametric optimization of lab-scale thickeners [61] . The authors used grey relational analysis to identify optimum process parameters including feed flow rate and solid percent. The researchers also conducted confirmation runs to compare the optimum parameters obtained from the grey relational analysis.

Gul et al. [62] investigated the multi-objective parametric optimization of industrial gas turbine fuels using grey- Taguchi and artificial neural networks (ANN). The authors conducted an ANOVA analysis to identify the most influential process parameters. Based on grey-Taguchi and ANN, the optimum process parameter is an air inlet filter to improve efficiency and horsepower and also lowers the specific fuel consumption.

Parametric optimization of powder mixed electric discharge machining of die steels was investigated by Phan et al. [63]. The authors used Taguchi-based AHP method to study the influence of process parameters on MRR, Ra, tool wear rate and white layer thickness. Based on the optimization results the optimum process parameters are pulse on time of 20 µs, pulse of time 57 µs and peak current of 8 A.

Ramon et al. [64] investigated the multi-objective parametric optimization of the turning process using GA. The authors studied the influence of feed, speed and depth of cut on conflicting objectives for tool life and operation time. Based on the micro-GA optimization technique Pareto optimal solutions were obtained for better tool life and less operation time.

Modeling and parametric multi-objective optimization of the casting process while squeezing LM 24 aluminum alloy using GA [65]. The authors used the L_9 orthogonal array for experimentation with process parameters such as squeeze pressure, preheat temperature and pressure duration. Based on the GA results, the optimum process parameters can be used to improve the ultimate tensile strength and hardness.

Rao et al. [66] investigated the multi-objective parametric optimization of heat exchangers using elastic JA. The authors used JA to optimize the total cost and effectiveness of heat exchangers. Based on the results of JA, they compared obtained results with other optimization techniques GA, teaching, and learning-based optimization (TLBO) algorithms in terms of computation time and the number of generations.

Dhiraj et al. [67] examined multi-objective parametric optimization of micromachining using a non-dominated TLBO method. The authors applied the TLBO algorithm for wire electric discharge machining process parameters and the optimum values are noted. As a result, the optimum values are compared with other well-known optimization techniques GA, and particle swarm optimization algorithms.

2.7 Research gaps and objectives

From the literature review, it is observed that hybrid MAF process has lot of potential especially in advance finishing research area and proven its potential in finishing various components related to automobile, medical and aerospace etc. However, there is scope exist to explore and improve the efficacy of the process particularly in few mentioned areas.

The following are the gaps and scope identified in MAF process.

- ✓ Very few researchers have focused on the performance of the MAF process on magnetic and non-magnetic materials.
- ✓ Limited research is available on finishing advanced materials using MAF and Hybrid MAF processes.
- ✓ Limited information is available in the literature on finishing forces and their effect on surface integrity and material removal (MR).
- ✓ Few researchers have focused on temperature distribution between workpieces and flexible magnetic brushes in MAF and UAMAF processes.
- ✓ Limited attention has been given to chemo based UAMAF process.
- ✓ The limited focus has been on the parametric optimization of MAF and hybrid variants of the MAF process.

The main **objectives** of the work are

- ✓ To develop a Laboratory based MAF and UAMAF setup for nano level finishing of advanced materials.
- ✓ To perform simulation studies of MAF & UAMAF Processes in order to analyze finishing forces and magnetic flux density
- ✓ To study the influence of process parameters on the finishing of Hastelloy C-276 using MAF process.
- ✓ To study the influence of process parameters on the finishing of Hastelloy C- 276 using UAMAF process.
- ✓ To carry out optimality checks and validation of results using suitable machine learning techniques.

2.8 Research Methodology

The methodology to be adopted is represented in Figure 2.1.

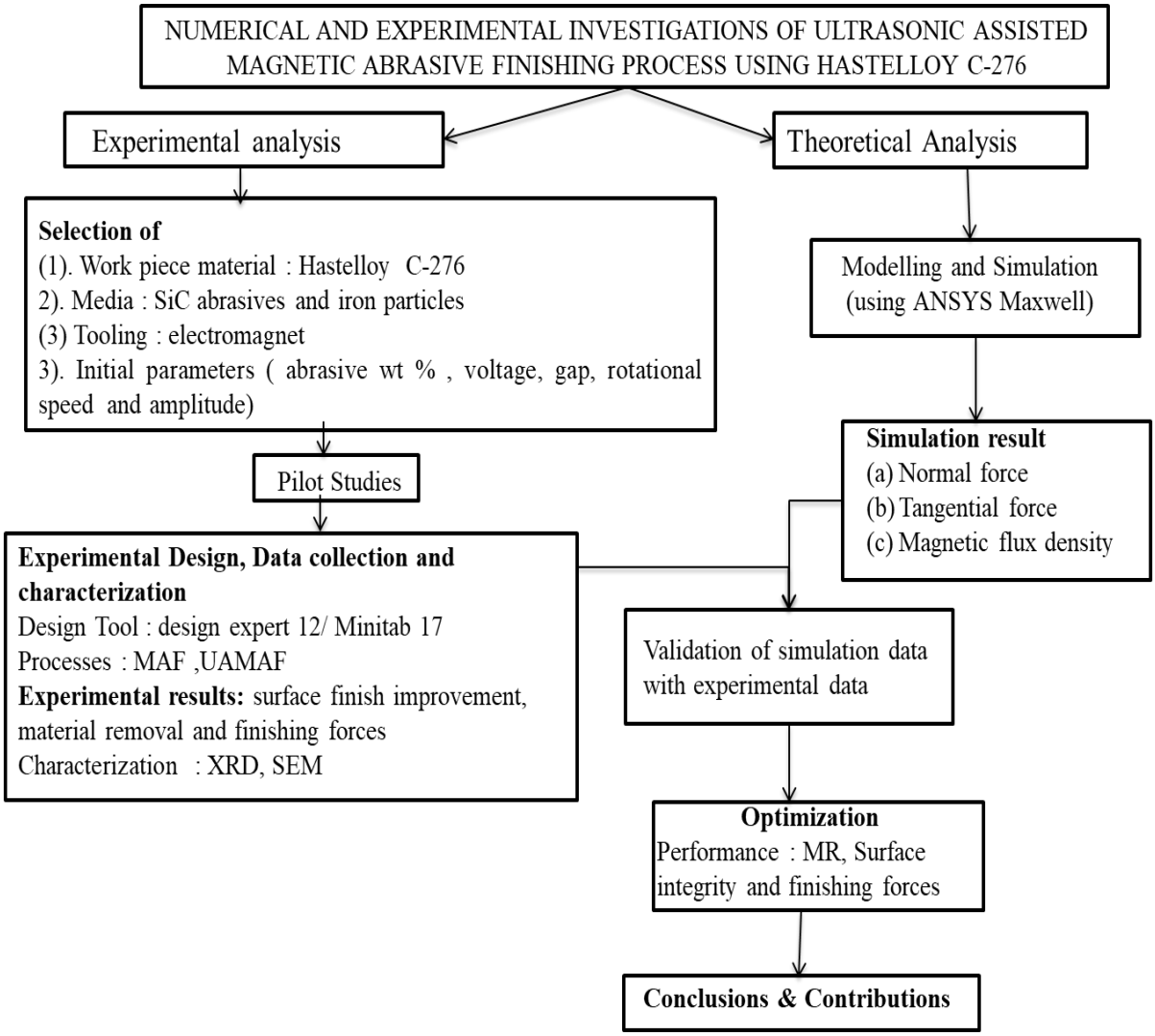

Figure 2.1: Research methodology

2.9 Summary

An overview of recent MAF and hybrid MAF advances as well as potential future research areas, are provided in this chapter. Based on earlier investigations, the process variables that effect on the performance are discussed. There are gaps in the current research and areas that might be looked into further. There have been presented the goals and parameters of the current effort. A flow chart that represents the work's methodology is suggested.

3 EXPERIMENTAL PROCEDURE AND DESIGN OF EXPERIMENTS

3.1 Introduction

Extensive experimental work had done throughout the entire inquiry. This chapter primarily investigates how the MAF and UAMAF setups are made. Additionally, the experimental methods employed, the characterization methods and tools used, the preparation of the workpiece and fixture, etc., are briefly presented with appropriate illustrations.

3.2 Development of MAF

In-situ developed MAF setup was arranged on a vertical milling machine with the required attachments, which is shown in Fig. 3.1. The main parts of MAF are an electromagnet unit, slip rings, winding unit, and work holding fixture. A stepped MS shaft acts as an electromagnet and it is connected to the milling machine rotating at different speeds. The workpiece holds to the working table with the help of a holding device. The spindle is mounted on an arbor and revolves at high speed. The working table has movements in horizontal as well as vertical directions.

Figure 3.1: Experimental setup on a vertical milling machine

3.2.1 The electromagnet

The electromagnet was fabricated to the required dimensions using a lathe machine. The electromagnet is in the form of a shaft with an overall length of 210 mm and step turned to the required dimensions as shown in Fig. 3.2. The slip ring is fixed on one step of the shaft,

and electrical winding is done over a length of 120mm using gauge 26 copper wire. The number of turns in the winding is approximately 500. The main purpose of the electromagnet is to study the influence of voltage on magnetic flux density and the strength of the flexible magnetic abrasive brush on the workpiece. It also addresses the variation of magnetic flux density (1-1.5 Tesla) by varying the voltage from (30-50 V). If the permanent magnet is considered for the purpose of experimentation, during the period of investigation, the magnetic flux density and the strength of the flexible magnetic brush become constant. Hence, an electromagnet is considered in this work to study the influence of variable magnetic flux density on a flexible magnetic abrasive brush.

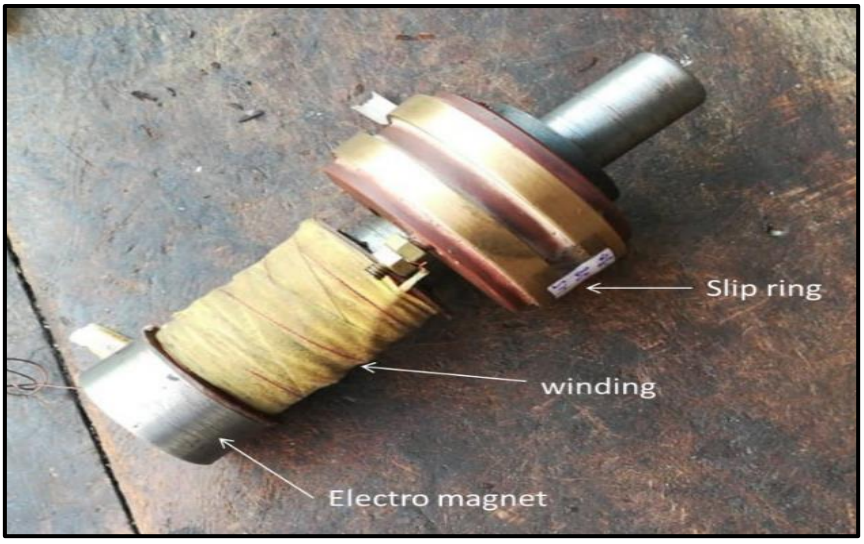

Figure 3.2: Electromagnet tool

3.2.2 Slip rings

Slip rings are electromechanical devices that are useful in transmitting power from a stationary structure to a rotating structure. These slip rings will improve mechanical performance, reduce the operation burden, and eliminate the risk of the wires swinging loosely in the setup.

Generally, a slip ring consists of a stationary metal contact that will be in contact with the outside diameter of a rotating metal ring, as shown in Fig. 3.3. This stationary metal contact or brush is generally made of graphite. The stationary brush in contact with the metal ring will conduct the electric current or signal by rotating the metal ring. With the use of a dimmer stat, this current is supplied. Because of this brush, the electrical circuit is finished. If there is a need for more than one electric circuit, more brushes and rings can be connected.

These slip rings are connected to the spindle of the vertical milling machine. The spindle also carries the electromagnet. The spindle consists of a stepped cylindrical housing.

This stepping is done with the help of a lathe machine. This cylindrical housing is usually made of mild steel or die steel. In this stepped cylindrical housing, the electromagnet is supported which is carried by the spindle. The current will be passing from the slip rings to this electromagnet. This completes the magnetic circuit.

Figure 3.3: Slip ring

3.2.3 Abrasives

The commonly used abrasives in the MAF process are Al_2O_3, SiC, B_4C, and diamond particles are used abrasives for industrial applications. The type of abrasives used depends on the application, hardness of the work material and the amount of required MRR. The abrasives are expressed in terms of mesh number. As the mesh size increases, the size of the abrasive particles reduces and the smaller mesh size abrasives give more MRR but give poor R_a, and vice versa[68].In the present study, SiC was used as an abrasive for both MS and Al 2024 alloy plates with an average mesh size of 325.

3.2.4 Magnetic particles

Magnetic particles influence the surface texture of the component. As the number of magnetic particles increases the strength of FMAB increases. FMAB improves the capturing capacity of the abrasives between these magnetic chains, thus improving the efficiency of the FMAB. In this current work, iron particles of 300 mesh size were used for the experimentation process. The SEM images of SiC abrasives and iron particles used for experimentation are shown in Fig. 3.4 (a) and Fig. 3.4 (b) before and after experimentation. Figure 3.4 (b) shows the broken abrasive particles which are into a small number of pieces due to abrasives' impacts on the workpiece. Girma et al. [36] suggested that the percentage of iron particles and abrasives varied from 80:20 to 70:30 for optimum performance.

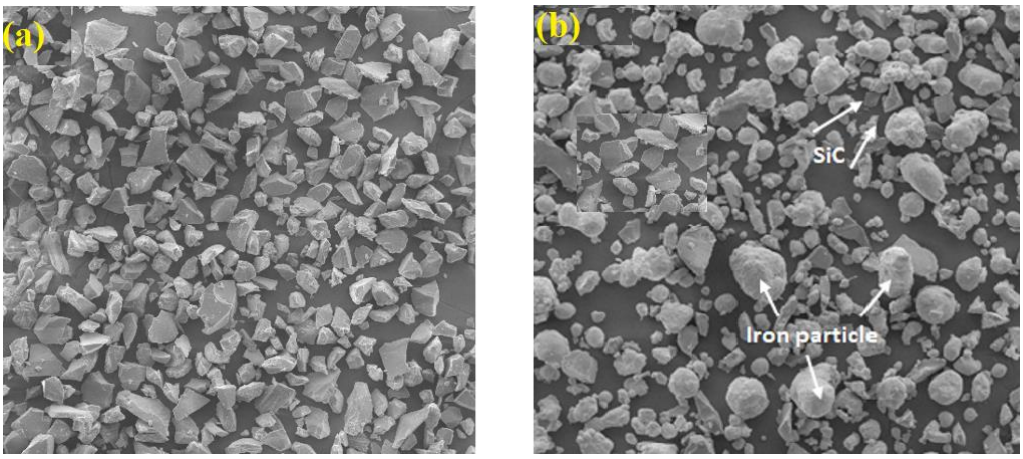

Figure 3.4: SEM image of (a) SiC abrasives (b) mix of iron particles and abrasives

3.2.5 Dimmerstat and rectifier

The dimmerstat used for varying voltage in the present experimentation for different levels is shown in Fig. 3.5. This voltage influences the magnetic field density of flexible magnetic brush and the range of dimmerstat is 10 A-230 V. The current is kept at a constant value throughout the experimentation. A rectifier was used to convert the alternating current (AC) into direct current (DC).

Figure 3.5: Dimmerstat

3.3 Workpieces

3.3.1 Mild steel

Mild steel (MS) is the most structural magnetic material used for engineering applications after stainless steel.

3.3.2 Aluminium alloy 2024

Al 2024 is a heat-treatable aluminium alloy with copper as the primary alloying element. Due to its high strength and fatigue resistance, 2024 is widely used in aircraft structures in wing and fuselage structures [69]. The chemical and physical properties of MS and Al 2024 alloy are listed in Tables 3.1 and 3.2. Also, the experimental details presented in Table 3.3.

Table 3.1: Chemical composition of MS plate

MS	Element	Mn	S	P	C	Fe
	Composition (wt. %)	0.6-0.9	0.05	0.04	0.14-0.2	Balance
Al 2024	Element	Cu	Mg	Si	Zn	Al
	Composition (wt. %)	3.8-4.9	1.2-1.8	< 0.5	< 0.25	Balance

Table 3.2: Physical properties of MS and Al 2024

	Yield Strength (MPa)	Tensile Strength (MPa)	Thermal conductivity (W/m K)	Melting point (°C)	Hardness (BHN)	Specific Heat capacity (J/g°C)
MS	275	475	51.9	1523	143	0.472
Al 2024	324	469	121	638	137	0.875

Table 3.3: Experimental details

Work materials	: Mild steel plate (MS) : Aluminum 2024 alloy (Al 2024)
Workpiece size	: 100mm×100mm×8mm
Abrasives used	: Silicon carbide (SiC)
Abrasive size	: SiC (220 mesh)
Magnetic particles & size	: Iron powder (300 meh)
Magnetic flux	: 1-1.5 Tesla
Run time	: 10 min
Dimmer stat	: 10A – 230 V
Rectifier	:0.5 A

3.3.3 Hastelloy C-276

The Hastelloy C-276 has significant proportions of molybdenum, nickel, and chromium. It also exhibits remarkable corrosion resistance at high temperatures. Because of its high hardness and rapid work hardening rate [70], machining Hastelloy is challenging. These materials are frequently employed in commercial applications such as transportation, aerospace, and healthcare. The chemical, physical and experimental details were listed in Tables 3.4,3.5 and 3.6.

Table 3.4: Chemical Composition

Element	Cr	Mo	Fe	W	Co	C	Si	Mn	V	P	S	Ni
Composition (wt.%)	15.5	16	5.5	3.5	2.5	0.02	0.08	1.0	0.35	0.03	0.03	Balance

Table 3.5: Mechanical properties

Melting point (°C)	Mass density (g/cm^3)	Ultimate tensile strength (MPa)	Hardness (HRB)	Modulus of elasticity (GPa)	Poisson's ratio
1350	8.89	792	90	410	0.31

Table 3.6: Experimental conditions

Workpiece materials	Hastelloy C-276
Workpiece size	100mm×100mm×6mm
Abrasives used	SiC
Abrasive size	SiC (220 & 325 mesh)
Magnetic particles & size	Iron powder (300 mesh)
Magnetic flux	1-1.5 Tesla
Run time	5 Mins for MAF & 2 Mins for UAMAF
Dimmer stat	10 A – 230 V
Rectifier	0.5
Details of the ultrasonic device	
Make	Roop Telesonic Ultrasonix Ltd.
Frequency	30 kHz
Power output	1000 W (variable in the steps of 0 to 100%)
Amplitude	12 microns

3.4 Development of UAMAF

The basic parts of the UAMAF setup, which are made on a vertical milling machine, are a slip ring, an electromagnet, a specifically made workpiece fixture, an ultrasonic setup, and an air compressor. A slip ring, copper winding, and an electromagnet make up the electromagnet, which is made of mild steel. It was stored next to the milling machine's cutting tool. The copper winding that is essential to the electromagnet's efficient operation receives electricity from the external source through the slip ring. The workpiece, ultrasonic head, and springs were all accommodated in the design of the work fixture. Springs effectively transfer the axial vibrations of the ultrasonic head to the workpiece. A uniquely constructed ultrasonic head and transducer make up the ultrasonic setup. For the ultrasonic head, the transducer transforms a high frequency of 30 kHz into an axial vibration of 8 to 12 microns. The ultrasonic horn's life was extended by using the compressor to cool the end of the horn. Diagrammatically depicted in Fig. 3.6 is the experimental setup for the UAMAF finishing procedure. Using a dimmerstat (10 A and 230 V), the external DC power source is delivered to the slide ring. Mild steel spindle is transformed into an electromagnet by the copper wrapping. FMAB was created between the workpiece and electromagnet using an external power source. Iron and abrasive particles both combined to form the FMAB. The iron particles become magnetised by the electromagnet's magnetism and become stuck with the abrasives, acting as a multipoint cutting tool. The tangential force and the indentation force because indentation is produced by the relative motion of the rotating FMAB with the workpiece. As a result, microchip-sized pieces of the workpiece are removed. Because the workpiece vibrates axially during the UAMAF process, the abrasive chains rotate every time, and this improves the surface quality of the workpiece.

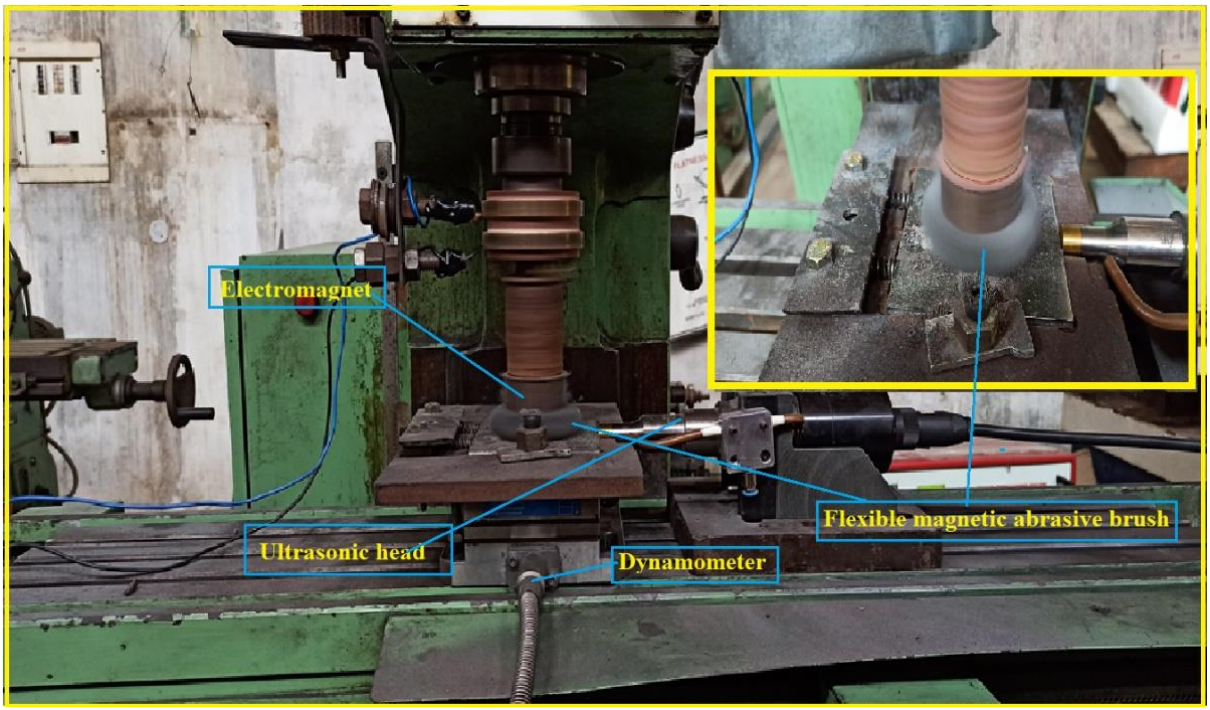

Figure 3.6: UAMAF process on milling machine

3.5 Spray coating technique

The workpiece's coating was applied via physical vapour deposition. Figure 3.7 (a) depicts the experimental setup, whereas Figure 3.7 (b) depicts the spray coating procedure in its schematic form. In this procedure, the chemical's weight, the hot chamber's temperature, and the quantity of coatings were all separately adjusted. In a 1:3 ratio, yttrium acetate and di-ethanolamine were combined to create the chemical etchant, according to Wen et al. [71]. Different weights of yttrium acetate, including 2, 4, 6, and 10 grams, were combined with a constant volume of 150 millilitres of ethanol. For optimum yttrium acetate mixing, the chemical etchant was handled with a vibrator and maintained at room temperature for four weeks. The Hastelloy C-276 workpiece, which was 10 cm by 10 cm in size, was coated with etchant four weeks later. To begin with, the ideal weight of the etchant was taken into consideration and kept consistent for subsequent tests. After that, depending on the surface finish attained, the ideal temperature and number of coats were forecasted.

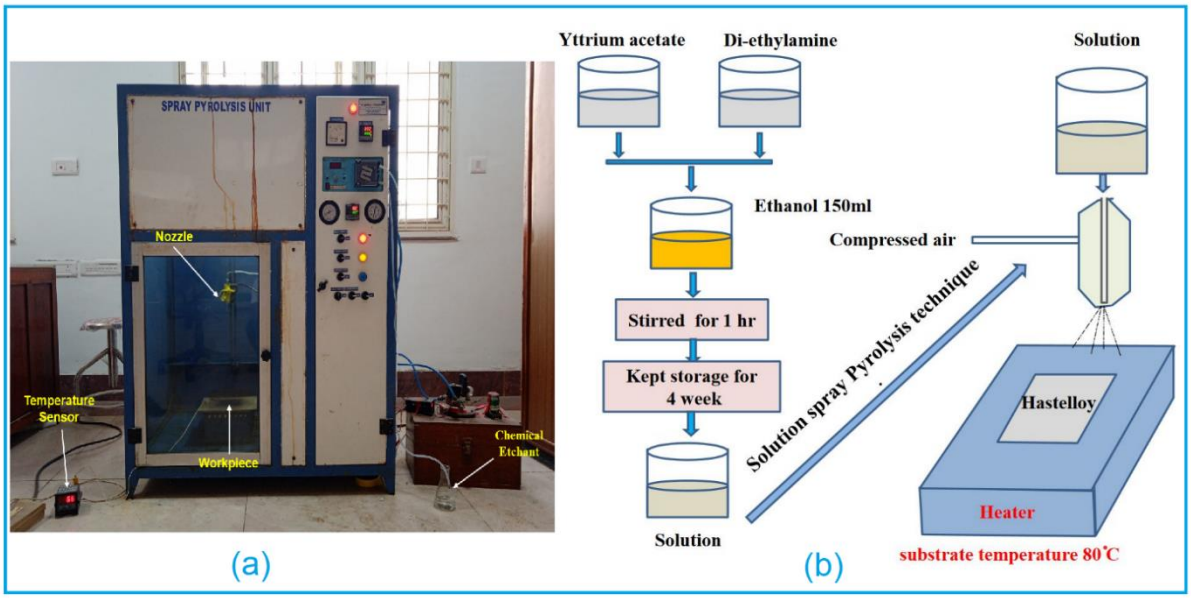

Figure 3.7: (a) Experimental setup for the spray coating process (b) Schematic process

3.6 Measurement of response parameters

3.6.1 Magnetic flux density measurement

Equipment from the STR Model S - 20B model was used to test the magnetic flux density. During the experiment, it was seen that the magnetic flux density ranged between 1 and 1.5 tesla. Equation 3.1 is also used to calculate the magnetic flux density (B) based on the theoretical study. (Yin et al. and Mulik et al. [72][73]).

$$B = \frac{\mu 0 N I}{g} \qquad \textit{Equation 3-1}$$

Where μ_0 = Permeability in vacuum = $4\pi \times 10^{-7}$ H/m Khairy et al. and Mori et al.[74][75]

N= Number of turns = 500

g = working gap = 2 to 3 mm

I = Current = 5 A

3.6.2 Surface roughness tester

Five distinct locations were used to measure the roughness of the surface, and the average value was used. The surface roughness tester, model TIME3220, and KTI manufacture were used to measure the R_a values; these specifications are provided in Table 3.7. The workpiece is surface-ground and kept at a constant surface roughness of 1.3 µm prior to the start of the experiment. Equations 3.2 and 3.3 were used to compute the material removal and surface finish improvement.

Figure 3.8: Surface roughness tester

$$\textit{Surface finish improvement } (\Delta R_a\ (\%)) = \frac{Intial\ Ra - Final\ Ra}{Intial\ Ra} * 100 \qquad \textit{Equation 3-2}$$

Material removal (MR (mg)) = (Initial Weight- Final Weight) *Equation 3-3*

Table 3.7: Surface roughness tester

Make	KTI Pvt. Ltd.
Model	Time3220
Cut of length	0.8 mm
Stylus speed	0.5 mm/s
Least count	0.001µm
Sensor	BFW non-skid head
Total evaluation length	5 mm

3.6.3 Material removal

Utilising a laboratory weighing balance with 0.1mg precision, the USS-DBS16 solid model, the material elimination was measured.

Figure 3.9: Weighing balance

3.6.4 Cutting force

The plug dynamometer fixed to the milling bed measured the cutting forces, and Dyno ware software was used to compile the results. Cutting forces in the X, Y, and Z directions were measured. Every second, a charge amplifier (5070A) shows the force values and lets the user know how the force measurement goes.

Dynamometer: The dynamometer of the Kistler (9257 B) type, which is depicted in Figure 3.10, forces were measured. A base plate and a top plate are the foundation of the dynamometer, which comprises four three-component force sensors that are tightly preloaded. Each sensor comprises three pairs of quartz plates, each responsive to shear in the x and y directions and one pair of pressure in the z-direction. Six components are measured without displacement: three orthogonal force components (F_x, F_y, and F_z) and three torque components (M_x, M_y, and M_z). These precision sensors' high rigidity, great sensitivity, outstanding repeatability, and long-term stability are their key distinguishing characteristics. The top plate of a six-component dynamometer sensor receives the forces and torque applied to the tool. Electrodes attached to the sensor's connector are used to gather the charges the quartz plates produce.

Figure 3.10: Kistler six-component 9257 B type dynamometer

Figure 3.11: Cutting force -charge amplifier &Data acquisition system

Charge Amplifier: The output of the dynamometer was amplified from microvolts to millivolts displayed in Figure 3.11 using the 5070A, 4-channel strain gauge amplifier. It is a tiny instrument that is affordable and ideal for high-resolution measurements. The spinning knob, adjusting, and measuring pushbuttons on the charge amplifier's front panel are used to configure the ranges of the measuring characteristics. It can function both analog and digital. The output signal in analog mode can be entered into an A/D converter or another device and is appropriate for up to +/- 10 volts of output voltage. An RS-232 serial connection serves as the output in digital mode. On the back of the case are conveniently situated single connectors for the amplifier's inputs and outputs.

Data Acquisition: The signals collected from the output from the charge amplifier are further examined using Dyno Ware data gathering and display software.

3.6.5 Surface Topography

The topography, morphology, composition, and crystallographic information are examined using scanning electronic microscopy. SEM creates images by using electrons as opposed to light. The fundamental idea behind SEM is that an electron beam created by a tungsten filament is focussed by magnetic lenses and strikes the specimen. Signals are produced when the electron beam interacts with the specimen's top surface. Each of these signals is sensitive to a different element of the specimen and provides a variety of information about the specimen by detecting the signals that are released. Figure 3.12 depicts the SEM system utilized in this investigation (TESCAN manufacture, Model: Vega LMU 3), together with information about its parameters are listed in Table 3.8.

Table 3.8: Specifications of Scanning Electron Microscope

Component	Details
Make and Model	TESCAN, Vega LMU 3
Electron gun	Tungsten heated cathode
Resolution	High Vacuum Mode (SE): 3 nm at 30 kV / 2 nm at 30 kV Low Vacuum Mode: 3.5 nm at 30 kV / 2.5 nm at 30 kV
Magnification	2 1,000,000
Scanning Speed	From 20 ns to 10 ms per pixel adjustable in steps or continuously
Chamber Vacuum	High Vacuum Mode: < 10-3 9 Pa Medium Vacuum Mode: 3 150 Pa Low Vacuum Mode: 3 500 Pa*
Chamber and Column Suspension	Pneumatic
Specimen Stage	Movements: X = 80 mm (40 mm to +40 mm) Y = 60 mm (30 mm to +30 mm) Z = 47 mm Rotation: 360° continuous tilt: 80° to +80° Maximum Specimen Height: 54 mm (with rotation stage) 81 mm (without rotation stage)

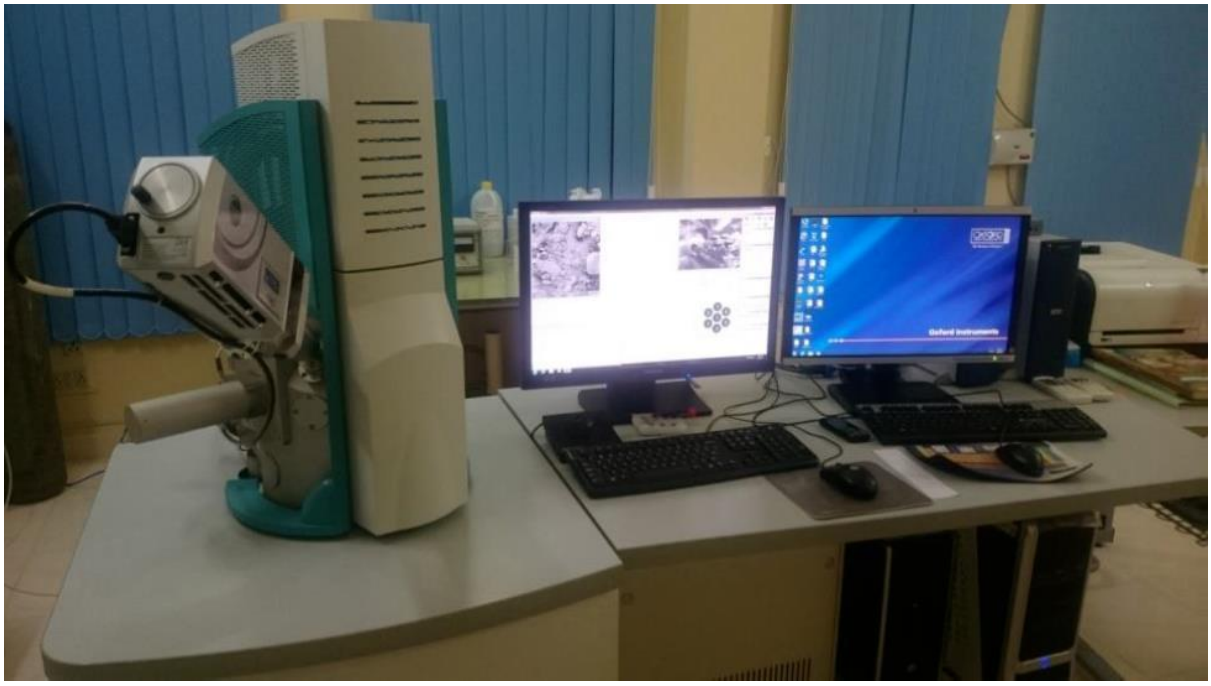

Figure 3.12: Scanning electron microscopy

3.6.6 Residual stresses

Figure 3.13 illustrates the use of X-ray diffraction, a common non-destructive testing method, to quantify the residual stress on the surface. Using portable or laboratory equipment, this technique can measure the residual stresses of the surface down to 30 m and the inter-atomic distance of the material. The X-Ray wavelength will be measured in angstroms (A^0), which is comparable to the sizes of the inter-planar or interatomic distances in polycrystalline materials. It takes the constructive interference of X-rays scattered from a polycrystalline solid to create the diffracted beams. Using Bragg's law, inter-planar spacing (d) is calculated from the angles of the maximum diffraction intensities of the diffraction planes and the unstressed spacing is d0. The magnitudes of the residual stresses in the workpiece are exactly proportional to the differential ($d-d_0$). In reality, the grains serve as internal strain gauges for residual tensions. Panalytical X'pert pro MRD with X'pert stress software is used to measure the profiles of stresses. Table 3.9 represents the X-Ray diffractometer's specifications

Figure 3.13: XRD equipment

Table 3.9: Specifications of the X-Ray diffractometer

Component	Details
Make & model	Panalytical X'Pert Pro
Source of X-rays	Cu-Kα, 1.54 Å wavelength
Detector	Pixel and Scintillation detector
Stage for sample	Fixed, with X-Ray source & Detector rotation
Filters	Nickel and copper
Range of masks	2 mm to 20 mm
Measurement range	5^{o} to 140^{o}

3.7 Statistical approach for predicting MAF output

3.7.1 Design of experiments

Design of experiments (DOE) is a branch of statistics that involves planning, analysing, conducting, and interpreting the tests to study the factors that control the experiment. DOE is the design of information gathering. DOE is the design of an information-gathering exercise where variation is present. It can be under the presence of an experimenter or not. DOE has a huge application and can be used as an analysis tool in various experimental situations. It is basically a systematic approach for investigating a

system, in which tests are designed by making changes to the input variables of the system. The effects of these changes on the output are then studied. [25].

DOE is a formal way of maximizing information gained while resources are required. It has something more to offer other than 'one change at a time' experimental methods because it allows judgment on the significance of the output of input variables acting alone, as well as input variables acting in combination with one another. There will always be a risk with 'one change at a time experimental methods that the experimenter may find the effect of one variable significantly on the output and may fail to discover the effect of other variables. This may happen because of the temptation to stop the test after finding one significant effect. Therefore 'one change at a time experimental method depends upon the experimenter carrying the job. However, DOE checks for all possible dependencies initially and then direct exactly what data are needed to assess them i.e., whether the response is changed by input variables on their own when combined with other variables or not at all. In terms of resources, the exact length and size of the experiment are set by design.

DOE is used to find the factors which have a major contribution to the system or process. It helps to find the performance of the system in the presence of noise and the best configuration values for which the variation due to noise is minimum. In the examples given above, these are problem-solving, parameter design, and robustness study. In each case, DOE helps to find the answer; the only thing that makes them different is which factors would be used in the experiment. The process of experimentation is shown in Figure 3.14

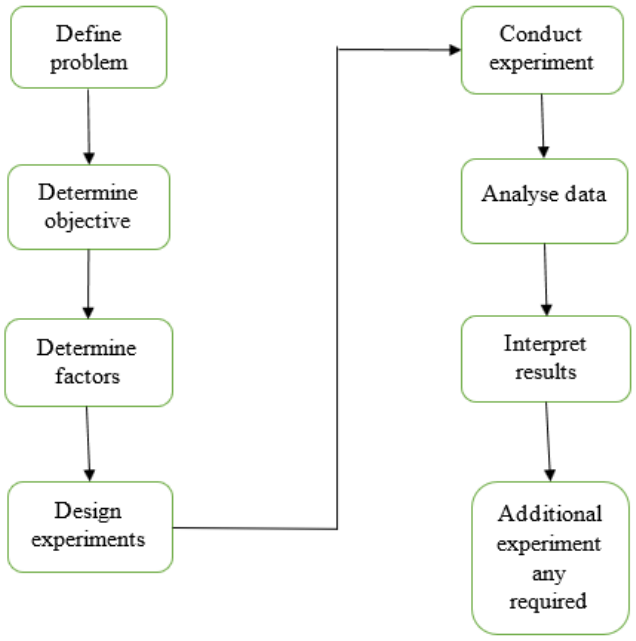

Figure 3.14*:* Process of experimentation

The order of tasks using the variable starts with the identification of input factors and output variables. For each input variable, the number of levels is defined that determines the range for which the effect of input variables is desired to be known. An experimental plan is produced by the experimenter that guides where to set each test parameter for each test run. Then the analysis is done for the response that is measured for each run and the difference in the output in each test is noticed. These differences are then attributed to the input variables acting alone (called a single effect) or in combination with another input variable (called an interaction).

The process parameters selected for finishing of MS and Al 2024 alloy using MAF were represented in Tables 3.10 & 3.11. The experimental designs for finishing of MS and Al 2024 alloy were represented in Tables 3.12 and 3.13.

Table 3.10: Process parameters for MS plate

Percentage of Abrasives (C_1) (%)	Speed of electromagnet (C_2) (rpm)	Voltage (C_3) (V)
20	180	30
25	350	40
30	500	50

Table 3.11: Process parameters for Al 2024 alloy

Percentage of abrasives (C_1) (%)	Speed of electromagnet (C_2) (rpm)	Voltage (C_3) (V)
20	1000	30
25	1400	40
30	2100	50

Table 3.12: Experimental conditions for MS

S. No	**C_1 (%)**	**C_2 (RPM)**	**C_3 (V)**	**% ΔR_a**
1	20	180	30	
2	20	180	40	
3	20	180	50	
4	20	350	30	
5	20	350	40	
6	20	350	50	

7	20	500	30	
8	20	500	40	
9	20	500	50	
10	25	180	30	
11	25	180	40	
12	25	180	50	
13	25	350	30	
14	25	350	40	
15	25	350	50	
16	25	500	30	
17	25	500	40	
18	25	500	50	
19	30	180	30	
20	30	180	40	
21	30	180	50	
22	30	350	30	
23	30	350	40	
24	30	350	50	
25	30	500	30	
26	30	500	40	
27	30	500	50	

Table 3.13: Experimental conditions for Al 2024 alloy

S. No	**C_1 (%)**	**C_2 (RPM)**	**C_3 (V)**	**% ΔR_a**
1	20	1000	30	
2	20	1000	40	
3	20	1000	50	
4	20	1400	30	
5	20	1400	40	
6	20	1400	50	
7	20	2100	30	
8	20	2100	40	

9	20	2100	50	
10	25	1000	30	
11	25	1000	40	
12	25	1000	50	
13	25	1400	30	
14	25	1400	40	
15	25	1400	50	
16	25	2100	30	
17	25	2100	40	
18	25	2100	50	
19	30	1000	30	
20	30	1000	40	
21	30	1000	50	
22	30	1400	30	
23	30	1400	40	
24	30	1400	50	
25	30	2100	30	
26	30	2100	40	
27	30	2100	50	

3.7.2 Response surface methodology

Response surface methodology was initially established by Box and Wilson (1951) to investigate the potential of the statistical design. With the use of this strategy, experiments can be planned, data can be analysed, and empirical models can be created that can be applied to process improvement or the identification of ideal circumstances. The objective of the RSM process is not only to study the influence of process parameters but also to identify the region of the optimal solution. The experimental design was developed to conduct experimentation for evaluating the process performance of the proposed MAF and UAMAF process. The Box Behnken technique is the experimental design employed in the study. The Box-Behnken Design (BBD), for the Response Surface Methodology, or RSM, is specifically made to match a second-order model, which is the main focus of most RSM investigations. The BBD requires just three levels for each factor, as opposed to five levels in the Central Composite Design (CCD), to build a second-order regression model (quadratic model).

The BBD set a mid-level between the original low- and high-level of the factors, avoiding the extreme axial (star) points as in the CCD. Moreover, the BBD uses face points, often more practical, rather than the corner points in CCD. The addition of the mid-level point allows the efficient estimation of the coefficients of a second-order model (Box et al., 2005). The BBD is almost rotatable as the CCD. Moreover, often, the BBD requires a smaller number of experimental runs. The process parameters selected for finishing Hastelloy C- 276 using MAF, UAMAF and surface coating are represented in Tables 3.14, 3.15 & 3.16. The experimental designs for MAF, UAMAF and surface coating while finishing Hastelloy C-276 were listed in Tables 3.17,3.18 and 3.19.

Table 3.14: Process parameters for MAF process

SiC Wt. % (%wt.) (C_1)	Voltage (V) (C_2)	Speed of electromagnet (rpm) (C_3)	Working Gap (mm) (C_4)
20	35	500	2
25	45	750	2.5
30	55	1000	3

Table 3.15: Process parameters for UAMAF process

SiC Wt.% (%wt.) (C_1)	Voltage (V) (C_2)	Speed of electromagnet (rpm) (C_3)	Working Gap (mm) (C_4)	Power intensity (W/m^2) (C_5)
20	35	500	2	80
25	45	750	2.5	90
30	55	1000	3	100

Table 3.16: Process parameters for surface coating process

Etchant weight (gm)	Temperature (^0C)	No. of coatings
2	60	5
6	80	15
10	100	25

Table 3.17: Experimental design matrix for MAF process

S. No	C_1 (wt.%)	C_2 (V)	C_3 (rpm)	C_4 (W/m^2)	ΔR_a (%)	MR (mg)	F_N (N)	F_T (N)
1	20	45	500	2.5				
2	25	45	500	2				
3	25	45	500	3				
4	25	35	500	2.5				
5	25	55	500	2.5				
6	30	45	500	2.5				
7	20	35	750	2.5				
8	20	55	750	2.5				
9	20	45	750	2				
10	20	45	750	3				
11	25	35	750	2				
12	25	55	750	2				
13	25	35	750	3				
14	25	55	750	3				
15	25	45	750	2.5				
16	25	45	750	2.5				
17	30	35	750	2.5				
18	30	55	750	2.5				
19	30	45	750	2				
20	30	45	750	3				
21	20	45	1000	2.5				
22	25	45	1000	2				
23	25	45	1000	3				
24	25	35	1000	2.5				
25	25	55	1000	2.5				
26	30	45	1000	2.5				

Table 3.18: Experimental design matrix for UAMAF process

S. No	C_1 (%)	C_2 (V)	C_3 (rpm)	C_4 (mm)	C_5 (W/m^2)	ΔR_a (%)	MR (mg)	F_N (N)	F_T (N)
1	25	45	500	2	90				
2	25	45	500	3	90				
3	25	45	500	2.5	80				
4	25	45	500	2.5	100				
5	20	45	500	2.5	90				
6	30	45	500	2.5	90				
7	25	35	500	2.5	90				
8	25	55	500	2.5	90				
9	20	35	750	2.5	90				
10	30	35	750	2.5	90				
11	20	55	750	2.5	90				
12	30	55	750	2.5	90				
13	25	35	750	2.5	80				
14	25	55	750	2.5	80				
15	25	35	750	2.5	100				
16	25	55	750	2.5	100				
17	20	45	750	2	90				
18	30	45	750	2	90				
19	20	45	750	3	90				
20	30	45	750	3	90				
21	25	35	750	2	90				
22	25	55	750	2	90				
23	25	35	750	3	90				
24	25	55	750	3	90				
25	25	45	750	2	80				
26	25	45	750	3	80				
27	25	45	750	2	100				
28	25	45	750	3	100				
29	20	45	750	2.5	80				

30	30	45	750	2.5	80				
31	20	45	750	2.5	100				
32	30	45	750	2.5	100				
33	25	45	750	2.5	90				
34	25	45	750	2.5	90				
35	25	45	1000	2	90				
36	25	45	1000	3	90				
37	25	45	1000	2.5	80				
38	25	45	1000	2.5	100				
39	20	45	1000	2.5	90				
40	30	45	1000	2.5	90				
41	25	35	1000	2.5	90				
42	25	55	1000	2.5	90				

Table 3.19: Experimental design matrix for Spray Coating

S. No	Etchant weight (gm)	Temperature (^{0}C)	No. of coatings	ΔR_a (%)
1	2	60	5	
2	2	60	15	
3	2	60	25	
4	2	80	5	
5	2	80	15	
6	2	80	25	
7	2	100	5	
8	2	100	15	
9	2	100	25	
10	6	60	5	
11	6	60	15	
12	6	60	25	
13	6	80	5	
14	6	80	15	
15	6	80	25	

16	6	100	5	
17	6	100	15	
18	6	100	25	
19	10	60	5	
20	10	60	15	
21	10	60	25	
22	10	80	5	
23	10	80	15	
24	10	80	25	
25	10	100	5	
26	10	100	15	
27	10	100	25	

3.7.3 Regression analysis

Modelling the link between the process variable and the answers is done using the regression analysis technique. The relationship between the dependent (responses) and independent (control factor) variables is the main focus of the regression study. Regression analysis is demonstrated via equation 4.4, where an empirical relationship is fit to predict the response Y in connection to independent variables like X1 and X2. As a result, the regression analysis can be performed with unknown parameters like B_0, B_1, B_2. Independent variable X and dependent variable can also be included. Through the use of a regression model, the relationship between the unknown parameter and the dependent variable Y is established.

$Y = F(X, B)$ *Equation 3-4*

The linear regression equation indicated in equation (3.4) can be written for several dependable variables as-

$Y = B0 + B_1X + E_{I,}\ I=1 \ldots\ldots, N.$ *Equation 3-5*

Adding a term X_i^2 to equation (3.5) leads to equation (3.6) as given below

$Y = B_0 + B_1X + B_2X_I^2 + E_{I,}\ I=1 \ldots\ldots, N.$ *Equation 3-6*

Equation (3.6) is still linear even though the right-hand independent terms are quadratic but it is linear in terms such as β_0, β_1, β_2. The term ε_i is an error term with the subscript *i* indicating the particular term. The residual of regression analysis is e_i which is a difference $(\hat{Y}_l – Y_i)$ between the value of the dependent variable predicted by the model $(\hat{Y}_l)$ and the true value of

the dependent variable (Y_i). The value of the dependent variable predicted by the model can be written as

$$\hat{Y}_L = \hat{\beta}_0 + \hat{\beta}_1 X_I \qquad \textit{Equation 3-7}$$

The parameters $\hat{\beta}_0$ and $\hat{\beta}_1$ are the estimators given in equations here under:

$$\hat{\beta}_1 = \frac{\Sigma(Xi-\bar{X})(Yi-\bar{Y})}{\Sigma(Xi-\bar{X})} \qquad \textit{Equation 3-8}$$

$$\hat{\beta}_0 = \bar{Y} - \hat{\beta}_1 \bar{X} \qquad \textit{Equation 3-9}$$

Where the mean average X values and $\hat{Y}$ is the mean average value of Y value. The residual of a regression analysis (e_i) is the estimated error which will coincide with the error term (ε_i) only if the parameters $\hat{\beta}_0$ and $\hat{\beta}_1$ are the exact estimate of regression parameters β_0 and β_1. The most common technique used for determining the coefficients $\hat{\beta}_0$ and $\hat{\beta}_1$ is the least square method of forecasting where the value of $\hat{\beta}_0$ and $\hat{\beta}_1$ are chosen to minimize the sum of squared residual error (SSE). The (SSE) can be written as

$$SSE = \sum(Y_I - \hat{\beta}_0 - \hat{\beta}_1 X_I^2) \qquad \textit{Equation 3-10}$$

With the assumption that the population error term has a constant variance the estimate of that variance known as the mean square error MFE of the regression, is given as

$$MFE = \frac{SSE}{N-2} \qquad \textit{Equation 3-11}$$

It should be noted that Σ denotes the summation $\sum_{i=1}^{N}$ Where N is the number of observations in the sample. The minimization of SSE is done by partial derivative operation of SSE with respect to parameter $\hat{\beta}_0$ and $\hat{\beta}_1$ and setting them equal to zero. This generates two equations which are then jointly solved to yield the estimated coefficient in the regression analysis. The SSE can be used to measure the 'goodness of fit' of the estimated equation term as R^2. This goodness-of-fit term R^2 is also known as the coefficient of determination which is calculated below.

$$R^2 = 1 - \frac{SSE}{\Sigma(Yi-\bar{Y})2} = 1 - \frac{SSE}{SST} \qquad \textit{Equation 3-12}$$

The expression $(\mathrm{Yi} - \bar{Y})^2$ in equation (4.14) represents the total variation, also known as the total sum of a square or SST. The SSE can be thought of as an unexplained variation in the dependent variable. So R^2 can be written as 1 minus the proportion of variation in Y_i that is not explained. Hence R^2 is the proportion variance in Y_i that is accounted for by the estimated equation the R^2 is bounded by 0 and 1.

The regression analysis is further forward by analysis of variance (ANOVA). ANOVA is useful for investigating the significance of factors and the interaction of process variables on the responses. In the ANOVA table, the means square (MS) is stated as below:

$$MS = \frac{(sum\ of\ square\ deviation)}{Degree\ of\ freedom} \qquad \textit{Equation 3-13}$$

The degree of freedom in ANOVA is used to calculate the MS. In the ANOVA table the F value indicates variance ratio or Fisher's ratio which is defined as

$$F = \frac{MS\ for\ a\ term}{MS\ for\ the\ error\ term} \qquad \textit{Equation 3-14}$$

The probability of significance (P-value) is then calculated based on the variance ratio (F value). If the probability of significance value (P value) is less than 0.05, then generally it can be stated that the effect of the control factor /interaction of factors had significant. From the regression analysis the interaction effects of the process variable can be observed.

3.8 Summary

The analysis of the experiment design and the experimental methodologies used are the key topics of this chapter. In order to impart forces in both normal and tangential directions, the MAF and UAMAF were built using suitable tooling. Additionally, combinations of other process parameters were devised, including axial vibrations and other process factors. We talked about the typical process for preparing the workpiece and the abrasive media. But appropriate figures were employed to depict the measurement and characterisation that were used in the study. It has been mentioned how the research activity's statistical analysis was done.

4 NUMERICAL STUDIES OF MAF AND UAMAF PROCESSES

4.1 Introduction

In this chapter, ANSYS Maxwell 16.0 software has been used to create a 3-D model and simulate the MAF and UAMAF process on a flat workpiece. According to the experimental setup dimensions, a milling machine's experimental setup for flat workpieces is modelled. ANSYS Maxwell 16.0 is then used to simulate these models. The generated numerical findings were compared with the experimental output after the model had been validated. However, it was discovered that the differences between the simulation and experiment results fell within an acceptable range, the simulation model was deemed to be valid.

4.2 Theoretical analysis of magnetic flux density

Finite elemental method (FEM) uses the classical Maxwell equation as a governing equation to calculate the distribution of magnetic flux density and the forces. The magnetic properties of materials are listed in Table 4.1.

The governing equation of the model:

$$\nabla \times E = \frac{\partial B}{\partial t} \qquad \textit{Equation 4-1}$$

$$\nabla \times H = J + \frac{\partial D}{\partial t} \qquad \textit{Equation 4-2}$$

$$\nabla \cdot B = 0 \qquad \textit{Equation 4-3}$$

Where,

E = Electric field

B = Magnetic flux density vector

H = Magnetic flux intensity vector,

J = Electric current density

D = Electric flux density vector, and

t = time

To simplify these equations, several assumptions are used, such as the strength of the magnetic field being constant while the remaining process parameters are kept constant

during MAF and UAMAF. Consider any magnetic field leakage to be insignificant due to the smaller working gap.

Because there is no current working gap, $\frac{\partial D}{\partial t} = 0$ and J = 0 may be assumed.

$$\nabla \times E = 0 \qquad \textit{Equation 4-4}$$

$$\nabla \times H = 0 \qquad \textit{Equation 4-5}$$

$$\nabla \cdot B = 0 \qquad \textit{Equation 4-6}$$

The relationship between H and B in a vacuum is:

$$B = \mu_o H \qquad \textit{Equation 4-7}$$

where $\mu_o = 4\pi \times 10{-}7$ (T· m/A), permeability of free space

The particles of magnetic abrasives cover the working gap, resulting in a magnetic flux density as shown in the equation.

$$B = \mu_o (H + M) \qquad \textit{Equation 4-8}$$

The magnetic flux intensity in terms of potential gradient

$$H = -\nabla \phi \qquad \textit{Equation 4-9}$$

where ϕ = potential gradient

also,

$$M = \chi H \qquad \textit{Equation 4-10}$$

where M = Internal magnetization of ferromagnetic

As a result, equation (4.8) may be written as:

$$B = \mu_o (1 + \chi) H \qquad \textit{Equation 4-11}$$

In equation (4.3), the values of B and H from equations (4.10) and (4.11) are substituted.

$$\nabla \cdot [\mu_o (1 + \chi)(-\nabla \phi)] = 0 \qquad \textit{Equation 4-12}$$

But μ_o is constant and $(1 + \chi) = \mu_r$, where

μ_r = relative permeability of MAPs, so (12) becomes:

$$\nabla \cdot [\mu_r \nabla \phi] = 0 \qquad \textit{Equation 4-13}$$

The gradient of the magnetic potential energy may be used to express the magnetic force F_m.

$$F_m = \mu_o 2 \nabla \int M \cdot H dV v \qquad \textit{Equation 4-14}$$

All V, M and H are assumed to be uniform. As a result, equation (14) may be reduced to

$$Fm = \mu_o (M \cdot \nabla) H \qquad \text{Equation 4-15}$$

Magnetic susceptibility χ calculated using Wiedemann's formula

$$\chi = \alpha \chi_{ferr} + (1 - \alpha)\, abr \qquad \text{Equation 4-16}$$

$$\mu r = \alpha \mu_{rferr} + (1 - \alpha)\, r_{abr} \qquad \text{Equation 4-17}$$

Table 4.1. Magnetic properties of materials

Relative magnetic permeability	**value**
Hastelloy C-276	1.002
Air	1
Iron	4500
Silicon carbide	0.99996
copper	1
Conductivity of copper coil	58×10^6 S/m

4.3 Simulation study

The simulation of MAF and UAMAF setup is performed on ANSYS Maxwell 16.0 software for flat workpieces. To study the influence of process variables on magnetic flux and finishing forces and results are listed and compared to the outcome of the experiment.

Assumptions

- It is assumed that the workpiece material is homogenous and isotropic.
- Magnetic field leakage is neglected
- The interaction with FMAB does not affect the material qualities of the workpiece.
- The magnetic abrasive particle's diameter and shape are considered to be identical and spherical.
- D_f or D_a =15.24/M (mm)
- The magnetic brush rotates at the same rpm as the tool
- The cross-sectional area of the magnetic brush is the same as the cross-sectional area of the air gap.

4.4 Procedure to be followed to perform the simulation

The simulation is performed on Ansoft Maxwell 16.0 software the input parameters and model specifications are listed in the previous sections. Results for magnetic flux density distribution is obtained

- ✓ Parameters such as force and torque can be determined
- ✓ Input parameters like machining gap, voltage and rpm are varied to observe the change in the magnetic flux density and magnetic force.

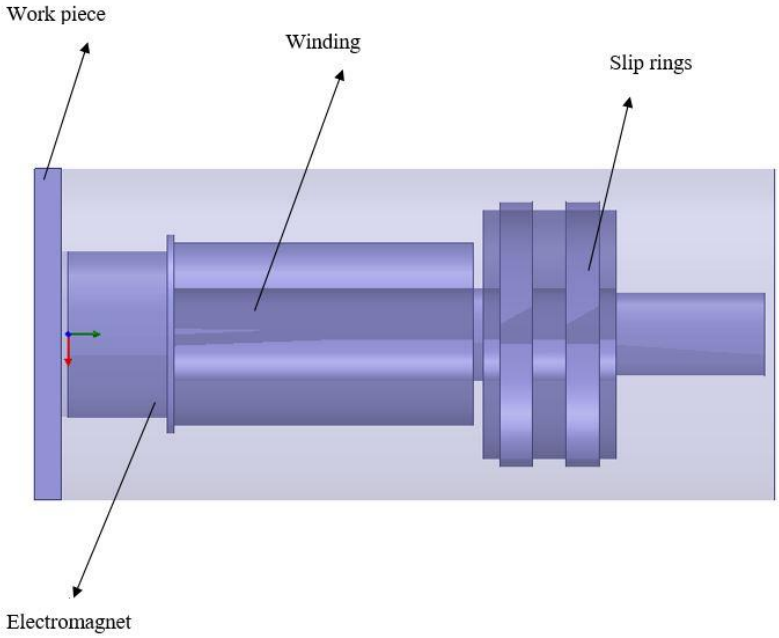

Figure 4.1: Schematic model of an electromagnetic tool

For assigning motion to the moving parts either rotary, translating, or periodic, firstly created the band which covers the moving part. Then assign the motion condition to bands, there are two types of motion setups in Figure 4.2. The rotational motion was given to the electromagnet in Figure 4.2 (a) and the transient axial motion was given to the workpiece in Figure 4.2 (d) is applied. An insulating boundary was given to the defined thickness for a perfectly insulating sheet between touching conductors in Figure 4.2 (b). This is particularly useful for separating winding and magnetic steel. The cross-sectional sides of the 3D conductors are designated by coil terminals. These can be found on the inside of a closed loop or on the outside of a conduction route shown in Figure 4.2 (c). A winding is formed by grouping the coil terminals and controlling the current in one or more conduction channels. The only things that the coil terminals define are the number of conductors and direction of current

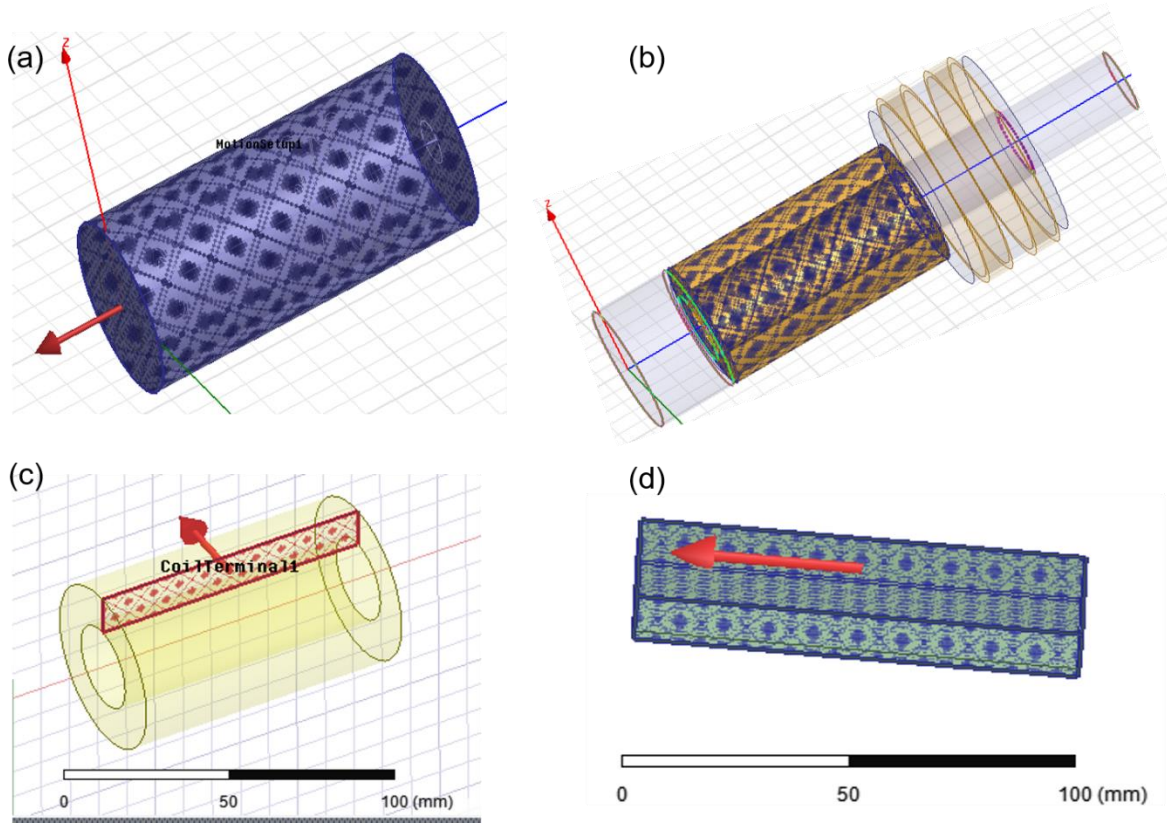

Figure 4.2 : Boundary conditions- Boundary conditions- (a) Rotational motion (b) Insulating boundary condition (c) Coil terminals (d) Axial transient motion

4.4.1 Meshing

In order to provide an efficient and precise solution in 3D the meshing operation was performed using the Ansoft Maxwell software. The mesh model of the electromagnet and workpiece is represented in figure 4.3. The grid size was chosen depending on the accuracy and convergent time. Research using a different grid was conducted to determine the optimal element number. Based on the output consistency, the optimal number of elements was found. However, to account for geometrical complications and increase the accuracy of the solution, numerical simulations employed a tetrahedron with the field approximated across it as a second-order basis function. An adaptive setup solution strategy was used to arrive at the final solution with 25 % mesh refinement per pass. To achieve the final solution, a total of 20 iterations steps were performed and the 541820 tetrahedral elements were generated.

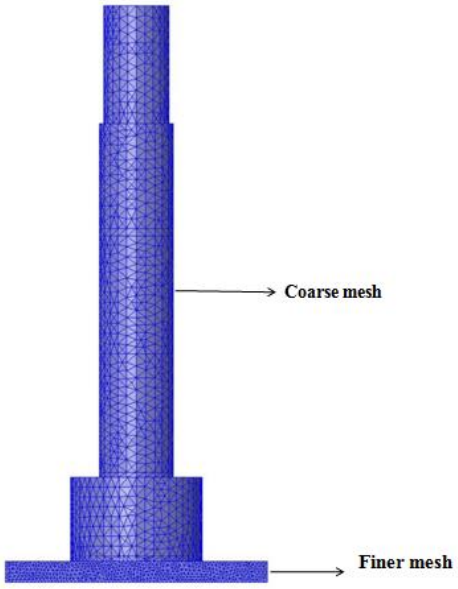

Figure 4.3: Mesh model of workpiece and electromagnet

The magnetic flux density distribution over the electromagnet and workpiece is shown in Figure 4.4. Figure 4.4 (a) shows the magnetic flux maximum of 3 Tesla at the operating conditions of input voltage 45 V, RPM 750, and machining gap of 2.5 mm. Also, it represents the variation of magnetic flux along with the length of the electromagnet. It is observed that at the centre part magnetic flux is maximum because the centre part on which winding is done due to this it is the source of a magnetic field. The variation of magnetic flux density on the workpiece as illustrated in Figure 4.4 (b). The maximum magnetic flux distributed on the workpiece surface is 2 Tesla at a similar condition of an electromagnet. The maximum magnetic flux is obtained on the circumference of the electromagnet and it is reducing away from the electromagnet due to weaker magnetic field lines.

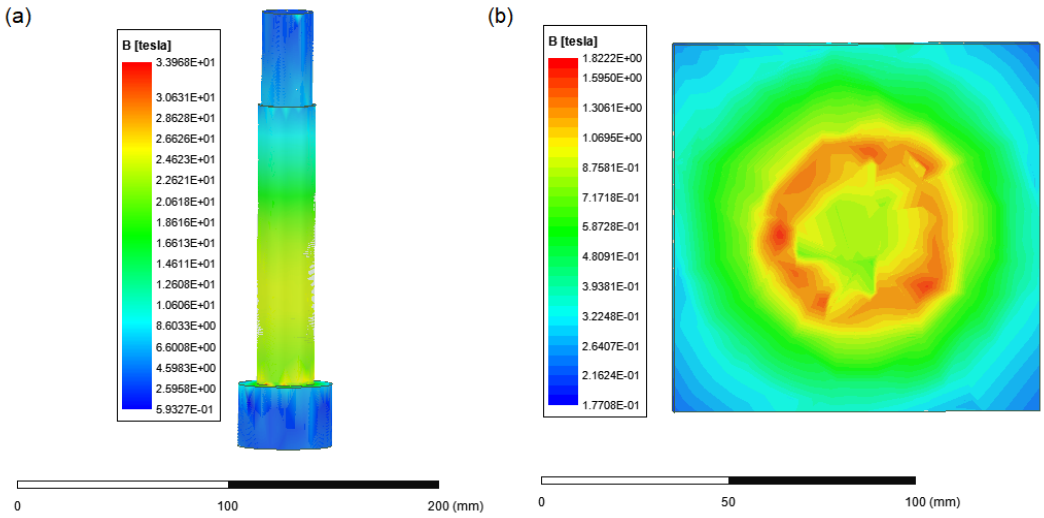

Figure 4.4 : Magnetic flux density distributions along the length of the electromagnet

The direction of magnetic field lines is represented in Figure 4.5. From the figure, the magnet-filed lines are passing along the axis of the electromagnet within the winding. Also, at the end of the electromagnet the magnetic field lines are distributed on the workpiece surface.

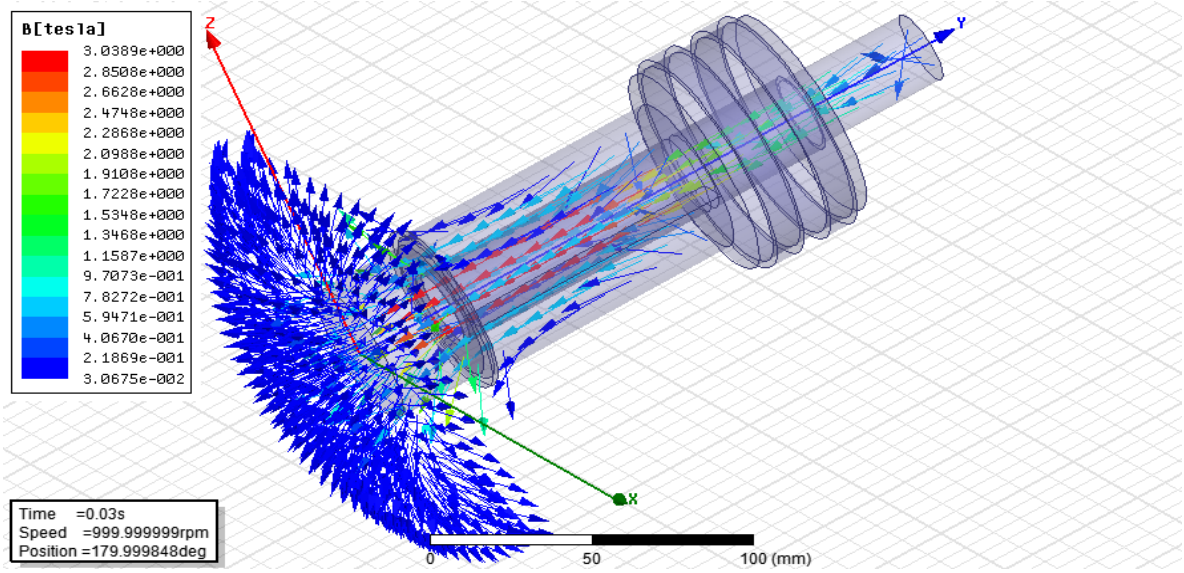

Figure 4.5: Schematic diagram of the magnetic field line of an electromagnet

Figure 4.6 represents the distribution of magnetic flux density over the workpiece surface for the UAMAF process at operating conditions of 45 volts, 750 rpm, 2.5mm gap, and 90 W/m^2 power intensity. The magnetic flux density is maximum at the centre of the workpiece and it is reducing while moving away from the FMAB due to reducing the strength of the magnetic field lines.

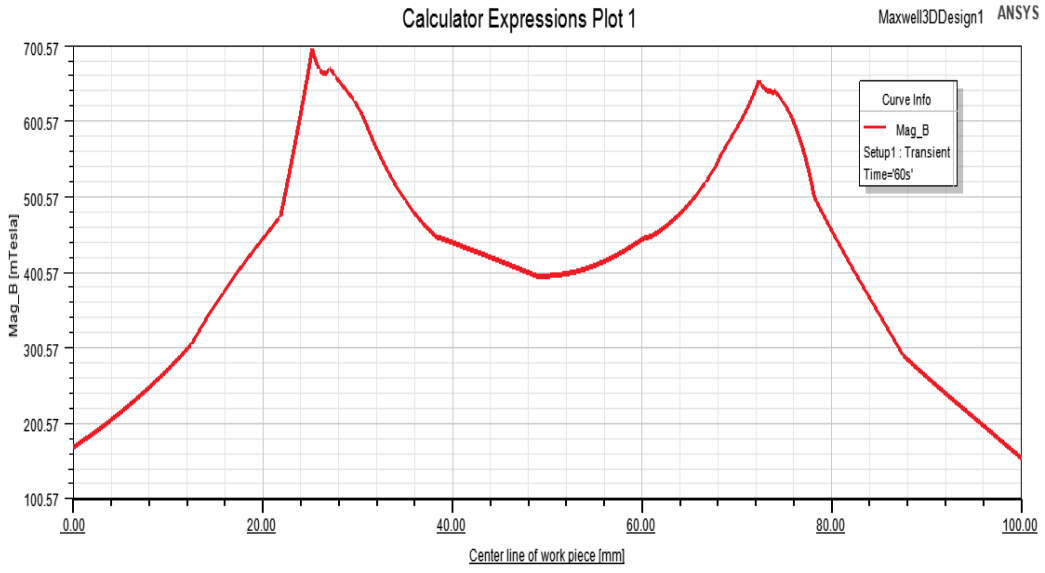

Figure 4.6: Magnetic flux density distributions over the workpiece surface (UAMAF)

4.5 Understanding the simulation results

In MAF and UAMAF processes, the force distribution during processing were observed in figure 4.7 (a) and (b) that there was variation in the magnitude of the cutting force during finishing time. In the MAF process there is only one velocity which is the rotational speed. That is why the cutting force was constant, but in UAMAF process due to ultrasonic vibration, the relative velocity of abrasive with respect to workpiece and there was variation with respect to finishing time as a result of variation in the cutting forces.

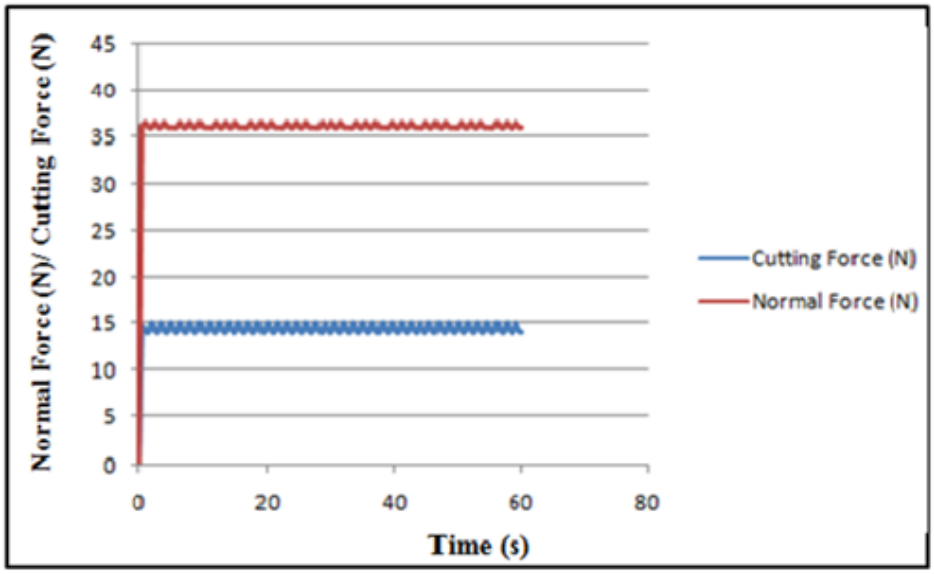

(a)

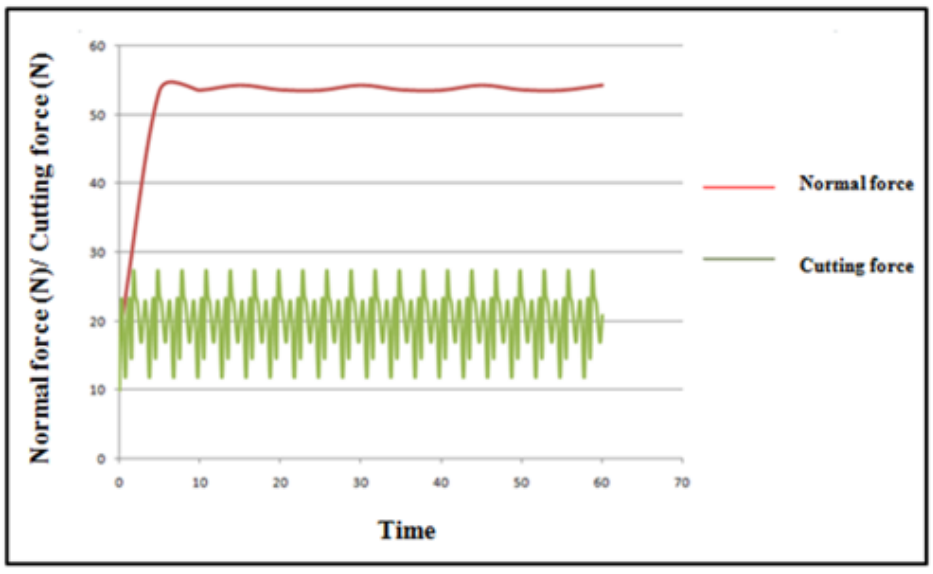

(b)

Figure 4.7: Variation of measured normal force with time (a) MAF and (b) UAMAF

4.6 Summary

In the context of MAF research, this chapter examines the notion of UAMAF. An axial direction was used to apply high-frequency ultrasonic vibrations to the workpiece. Software called ANSYS Maxwell was used to conduct the simulation studies for the UAMAF process. It is employed to examine how varying levels of process parameters such as power intensity, voltage, speed, and working gap affect the magnetic flux density, normal force, and cutting forces. It has been theoretically and computationally examined how micro abrasives interact with workpiece asperities.

5 FINISHING OF HASTELLOY C- 276 USING MAF PROCESS

5.1 Introduction

There is no particular profile limitation for finishing the Magnetic abrasive finishing (MAF) process. However, suitable fixtures are required for complex surface finishing and proper control of the magnetic flux density is required. The present chapter discusses the experimental investigation of Hastelloy C-276. Initial experiments were conducted on low-strength material mild steel (MS) and medium strength material aluminium 2024 alloy (Al 2024). Mild steel (MS) is the most structural magnetic material used for engineering applications after stainless steel Al 2024 is a heat-treatable aluminium alloy with copper as the primary alloying element. Due to its high strength and fatigue resistance, 2024 is widely used in aircraft structures in wing and fuselage structures [69]. The experiments are conducted using in situ developed MAF on a vertical milling machine. For MS and Al 2024 alloy the full factorial experiments were conducted with process parameters wt.% of abrasives, voltage and rotational speed of the electromagnet to evaluate the process response such as surface finish improvement (%ΔR_a). Further, the experiments were carried out on Hastelloy C-276 using box Behnken design of the RSM technique. To identify the factors that have the greatest influence on a material's surface quality, analysis of variances (ANOVA) was carried out using the Minitab 17 software. Also, a comparative study on the surface morphology of both materials was recorded using scanning electron microscopy (SEM) and surface roughness measurement.

5.2 Selection of process parameters

Preliminary experiments were conducted before the main experimentation process to identify the parameter levels and ranges. The experimental setup was set on a vertical milling machine in which the electromagnet is mounted in place of the tool. The experiments are conducted so that one parameter is varied and keeps all others at constant values. Experiments were conducted for the selected magnetic and nonmagnetic materials using different process variables along with ranges listed in Tables 5.1 and 5.2. The experimentation aimed to study the influence of process parameters on the surface characteristics of magnetic and nonmagnetic materials.

Table 5.1: Experimental conditions for MS plate

Percentage of Abrasives (C_1) (%)	Speed of electromagnet (C_2) (rpm)	Voltage (C_3) (V)
20	180	30
25	350	40
30	500	50

Table 5.2: Experimental conditions for Al 2024 alloy

Percentage of abrasives (C_1) (%)	Speed of electromagnet (C_2) (rpm)	Voltage (C_3) (V)
20	1000	30
25	1400	40
30	2100	50

Table 5.3: Experimental conditions for Hastelloy C-276

SiC Weight % (%wt.) (C_1)	Voltage (V) (C_2)	Speed of electromagnet (rpm) (C_3)	Working Gap (mm) (C_4)
20	35	500	2
25	45	750	2.5
30	55	1000	3

For the experiment, five samples were used, and the result was determined by averaging the results. Experiments were successfully conducted on in situ developed MAF process and $\%\Delta R_a$, $\%\Delta R_z$, $\%\Delta R_t$ and $\%\Delta R_q$ values were measured from the finished surfaces. The experimental responses are listed in Tables 5.4 and 5.5 for MS and Al 2024 respectively. The percentage improvement of the surface texture parameters was calculated from equation 1 [76]. The experimental responses are listed in Table 5.6. After grinding, the surface finish of the workpiece was measured by considering the average of four observations at different locations and at the same locations, roughness values were calculated after the MAF process.

$$\%\,\Delta R_i = \frac{Initial\,R_i - Final\,R_i}{Initial\,R_i} * 100 \qquad \textit{Equation 5-1}$$

Table 5.4: Experimental results of MS

S. No	C_1 (%)	C_2 (RPM)	C_3 (V)	% ΔR_a	% ΔR_z	% ΔR_t	% ΔR_q
1	20	180	30	20.50	17.00	14.50	14.00
2	20	180	40	21.80	17.50	15.60	15.25
3	20	180	50	26.45	22.65	20.25	19.50
4	20	350	30	26.45	23.25	21.50	20.75
5	20	350	40	45.65	42.50	35.00	34.00
6	20	350	50	48.50	45.00	37.00	35.75
7	20	500	30	63.25	46.25	39.65	38.50
8	20	500	40	65.50	56.75	48.50	47.65
9	20	500	50	77.75	71.65	55.75	55.00
10	25	180	30	22.65	19.00	17.25	16.50
11	25	180	40	24.65	21.50	18.00	17.25
12	25	180	50	28.50	24.50	22.50	21.65
13	25	350	30	29.45	26.00	23.65	22.75
14	25	350	40	48.50	44.50	38.00	37.00
15	25	350	50	51.65	47.50	40.25	39.75
16	25	500	30	65.25	48.65	42.45	41.65
17	25	500	40	67.65	59.50	50.65	49.50
18	25	500	50	79.50	74.25	58.50	57.50
19	30	180	30	24.50	20.50	20.25	19.50
20	30	180	40	28.65	24.65	21.65	21.00
21	30	180	50	30.25	26.45	25.65	24.75
22	30	350	30	34.50	32.50	27.50	26.65
23	30	350	40	51.75	47.75	41.50	40.50
24	30	350	50	55.45	52.50	44.75	44.00
25	30	500	30	66.65	55.65	48.25	47.65
26	30	500	40	69.25	66.25	56.50	56.25
27	30	500	50	83.00	76.20	65.50	65.00

From Table 5.4, 27th treatment was observed to be the best among the values reported in all the experiments for MS $\%\Delta R_a = 83$, $\%\Delta R_z = 65$, $\%\Delta R_t = 65.5$ and $\%\Delta R_q = 76.20$

improvement of surface texture. The input parameters at maximum response values are 30% abrasive wt. percentage, 500rpm electromagnet speed, and 50V voltage.

Table 5.5: Experimental results of Al 2024 alloy

S. No	C_1 (%)	C_2 (RPM)	C_3 (V)	% ΔR_a	% ΔR_z	% ΔR_t	% ΔR_q
1	20	1000	30	18.00	12.50	13.25	15.65
2	20	1000	40	21.50	14.50	15.00	18.50
3	20	1000	50	33.50	22.50	23.50	30.50
4	20	1400	30	21.25	15.00	15.75	18.25
5	20	1400	40	25.75	16.65	17.25	22.75
6	20	1400	50	40.65	30.75	32.00	37.50
7	20	2100	30	32.25	24.50	25.65	29.00
8	20	2100	40	42.65	32.00	33.50	38.50
9	20	2100	50	54.00	41.25	42.50	49.00
10	25	1000	30	21.65	15.65	16.75	18.50
11	25	1000	40	24.65	16.50	17.50	21.65
12	25	1000	50	35.75	26.00	27.25	32.75
13	25	1400	30	24.75	17.00	18.00	21.75
14	25	1400	40	29.50	22.50	23.75	26.50
15	25	1400	50	45.65	35.75	37.00	42.65
16	25	2100	30	37.00	28.65	29.50	34.00
17	25	2100	40	48.75	38.00	39.25	45.75
18	25	2100	50	58.00	42.50	43.75	51.50
19	30	1000	30	24.50	16.25	17.00	21.50
20	30	1000	40	29.25	20.75	21.50	26.25
21	30	1000	50	39.50	29.50	31.75	36.50
22	30	1400	30	27.65	18.75	19.50	24.50
23	30	1400	40	37.25	28.65	29.75	34.25
24	30	1400	50	48.50	36.00	37.50	43.65
25	30	2100	30	40.75	30.45	31.00	37.50
26	30	2100	40	54.50	43.00	44.50	48.50
27	30	2100	50	65.00	50.00	51.00	55.00

From Table 5.5, 27th treatment is observed to be the best of all the experiments for Al 2024 alloy has $\%\Delta R_a$ = 65, $\%\Delta R_z$ =50, $\%\Delta R_t$ = 51 and $\%\Delta R_q$ = 55 improvements of surface texture. The input parameters at maximum response values are 30% abrasive wt. percentage, 2100rpm electromagnet speed, and 50V voltage.

Table 5.6: Experimental details of Hastelloy C-276 after MAF process

S. No	C_1 (Wt. %)	C_2 (V)	C_3 (rpm)	C_4 (W/m^2)	ΔR_a (%)	MR (mg)	F_N (N)	F_T (N)
1	20	45	500	2.5	30.09	12.11	33.92	18.83
2	25	45	500	2	32.65	13.13	36.77	19.57
3	25	45	500	3	27.52	11.81	33.06	17.75
4	25	35	500	2.5	24.38	10.41	29.16	20.38
5	25	55	500	2.5	32.71	13.97	39.13	17.89
6	30	45	500	2.5	33.36	12.77	35.75	18.17
7	20	35	750	2.5	25.45	9.56	26.78	16.35
8	20	55	750	2.5	41.65	12.73	35.65	20.55
9	20	45	750	2	35.78	11.60	32.49	16.87
10	20	45	750	3	35.32	11.01	30.82	18.17
11	25	35	750	2	29.44	10.68	28.51	20.51
12	25	55	750	2	46.10	13.05	36.53	21.35
13	25	35	750	3	26.66	9.83	27.51	15.75
14	25	55	750	3	43.32	12.10	33.89	20.38
15	25	45	750	2.5	37.25	11.03	30.89	17.43
16	25	45	750	2.5	37.25	11.03	30.89	21.91
17	30	35	750	2.5	33.25	10.24	28.68	20.97
18	30	55	750	2.5	51.37	13.70	38.37	21.77
19	30	45	750	2	44.30	12.11	33.92	17.75
20	30	45	750	3	41.04	11.43	32.01	19.57
21	20	45	1000	2.5	39.65	9.90	27.73	20.55
22	25	45	1000	2	44.51	10.86	30.42	20.16
23	25	45	1000	3	41.73	9.46	27.98	17.89
24	25	35	1000	2.5	30.26	9.33	26.13	18.37
25	30	55	1000	2	75.5	14.15	31.23	20.38
26	30	45	1000	2.5	50.51	10.59	29.65	21.35

The optimum process parameters are 30% abrasives, 1000 rpm rotating speed, 2 mm working gap, and 55V voltage.

5.3 Regression Equations and ANOVA analysis

5.3.1 Regression analysis

Regression analysis gives the relationship between the responses and input factors (variables). Eq.3 represents a sample regression equation and Eq.4 represents a simple linear regression equation in which the relationship of response *Y* and input factors such as A, B, C, and D [77]. Therefore, the analysis may include unknown regression parameters, for example, β_0, β_1, β_2, β_3, and β_4. For example

$Y = F(C, B)$ *Equation 5-2*

Equation 2 represents the linear type regression:

$Y = B_0 + B_1 A + B_2 B + B_3 C + B_3 D + \mathcal{E}$ *Equation 5-3*

Ɛ = error term of the regression equation

Based on regression analysis the quadratic fitted models are obtained for $\%\Delta R_a$ of MS and Al 2024 alloy and Hastelloy C-276 are represented in EQs. 5.4 to 5.9 and 6 respectively.

$$\%\,\Delta \boldsymbol{R_a} = -6.1 + 0.10\,C1 - 0.0723\,C2 + 0.73\,C3 + 0.0094\,C1*C1 + 0.000234\,C2*C2 - 0.0070\,C3*C3 - 0.00020\,C1*C2 + 0.0009\,C1*C3 + 0.001506\,C2*C3 \quad \textit{Equation 5-4}$$

$$\%\,\Delta \boldsymbol{R_a} = 39.7 - 0.42\,C1 - 0.02005\,C2 - 1.470\,C3 + 0.0112\,C1*C1 + 0.000006\,C2*C2 + 0.02264\,C3*C3 + 0.000328\,C1*C2 + 0.0057\,C1*C3 + 0.000317\,C2*C3 \quad \textit{Equation 5-5}$$

$$\%\,\Delta \boldsymbol{R_a} = 73.7 - 3.606\,C1 + 0.244\,C2 - 0.0822\,C3 - 0.91\,C4 + 0.0700\,C1*C1 - 0.00991\,C2*C2 - 0.000010\,C3*C3 + 0.31\,C4*C4 + 0.00959\,C1*C2 + 0.001519\,C1*C3 - 0.281\,C1*C4 + 0.001666\,C2*C3 + 0.0000\,C2*C4 + 0.00470\,C3*C4 \quad \textit{Equation 5-6}$$

$$\boldsymbol{MR} = 20.4 - 0.596\,C1 + 0.081\,C2 + 0.00319\,C3 - 4.83\,C4 + 0.01225\,C1*C1 + 0.00181\,C2*C2 + 0.000000\,C3*C3 + 0.878\,C4*C4 + 0.00145\,C1*C2 + 0.000007\,C1*C3 - 0.0085\,C1*C4 - 0.000174\,C2*C3 - 0.0045\,C2*C4 - 0.00015\,C3*C4 \quad \textit{Equation 5-7}$$

$$F_N = 50.8 - 1.660\,C1 + 0.574\,C2 - 0.0024\,C3 - 12.31\,C4 + 0.0341\,C1*C1 + 0.00330\,C2*C2 + 0.000004\,C3*C3 + 2.49\,C4*C4 + 0.00405\,C1*C2 + 0.000019\,C1*C3 - 0.024\,C1*C4 - 0.000488\,C2*C3 - 0.0821\,C2*C4 + 0.00255\,C3*C4 \quad \text{Equation 5-8}$$

$$F_T = -1.54 + 0.296\,C1 + 0.275\,C2 + 0.00041\,C3 - 1.02\,C4 - 0.00245\,C1*C1 - 0.00078\,C2*C2 + 0.000005\,C3*C3 + 0.770\,C4*C4 - 0.00166\,C1*C2 + 0.000166\,C1*C3 - 0.0600\,C1*C4 - 0.000098\,C2*C3 + 0.0130\,C2*C4 - 0.001060\,C3*C4 \quad \text{Equation 5-9}$$

5.3.2 Statistical Analysis

ANOVA analysis was performed using Minitab 17 software for both MS and Al 2024 alloy to identify the effect of input variables on responses represented in (Tables 5.5 and 5.6).

Table 5.7: Analysis of variances (ANOVA) for MS

Response	Source	D O F	Adj. SS	Adj. MS	F- Ratio	P-Value
% ΔR_a	C_1	2	180.2	90.11	3.97	0.001
	C_2	2	7669.9	3834.97	169.09	0.001
	C_3	2	1451.9	725.94	32.01	0.001
	Error	20	453.6	22.68		
	Total	26	9755.6			
	Model Summary	S	R- Sq.	Adj R- Sq.	Pred. R- Sq.	
		3.15	0.9971	0.9886	0.9166	

Based on Table 5.7 The influential parameters were decided based on F-value and P-value at confidence level of 95% ($P < 0.05$). The most efficient input parameters on the responses are C_2, C_3 and C_1.

Table 5.8: Analysis of variances (ANOVA) for Al 2024

Response	Source	D O F	Adj. SS	Adj. MS	F- Ratio	P-Value
% ΔR_a	C_1	2	332.86	166.43	33.36	0.001
	C_2	2	2009.63	1004.81	201.43	0.001
	C_3	2	1688.67	844.34	169.26	0.001
	Error	20	99.77	4.99		
	Total	26	4130.93			
	Model Summary	S	R- Sq.	Adj R- Sq.	Pred. R- Sq.	
		2.23	0.9875	0.9816	0.9560	

Based on Table 5.8 the parameters that exercise maximum impact were decided based on F-value and P-value at a confidence level of 95% ($P < 0.05$). The most efficient input parameters on the response are C_2, C_3 and C1.

Table 5.9: Analysis of variances for Hastelloy C-276

Response	**Source**	**D O F**	**Adj. SS**	**Adj. MS**	**F- Ratio**	**P-Value**
$\% \Delta R_a$	C_1	1	175.47	175.47	383.56	0.001
	C_2	1	849.38	849.38	1856.69	0.000
	C_3	1	549.37	549.37	1200.89	0.000
	C_4	1	24.60	24.60	53.79	0.003
	Error	11	5.03	0.503		
	Total	25	1727.64			
	Model Summary	S	R- Sq.	Adj. R-Sq.	Pred. R-Sq.	
		0.6764	0.9971	0.9934	0.9832	
MR	C_1	1	1.28	1.28	15.30	0.004
	C_2	1	23.11	23.11	275.25	0.001
	C_3	1	13.87	13.87	165.20	0.001
	C_4	1	2.80	2.80	33.39	0.002
	Error	11	0.9239	0.0840		
	Total	25	43.37			
	Model Summary	S	R- Sq.	Adj. R-Sq.	Pred. R-Sq.	
		0.2898	0.9787	0.9516	0.8773	
F_N	C_1	1	10.07	10.07	20.27	0.004
	C_2	1	192.23	192.23	386.76	0.001
	C_3	1	99.98	99.98	201.16	0.001
	C_4	1	14.87	14.87	29.93	0.003
	Error	11	5.467	0.497		
	Total	25	333.64			
	Model Summary	S	R- Sq.	Adj. R-Sq.	Pred. R-Sq.	
		0.7049	0.9836	0.9628	0.9056	

F_T	C_1	1	1.614	1.614	28.55	0.001
	C_2	1	17.98	17.98	318.12	0.001
	C_3	1	13.95	13.95	246.80	0.000
	C_4	1	3.75	3.75		0.005
	Error	11	0.6219	0.0565		
	Total	25	39.38			
	Model Summary	S	R- Sq.	Adj. R-Sq.	Pred. R-Sq.	
		0.2378	0.9842	0.9641	0.9091	

The influential parameters were decided based on F-value and P-value at confidence level of 95% ($P < 0.05$). The most efficient input parameters on the responses are C_2, C_3, C_4 and C_1.

5.4 Influence of process parameters

5.4.1 Influence of voltage on $\%\Delta R_a$, MR (mg), F_N (N) and F_T (N)

Figure 5.1 illustrates the impact of abrasives' weight percentage on variations in surface finish, material removal, normal force, and tangential force at various voltage levels in the MAF process. From Figure 5.1(a), it is observed that the $\%\Delta R_a$ value increased with the % of abrasives. This is because of increase in the amount of abrasives percentage in FMAB increased the number of cutting edges in the cutting action that removes material in the form of microchips. Additionally, a rise in abrasive % strengthens the bonds between magnetic abrasives chains, enhancing cutting forces in both the normal and tangential directions. which is described in figures 5.1(c) and 5.1(d). Due to an increase in forces, more material removal takes at a higher abrasives percentage which is observed in Figure 5.1(b). From Figure 5.1(a), it is observed that an increase in $\%\Delta R_a$ is observed with an increase in voltage. This is because of higher magnetic flux at higher voltage and forms a strong bonding between abrasives and magnetic particles leading to a better finish at higher voltages. From figure 5.1(b) it is observed that an increase in MR is observed with an increase in voltage. This is because of higher bond strength in FMAB at a higher voltage with remove higher amount of material at the same time compared to a lower voltage. MR, $F_{N,}$ and F_T proportionally as the increase in voltage at different levels. From Figures 5.1(c) and 5.1(d), it is observed that an increase in forces with an increase in voltage. It is because the voltage increases the magnetic flux density and the strength of the FMAB. Due to the high strength of

FMAB, the effect of normal force increases causing a strong impact of abrasive chains on the workpiece also the shear force increases due to the centrifugal action of the electromagnet. Moreover, this increase in finishing forces imparts rubbing and ploughing action between the electromagnet and workpiece resulting in a high amount of force in both normal and tangential directions.

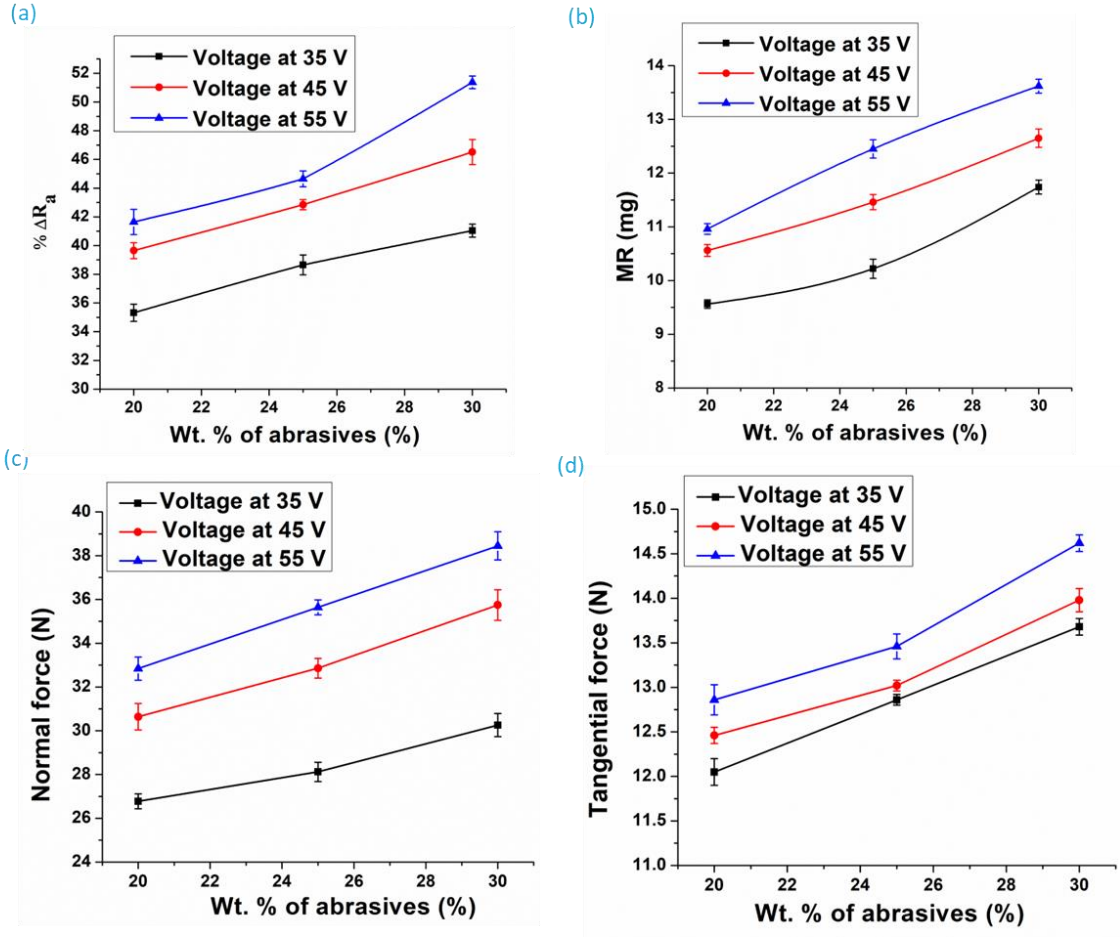

Figure 5.1: Influence of voltage on %ΔR_a, MR, F_N and F_T

5.4.2 Influence of speed on %ΔR_a, MR (mg), F_N (N) and F_T (N)

From Figure 5.2(a) it is observed that an increase in % ΔR_a is observed with a increase in speed. As the speed rises, the frequency of the abrasives hitting the workpiece surface is increases. Along with this the effect of circumferential force is higher at high speeds supports the better surface finish. From Figure 5.2(b), it is observed that a decrease in MR is observed with an increase in the speed of the electromagnet. This is because at higher speeds, the indentation force on the workpiece was very less because of the centrifugal action of FMAB between the electromagnet and the workpiece. From Figure 5.2(c), F_N proportionally reduces with an increase in the rotational speed of the electromagnet at different levels. This is at high speeds the strength of magnetic abrasives chains is reducing, also the impact force of

abrasives on the workpiece is reducing. Figure 5.2(d) shows an increase in tangential force with an increase in rotational speed. An increase in speed increases the centrifugal action of the electromagnet. Moreover, this increase in finishing force imparts rubbing and ploughing action between electromagnet and workpiece, resulting in a high amount of force in circumferential directions.

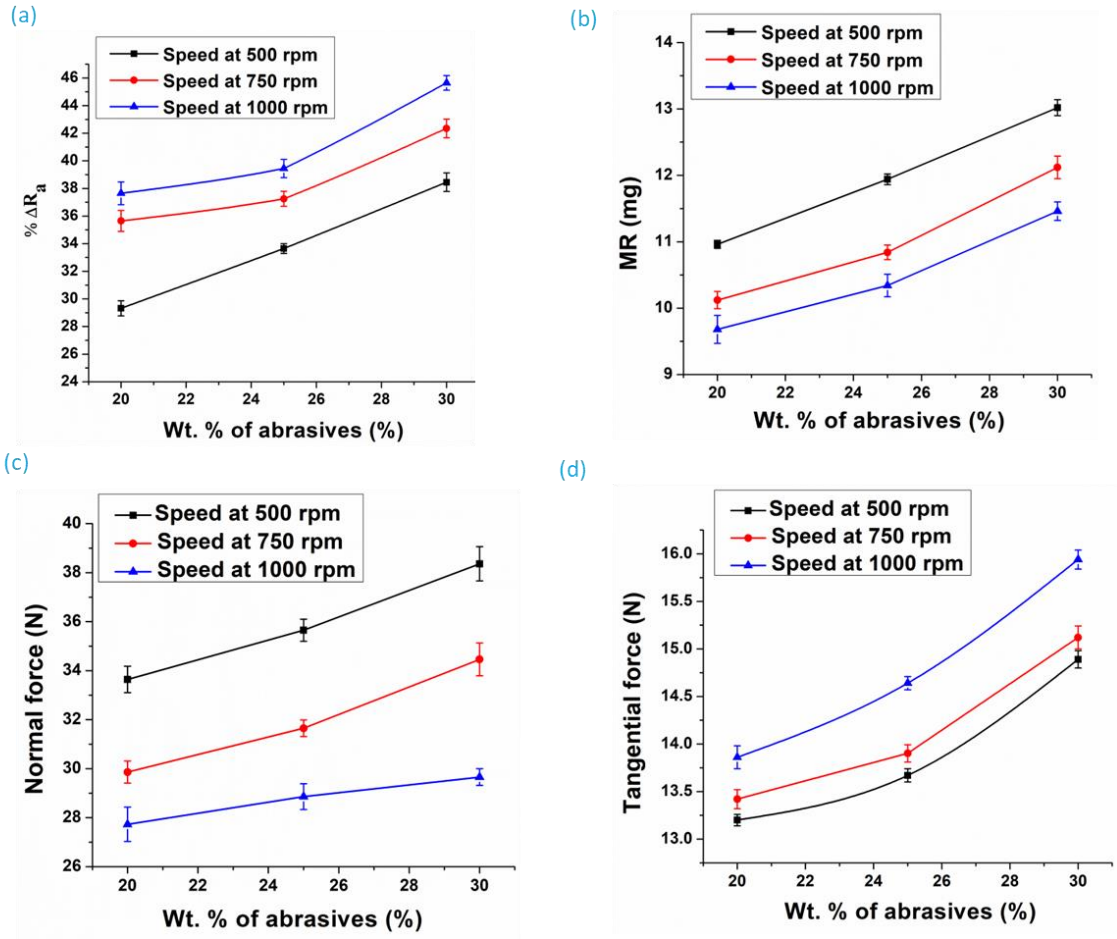

Figure 5.2: Influence of speed on $\%\Delta R_a$, MR, F_N and F_T

5.4.3 Effect of working gap on $\%\Delta R_a$, MR (mg), F_N (N) and F_T (N)

Figure 5.3(a) shows that the $\%\Delta R_a$ increases with decrease in working gap. As the working gap is at a low condition. Due to the high strength of the magnetic abrasive chains, which increased the impact of the abrasives on the workpiece surface, the number of abrasives in FMAB was growing at the lower working gap, which resulted in the improvement of removal of material and surface finish. As the working gap further increases the gap between the workpiece and electromagnet increases also the strength of abrasives reduces. A similar condition is observed for MR also as shown in Figure 5.3(b). Figures 5.3(c) and 5.3(d) showed that as the working gap increases, the F_N and F_T forces increase with decrease in working gap. This is because at a low working gap the number of active

abrasives is more, due to this the normal indentation force and tangential force of these abrasives are more. The number of active abrasives rises, their impact on the workpiece grows, and both normal and shear action are used to remove material at the lower working gap.

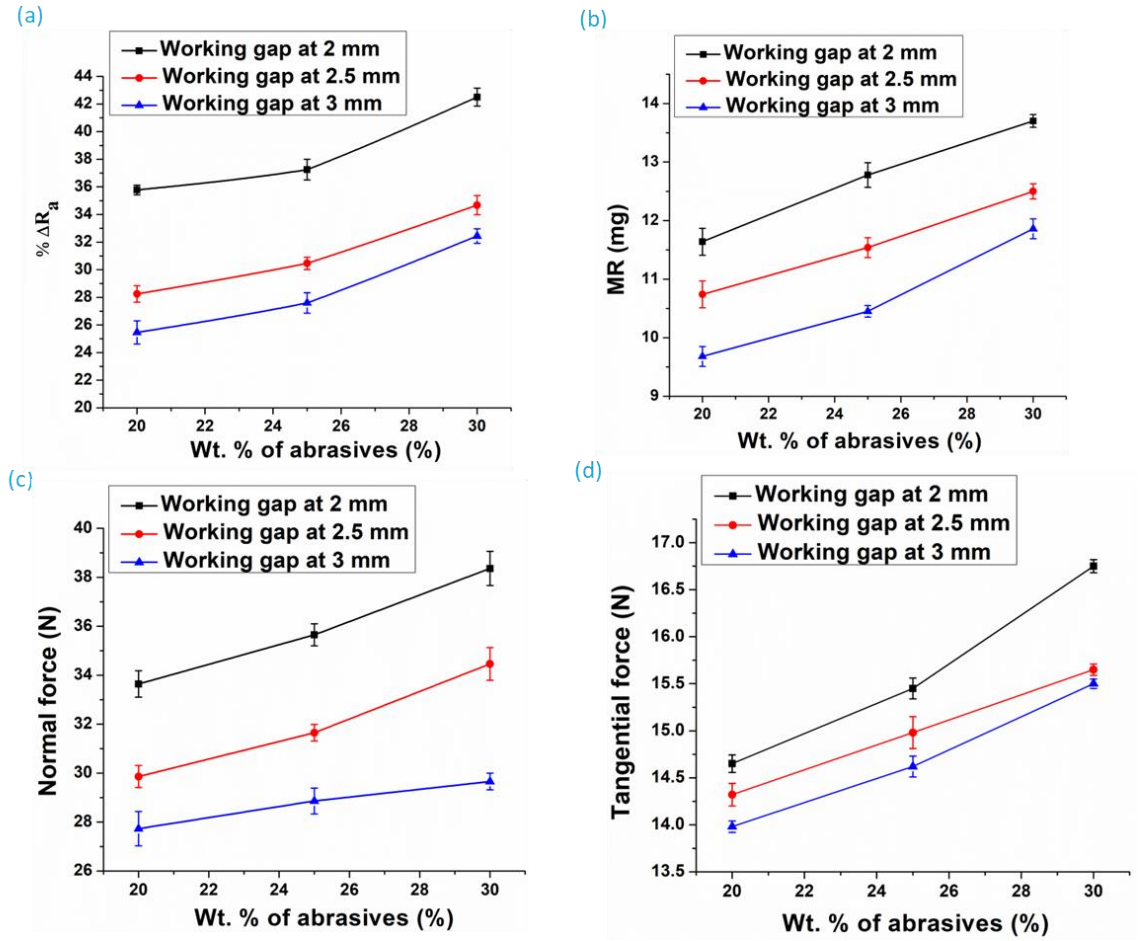

Figure 5.3 : Influence of working gap on $\%\Delta R_a$, MR, F_N and F_T

5.4.4 Surface topography and surface profiles

The surface morphology of Hastelloy before and after MAF finishing are represented with SEM images in Figure 5.4. Figure 5.4(a) before MAF experimentation, the workpiece was surface grinded and the grinding marks and pit holes are observed due to the high cutting forces of the grinding operation. Figure 5.4(b) represents the surface morphology after MAF finishing and the surface texture illustrates that there are no further grinding marks and irregularities. The abrasive cutting marks are seen on the finished surface due to random movement, and no lay direction is observed in particular [78].

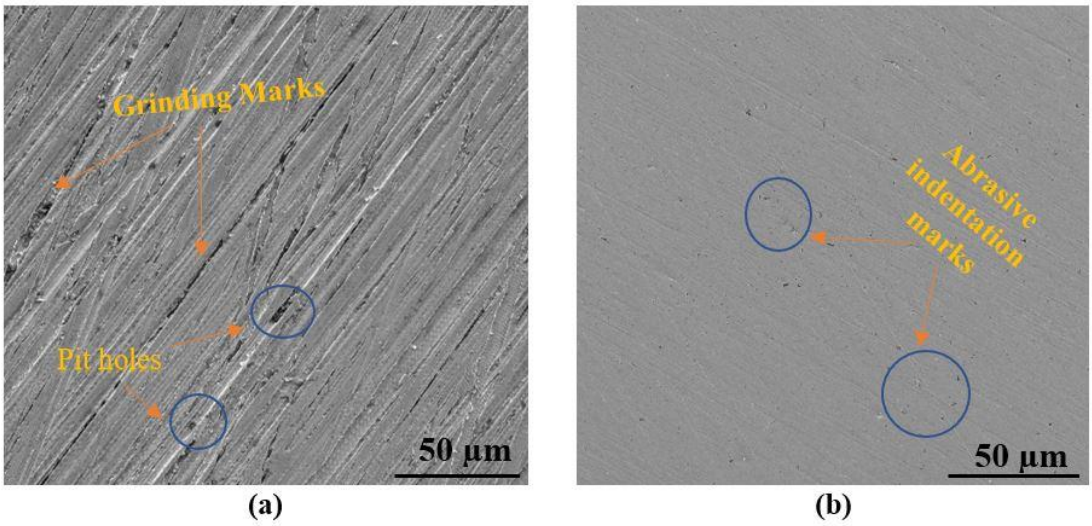

Figure 5.4: - SEM images (a) Surface grinded (b) MAF finished process

The surface finish profiles are measured from Suftronic S-100 series surface roughness tester. Prior to MAF process, the MS and Al 2024 plates were surface grounded. Figure 5.5 shows the initial average R_a value observed as 0.160µm and the final average R_a value obtained is 0.0272µm for MS plate. Figure 5.6 shows the initial average R_a value of 0.160µm and the final average R_a value is 0.056µm for Al 2024 alloy. The $\%\Delta R_a$ improvement in case of MS plate is 83% whereas for Al 2024 it is 65%.

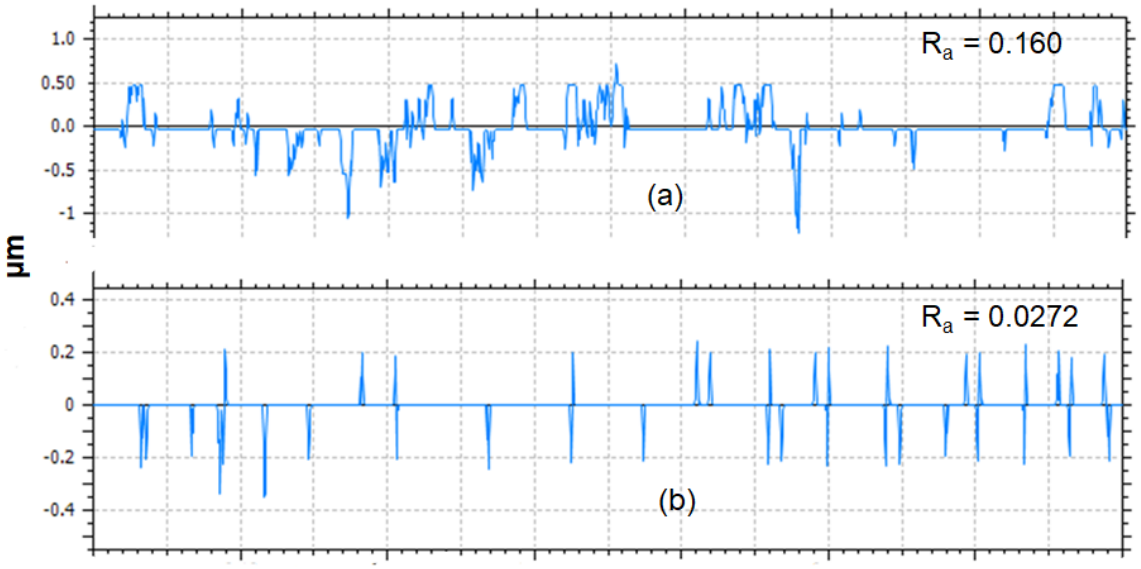

Figure 5.5: MS plate R_a values (a) before and (b) after MAF process

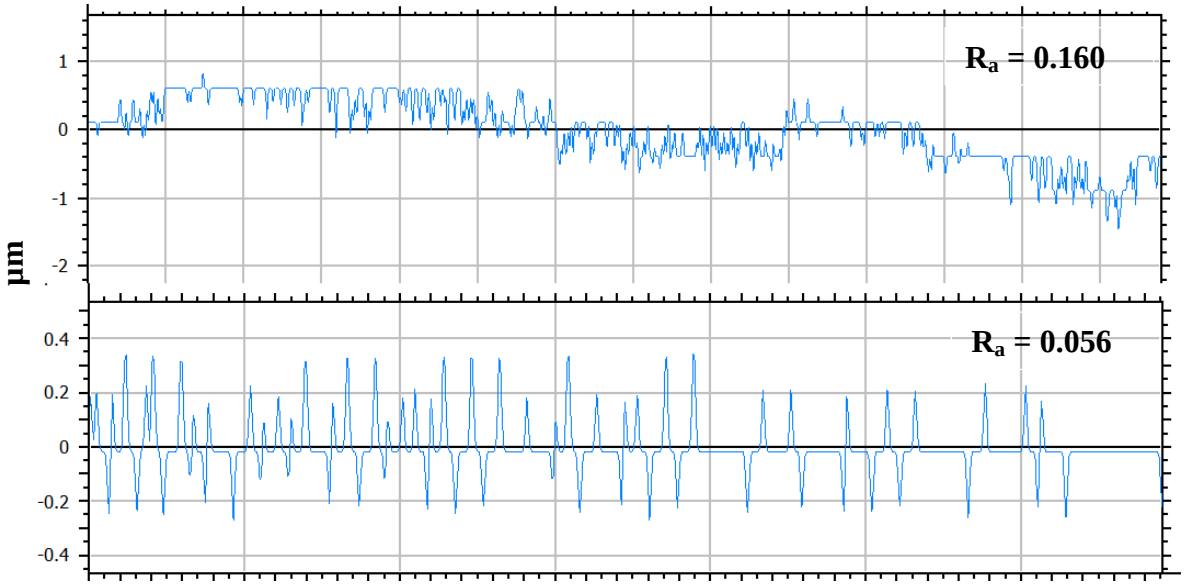

Figure 5.6: Al 2024 alloy plate R_a values (a) before and (b) after MAF process

The surface profiles of the Hastelloy C-276 workpiece before and after finishing at optimum process parameters are shown in Figure 5.7. The workpiece was surface-ground and kept at a constant surface roughness of 1.3 µm as illustrated in Figure 5.7(a) before the experiment. After experimentation at optimum process parameters, the surface roughness of 0.325 µm is achieved in Figure 5.7(b). From the surface profiles, the change in surface roughness after experimentation is 90.4% compared to the initial surface roughness.

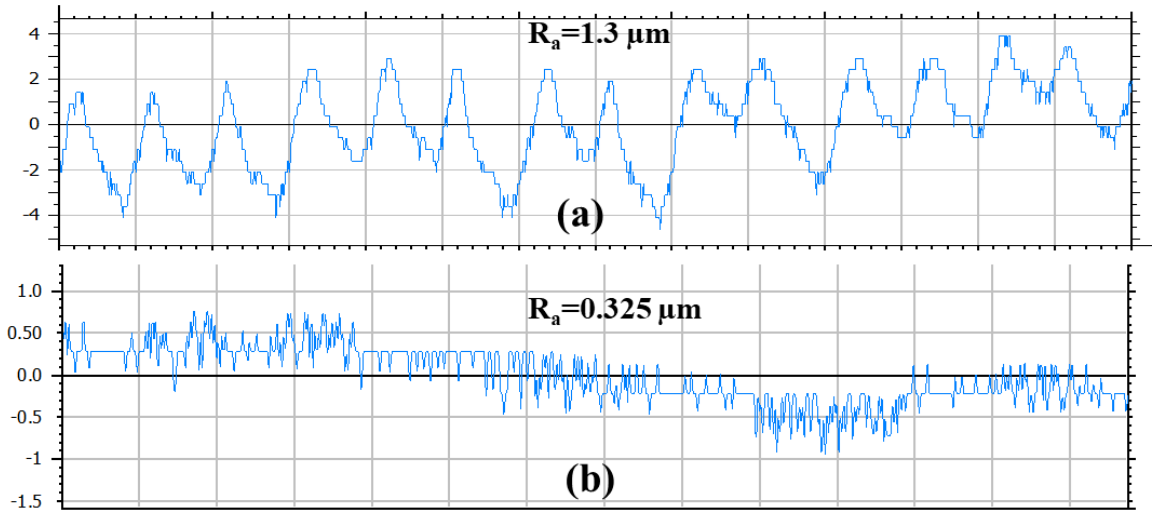

Figure 5.7:- Hastelloy C-276 alloy plate R_a values (a)before and (b) after MAF process

5.5 Summary

In this chapter, the surface texture study of MS, Al 2024 and Hastelloy C-276 was carried out using a laboratory-developed MAF process. The surface finish improvement of MS is better compared to the Al 2024. This is because MS is a magnetic material and the magnetic field generated between the workpiece and tool is strong and the strength of the FMAB is more. Hence, the abrasive chains penetrate the work surface due to strong magnetic field interaction, giving better surface texture values. 2-D surface profiles are used to illustrate the results in terms of responses.

6 FINISHING OF HASTELLOY C-276 USING UAMAF PROCESSES

6.1 Introduction

In industries like aerospace, automobile, and marine, the surface integrity of the machined component is critical because it affects the corrosion and fatigue life. The high hot strength, high temperature resistance, and high corrosion resistance of Hastelloy C-276, a nickel-based superalloy, make it ideal for application in the chemical and petrochemical sectors. The finishing of Hastelloy C-276 in this chapter was accomplished using the UAMAF (ultrasonic-assisted magnetic abrasive finishing) process. The traditional MAF process, which provides axial vibrations to the workpiece at a frequency of (10–30 kHz), has an additional attachment called an ultrasonic horn added as part of the UAMAF process. The responses to changes in the surface finish ($\%\Delta R_a$) and material removal (MR), the normal force (F_N), and the tangential force (F_T) are investigated in this process at various process variables, including power intensity, voltage, speed, weight percentage of abrasives, and working gap. The outcomes under UAMAF are contrasted with the reactions of MAF under comparable experimental circumstances. The Minitab 17 programme was used to do regression and analysis of variances (ANOVA) in order to identify the factors that have the greatest influence on a material's surface quality. UAMAF specimens were given an additional chemical coating by physical vapour deposition that included yttrium acetate and di-ethanolamine. The coating process considers variables including coating quantity, chamber temperature, and etchant weight. Additionally, utilising scanning electron microscopy (SEM) and surface roughness testing, a comparison of the surface morphologies of the two materials was made.

6.2 Selection of process parameters

The finishing was initially carried out using the MAF process. Subsequently, an ultrasonic attachment was attached to the MAF and carried out the finishing operation under identical operating conditions. The input parameters working gap (mm), voltage (v), electromagnet speed (rpm), and abrasive weight (%wt.) were changed at various levels in both procedures. The UAMAF experimented with the amplitude (mm) variable as well. For MAF, the finishing time was 5 minutes, however for UAMAF, it was 2 minutes. The levels of input parameters are represented in Tables 6.1 for UAMAF and Table 6.2 for surface coating processes.

Table 6.1: Process parameters for UAMAF process

SiC Weight % (%wt.) (C_1)	Voltage (V) (C_2)	Speed of electromagnet (rpm) (C_3)	Working Gap (mm) (C_4)	Power intensity (W/m^2) (C_5)
20	35	500	2	80
25	45	750	2.5	90
30	55	1000	3	100

Table 6.2: Process parameters for spray coating process

Etchant weight (gm) C_1	Temperature (°C) C_2	No. of coatings C_3
2	60	5
6	80	15
10	100	25

Five samples were chosen for the experiment, and the result was determined by averaging the findings. Experiments were successfully conducted on in situ developed MAF and UAMAF processes and $\%\Delta R_a$, MR, F_N and F_T values were measured from the finished surfaces. The experimental responses for UAMAF and surface coating processes are listed in Tables 6.3, 6.4, respectively. The percentage improvement of the surface texture parameters was calculated from equation 6.1 [76] and the material removal was based on equation 6.2. After grinding, the surface finish of the workpiece was measured by considering the average of four observations at different locations and at the same locations, roughness values were calculated after the MAF, UAMAF and surface coating process. The responses F_N and F_T which was measured by using a dynamometer setup.

The responses are calculated based on the following equations.

Surface finish improvement (ΔR_a (%)) = $\frac{Intial\ Ra - Final\ Ra}{Intial\ Ra} * 100$ *Equation 6-1*

Material removal (MR (mg)) = (Weight before - Weight after) *Equation 6-2*

Table 6.3: Experimental results after UAMAF process

S. No	C_1 (%)	C_2 (V)	C_3 (rpm)	C_4 (mm)	C_5 (W/m^2)	ΔR_a (%)	MR (mg)	F_N (N)	F_T (N)
1	25	45	500	2	90	48.98	20.86	49.64	18.83
2	25	45	500	3	90	41.28	18.75	44.63	19.57
3	25	45	500	2.5	80	42.98	18.43	43.86	17.75
4	25	45	500	2.5	100	49.28	21.94	52.21	20.38
5	20	45	500	2.5	90	45.14	19.24	45.79	17.89
6	30	45	500	2.5	90	50.04	20.28	48.26	18.17
7	25	35	500	2.5	90	36.56	16.54	39.36	16.35
8	25	55	500	2.5	90	49.05	22.19	52.82	20.55
9	20	35	750	2.5	90	38.18	15.94	37.95	16.87
10	30	35	750	2.5	90	49.88	16.27	38.72	18.17
11	20	55	750	2.5	90	62.48	20.22	48.13	20.51
12	30	55	750	2.5	90	77.04	21.13	50.28	21.35
13	25	35	750	2.5	80	40.17	14.88	35.41	15.75
14	25	55	750	2.5	80	56.25	19.33	46.01	20.38
15	25	35	750	2.5	100	45.83	18.43	43.86	17.43
16	25	55	750	2.5	100	63.83	21.94	52.21	21.91
17	20	45	750	2	90	53.67	18.43	43.86	20.97
18	30	45	750	2	90	66.45	19.24	45.79	21.77
19	20	45	750	3	90	52.98	17.48	41.61	17.75
20	30	45	750	3	90	61.65	18.16	43.21	19.57
21	25	35	750	2	90	44.16	16.17	38.49	20.55
22	25	55	750	2	90	69.38	20.72	49.32	20.16
23	25	35	750	3	90	39.99	15.61	37.14	17.89
24	25	55	750	3	90	64.98	19.22	45.75	18.37
25	25	45	750	2	80	46.88	17.89	42.57	20.38
26	25	45	750	3	80	44.48	17.08	40.64	21.35
27	25	45	750	2	100	60.75	20.72	49.32	17.33
28	25	45	750	3	100	59.78	19.74	46.97	18.23
29	20	45	750	2.5	80	45.38	17.08	40.64	16.37

30	30	45	750	2.5	80	53.48	18.43	43.86	16.74
31	20	45	750	2.5	100	59.48	20.22	48.13	18.69
32	30	45	750	2.5	100	61.88	20.86	49.64	19.95
33	25	45	750	2.5	90	55.88	17.52	41.70	19.46
34	25	45	750	2.5	90	55.88	17.52	41.70	19.46
35	25	45	1000	2	90	66.75	16.69	39.71	20.97
36	25	45	1000	3	90	62.63	16.17	38.49	22.09
37	25	45	1000	2.5	80	63.83	15.46	36.79	19.15
38	25	45	1000	2.5	100	68.40	18.16	43.21	22.06
39	20	45	1000	2.5	90	59.48	15.73	37.43	20.47
40	30	45	1000	2.5	90	75.77	16.82	40.03	21.91
41	25	35	1000	2.5	90	45.38	14.82	35.28	20.05
42	30	55	1000	2	90	82.88	17.71	42.15	22.88

The optimum process parameters are 30% abrasives, a rotational speed of 1000 rpm, a working gap of 2 mm and a voltage of 55V.

Table 6.4: Experimental details of ΔR_a (%) after spray coating process

S. No	C_1 (gm)	C_2 (°C)	C_3	ΔR_a (%)
1	2	60	5	27.68
2	2	60	15	37.8
3	2	60	25	32.5
4	2	80	5	35.65
5	2	80	15	46.8
6	2	80	25	36.7
7	2	100	5	31.6
8	2	100	15	40.56
9	2	100	25	34.5
10	6	60	5	36.5
11	6	60	15	52.4
12	6	60	25	41.8
13	6	80	5	48.6
14	6	80	15	75

15	6	80	25	56.5
16	6	100	5	42.5
17	6	100	15	58.6
18	6	100	25	48.4
19	10	60	5	32.8
20	10	60	15	46.5
21	10	60	25	35.6
22	10	80	5	41.6
23	10	80	15	58.2
24	10	80	25	45.6
25	10	100	5	37.2
26	10	100	15	51.6
27	10	100	25	41.5

6.3 Regression equations and ANOVA analysis

6.3.1 Regression analysis

The regression equations for Hastelloy C-276 after MAF, UAMAF and surface coating processes are represented in equations 6.4 to 6.12.

UAMAF Process

$$\%\Delta R_a = 146 - 2.07\,C1 + 0.11\,C2 - 0.1339\,C3 - 0.7\,C4 + 4.59\,C5 + 0.0861\,C1*C1 + 0.000002\,C3*C3 - 0.79\,C4*C4 - 0.0204\,C5*C5 + 0.0143\,C1*C2 + 0.00228\,C1*C3 - 0.411\,C1*C4 - 0.0285\,C1*C5 + 0.002501\,C2*C3 - 0.012\,C2 + 0.0048\,C2*C5 + 0.0072\,C3*C4 - 0.000173\,C3*C5 + 0.071\,C4*C5$$

Equation 6-3

$$MR = 75.5 - 0.811\,C1 + 0.506\,C2 + 0.00299\,C3 - 7.02\,C4 - 1.336\,C5 + 0.02222\,C1*C1 + 0.001879\,C2*C2 + 0.000001\,C3*C3 + 1.355\,C4*C4 + 0.009771\,C5*C5 + 0.00290\,C1*C2 + 0.000010\,C1*C3 - 0.0130\,C1*C4 - 0.00355\,C1*C5 - 0.000276\,C2*C3 - 0.0470\,C2*C4 - 0.00235\,C2*C5 + 0.003180\,C3*C4 - 0.000081\,C3*C5 - 0.0085\,C4*C5$$

Equation 6-4

F_N = 178.5 - 1.914 C1 + 1.204 C2 + 0.0072 C3 - 16.59 C4 - 3.163 C5+ 0.05279 C1*C1 + 0.00449 C2*C2 + 0.000003 C3*C3 + 3.216 C4*C4 + 0.02320 C5*C5 + 0.00690 C1*C2 + 0.000026 C1*C3 - 0.033 C1*C4 - 0.00855 C1*C5 - 0.000659 C2*C3 - 0.1110 C2*C4 - 0.00563 C2*C5 + 0.00758 C3*C4 - 0.000193 C3*C5 - 0.0210 C4*C5 *Equation 6-5*

F_T= -3.58 + 0.0797 C1 + 0.0195 C2 - 0.00252 C3 - 0.306 C4 + 0.0691 C5+0.00001 C3*C3+ 0.1092 C4*C4- 0.000477 C5*C5- 0.000200 C1*C2- 0.01800 C1*C4+ 0.000400 C1*C5+ 0.000007 C2*C3- 0.00050 C2*C4- 0.000025 C2*C5+ 0.000180 C3*C4 + 0.000017 C3*C5 + 0.00200 C4*C5 *Equation 6-6*

Spray Coating process

% ΔR_a= -144.8 + 8.89 C1 + 3.615 C2 + 3.976 C3 - 0.7160 C1*C1 - 0.02212 C2*C2 - 0.1265 C3*C3 + 0.0070 C1*C2 + 0.0049 C1*C3 + 0.00008 C2*C3 *Equation 6-7*

6.3.2 Statistical Analysis

ANOVA analysis was performed using Minitab 17 software to identify the effect of input variables on responses for UAMAF and spray coating represented in (Tables 6.5 and 6.6)

Table 6.5: Analysis of variances (ANOVA) for UAMAF Process

Response	Source	D O F	Adj. SS	Adj. MS	F- Ratio	P-Value
% ΔR_a	C_1	1	394.12	394.12	43.87	0.002
	C_2	1	2156.33	2156.33	240.05	0.001
	C_3	1	1636.30	1636.30	182.16	0.001
	C_4		53.47	53.47	5.95	0.005
	C5		358.91	358.91	39.95	0.003
	Error	21	188.64	8.98		
	Total	41	5133.20			
	Model Summary	S	R- Sq.	Adj. R- Sq.	Pred. R- Sq.	
		2.99	0.9633	0.9283	0.8530	
	C_1	1	2.916	2.916	58.87	0.002
	C_2	1	71.476	71.476	1442.71	0.001
	C_3	1	44.34	44.34	896.81	0.001

MR	C_4	1	4.52	4.52	91.25	0.004
	C5	1	34.328	34.328	692.89	0.003
	Error	21	1.040	0.0495		
	Total	41	169.52			
	Model Summary	S	R- Sq.	Adj. R- Sq.	Pred. R- Sq.	
		0.222	0.9939	0.9880	0.9755	
F_N	C_1	1	16.52	16.52	58.87	0.005
	C_2	1	404.87	404.87	1442.71	0.000
	C_3	1	251.67	251.67	896.81	0.001
	C_4		25.60	25.60	91.25	0.003
	C5		194.45	194.45	692.89	0.002
	Error	21	5.89	0.295		
	Total	41	960.239			
	Model Summary	S	R- Sq.	Adj. R- Sq.	Pred. R- Sq.	
		0.5297	0.9939	0.9880	0.9658	
F_T	C_1	1	3.003	3.003	10.00	0.006
	C_2	1	56.79	56.79	189.10	0.003
	C_3	1	25.19	25.19	83.88	0.004
	C_4	1	4.39	4.39	14.64	0.005
	C5	1	24.38	24.38	81.21	0.002
	Error	21	6.307	0.3153		
	Total	41	136.188			
	Model Summary	S	R- Sq.	Adj R- Sq.	Pred. R- Sq.	
		0.548	0.9537	0.9096	0.8148	

Based on Table 6.5 the parameters that exercise maximum impact were decided based on F-value and P-value at a confidence level of 95% ($P < 0.05$). The most efficient input parameters on the response are C_2, C_3, C_5, C_4 and C1.

Table 6.6: Analysis of variances (ANOVA) for Spray coating process

Response	Source	D O F	Adj. SS	Adj. MS	F- Ratio	P-Value
	C_1	1	247.98	247.98	22.36	0.001
	C_2	1	102.15	102.15	9.21	0.004

% ΔR_a	C_3	1	84.37	84.37	7.61	0.003
	Error	17	188.54	11.09		
	Total	26	2844.46			
	Model Summary	S	R- Sq.	Adj. R-Sq.	Pred. R-Sq.	
		3.3302	0.9337	0.8986	0.8433	

Based on Table 6.6 the parameters that exercise maximum impact were decided based on F-value and P-value at a confidence level of 95% ($P < 0.05$). The most efficient input parameters on the response are C_1, C_2 and C_3.

6.4 Influence of process parameters

6.4.1 Influence of process variable on %ΔR_a (%)

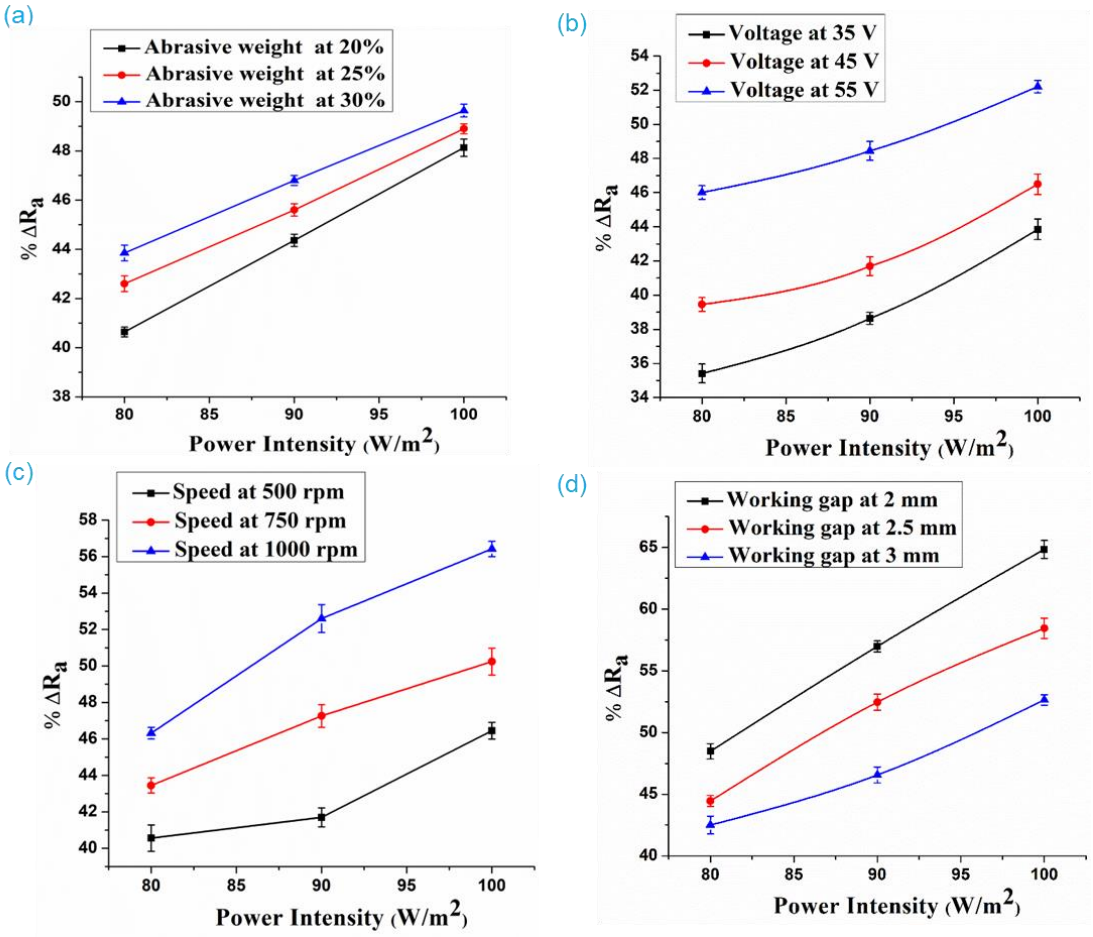

Figure 6.1: Influence of power intensity and (a) wt. % of abrasives (b) voltage (c) speed and (d) working gap on %ΔR_a

The impact of power intensity on changes in surface quality at different abrasive weight percentages during the UAMAF process is shown in Figure 6.1. Because of the amplitude and frequency of vibrations increased with increasing power intensity, the $\%\Delta R_a$ increases with power intensity (Figure 6.1 (a)). Consequently, it increases the random movement of the abrasives along with indentation of the abrasives between the workpiece and FMAB. Additionally, the abrasives particles participating in the finishing operation were changed rapidly to form the new FMAB abrasives of a greater intensity, and the combination of all these elements produced a better surface finish at a higher power intensity. Figure 6.1 (a) illustrates how the $\%\Delta R_a$ increases with the abrasive wt.%. This is a result of the more cutting edges that are present at greater weight percentages and may effectively remove materials. The number of active abrasives in FMAB forced out the blunt abrasives since there were more abrasives available. In addition to providing a superior surface quality at higher wt.% of abrasives, this reduces the number of blunt edges rubbing against the surface. Further, increase in abrasives percentage in FMAB, the formation of magnetic abrasive chains reduces as the weight percentage of abrasives increased. The barrier to the development of magnetic abrasive chains is subsequently decreased as a result. Additionally, the FMAB strength and the overall magnetic force are diminished. A similar trend was also observed by Nitesh et al.[79].

It can also be seen from Figure 6.1(b) that the $\%\Delta R_a$ increased when voltage was increased. The magnetic field strength of FMAB is directly determined by voltage; at higher voltages, a strong magnetic field is produced. This improves the connection between the electromagnet and the abrasives, allowing for the precise removal of material from the workpiece. Figure 6.1(c) also shows that the $\%\Delta R_a$ increases as the electromagnet's speed increases. At lower speeds sticking the removed material back on the workpiece's surface during the finishing process degrades the surface finish. High centrifugal forces at high speeds cause the particles to be pushed outward, improving the surface quality. The percentage $\%\Delta R_a$ grew with decrease in working gap, as shown in Figure 6.1 (d). This is because at a lower working gap the magnetic strength of FMAB is more. Also, the influence of finishing forces is more on workpiece surface at lower working gap gives better finishing results. However, as the working gap increase, the impact force is reduced, which caused the reduced surface finish.

6.4.2 Influence of process variable on MR (mg)

The impact of power intensity on material removal at different abrasive percentages in the UAMAF process is depicted in Figure 6.2. According to Figure 6.2(a), the MR value increased as power intensity increased. The axial vibrations to the workpiece grow along with intensity as well as the number of impacts and randomness of the abrasives, enhancing both. Along with this, the indentation or impact force of active abrasives increases. Additionally, the workpiece surface shears more frequently as a result of the electromagnet's relative motion to the workpiece, which all work together to improve material removal. Figure 6.2(a) shows that the MR increases as the abrasive wt.% increased. This is as a result of the rise of cutting edges at greater weight percentages, which may remove materials effectively and quickly. The number of active abrasives fluctuates as the abrasive % rises, and the interaction between the new cutting edges and the work surface results in significant material removal. As more voltage was given to the electromagnet, the MR increased, as seen in Figure 6.2(b).

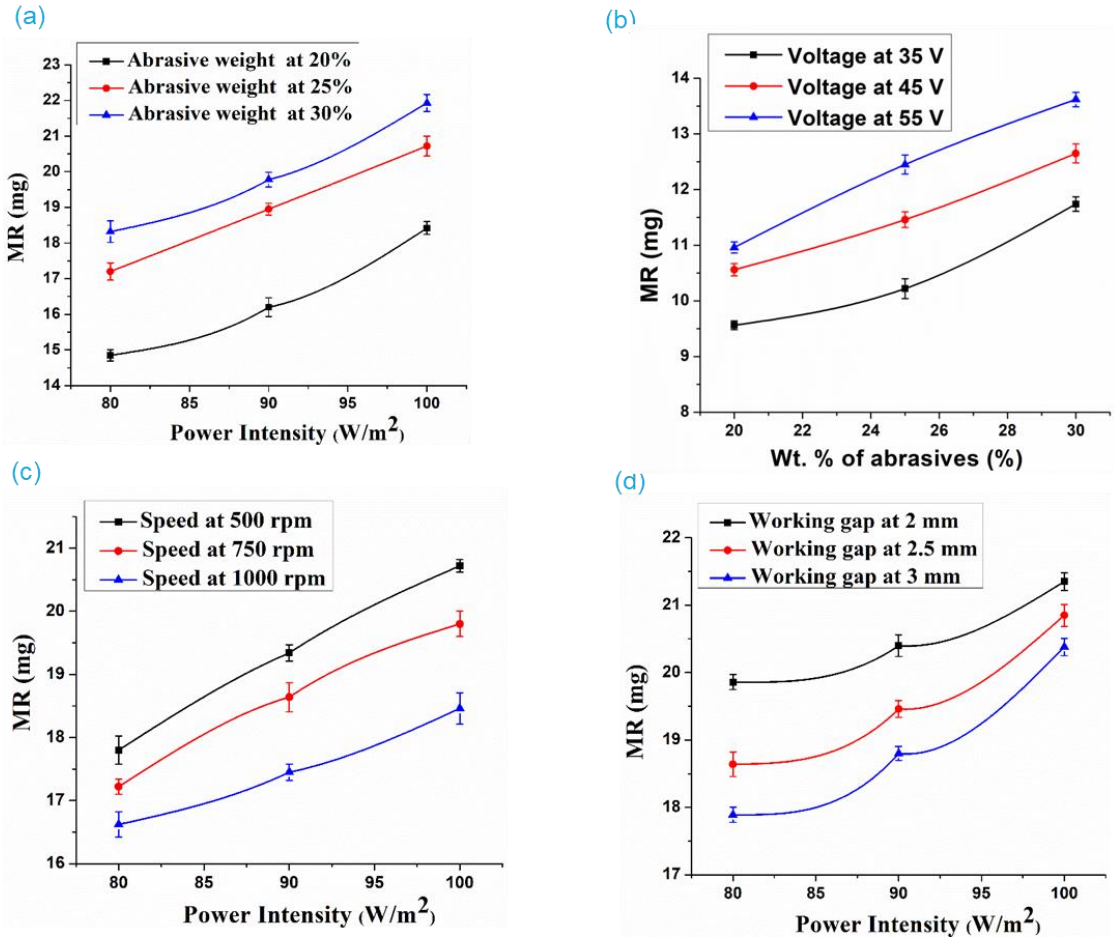

Figure 6.2: Influence of power intensity and (a) wt. % of abrasives (b) voltage (c) speed and (d) working gap on MR

The FMAB's magnetic field strength is directly influenced by the voltage. The FMAB's strength rises with increased voltage. As a result, the workpiece and electromagnet's magnetic and abrasive particle bonds were stronger. This results in a high material removal rate and removes the material from microchips. Additionally, it can be shown in Figure 6.2(c) that the MR decreased as the electromagnet's speed increased. Only rubbing action occurs between FMAB and the workpiece during the finishing operation as the electromagnet's speed increases, as opposed to indentation force. The amount of material removed at faster speeds is reduced because the impact force is so small in comparison to the rubbing action. The MR diminishes as the working gap increases, as seen in Figure 6.2(d). This is so that more material may be removed because to the higher impact of the abrasive chains at the lower working gap. As the working space widens, less material is removed because of weaker magnetic abrasive chains between FMAB and the workpiece surface. contrasted with a smaller working gap.

6.4.3 Influence of process variables on Normal force (N)

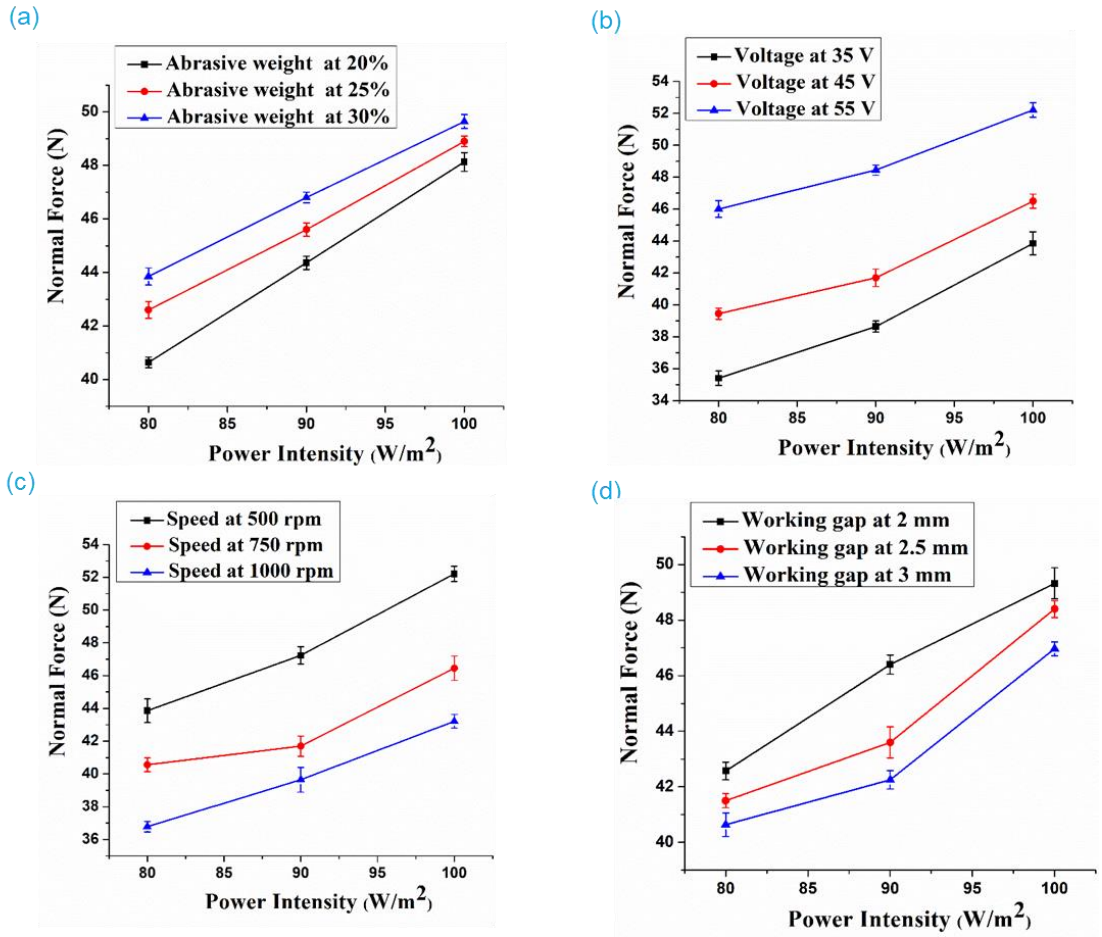

Figure 6.3: Influence of power intensity and (a) wt. % of abrasives (b) voltage (c) speed and (d) working gap on Normal force

Figure 6.3 illustrates how normal force (F_N) is affected by power intensity in the UAMAF process at varying abrasive percentages. As power intensity is more, the F_N value also more (Figure 6.3(a)). Axial vibrations to the workpiece become more intense at greater intensities, which boosts the abrasives' unpredictability and number of hits. The impact force or indentation of active abrasives also grows along with this. As can be seen from Figure 6.3(a), the F_N grew as the abrasive wt.% increased. This is because more cutting edges are present at larger weight percentages, which enable faster and more effective material removal. The number of active abrasives fluctuates as the abrasive % rises, and the interaction between the new cutting edges and a work surface causes an increase in normal force. Figure 6.3(b) shows that the F_N grew when more voltage was added to the electromagnet. The FMAB's magnetic field strength is directly influenced by voltage. The FMAB's strength rises with increased voltage. As a result, the workpiece and electromagnet's magnetic and abrasive particle bonds were stronger. It results in an increase in the typical cutting force by removing the material in the form of microchips. From Figure 6.3 (c), it is also observed that the F_N decreased with the speed of the electromagnet. It can also be seen from Figure 6.3(c) that the F_N dropped as the electromagnet's speed increased. Only rubbing action occurs between FMAB and the workpiece during the finishing operation as the electromagnet's speed increases and its circumferential force grows relative to its indentation force. Since the rubbing action causes a reduction in normal force at higher speeds, the impact force is smaller than the rubbing action. Figure 6.3(d) demonstrates that as the working gap decreases, the F_N value increases. At lower working gap the strength of the FMAB is more and it supports the indention of abrasives. Additionally, as the working space widens, the F_N value falls as a result of the weaker magnetic abrasive chains between the FMAB and the workpiece surface, leading to reducing in normal force when compared to a lower working gap.

6.4.4 Influence of process variables on Tangential force (N)

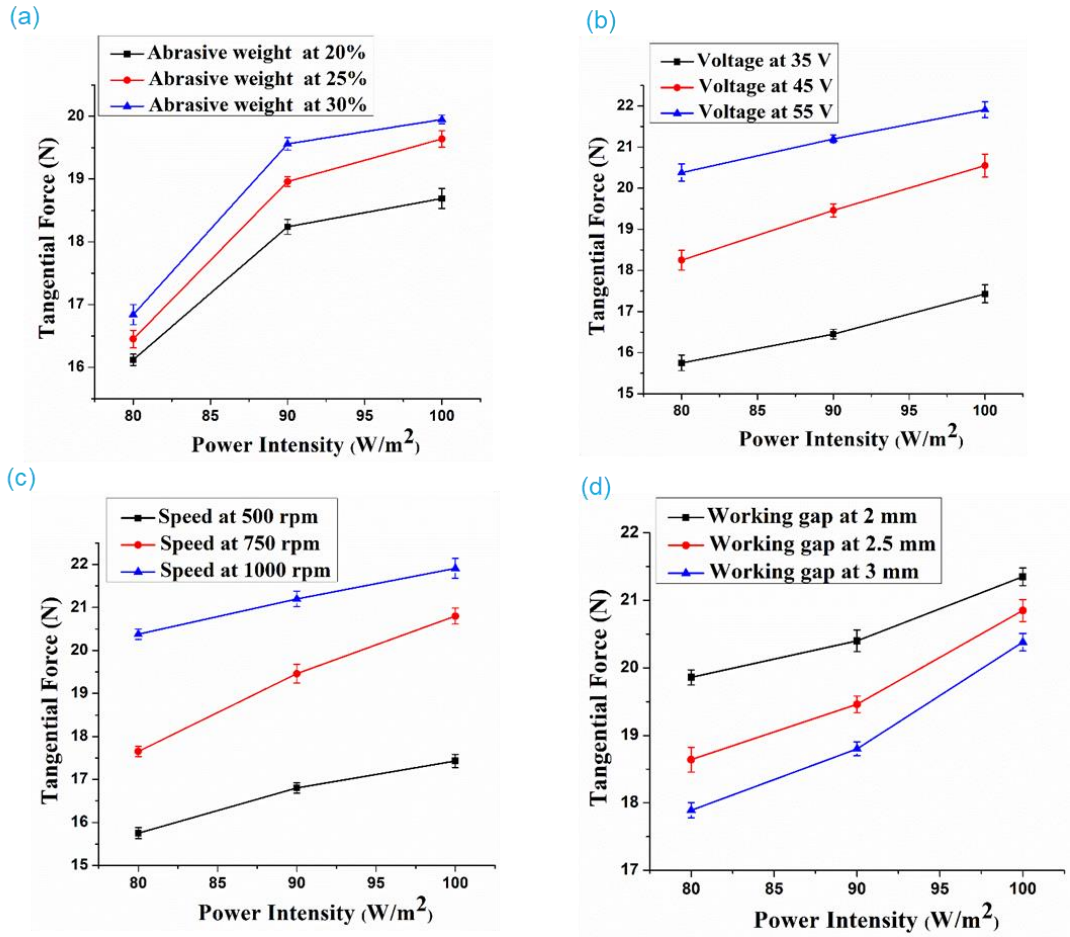

Figure 6.4: Influence of power intensity and (a) wt. % of abrasives (b) voltage (c) speed and (d) working gap on Tangential force

The impact of power intensity on tangential force (F_T) at varying wt.% of abrasives in the UAMAF process is shown in Figure 6.4. Due to the increased amplitude and frequency of vibrations at higher intensities, the tangential force increased with power intensity (Figure 6.4(a)). As a result, it increases the quantity of hits and randomness of the active abrasives between the workpiece and FMAB. All these elements together result in a large tangential force at greater power intensities. In addition, the abrasive particles in the finishing process were replaced with new abrasives of FMAB at a higher intensity.

Figure 6.4(b) similarly shows that the tangential increased as voltage was added. When the voltage was higher, a strong magnetic field was produced, directly affecting the FMAB's magnetic field strength. As a result, the connection between the magnetic and abrasives was strengthened, improving tangential force. Figure 6.4(c) also shows that the tangential force rose as the electromagnet's speed grew. The time for sticking was shorter at faster speeds, resulting in successful removal. High centrifugal forces at high speeds cause

the particles to be pushed outward, improving the surface quality. The tangential force increases as the working gap increases, as seen in Figure 6.4(d). shows that the tangential force increases as the working gap reduces. Additionally, the weaker magnetic abrasive chains between the FMAB and the workpiece surface cause the tangential force value to decrease as the working space widens, which results in a reduction in normal force as compared to a working gap that is smaller. Jain et al. [37] also explored a related pattern.

6.4.5 Influence of coating process parameters on $\%\Delta R_a$

The impact of etchant weight, temperature, and number of coats on surface quality improvement is shown in Figure 6.5. The $\%\Delta R_a$ value rises up to a certain point and falls as etchant weight grows further (Figure 6.5(a)) at various temperatures and coating counts. At first, the coating improves the finish by filling up any gaps on the surface. However, after a certain etchant weight, oxidation reduces the finish. The effect of temperature on $\%\Delta R_a$ at different levels of etchant weight and coating count is depicted in Figure 6.5 (b). When the temperature reaches 80°C, the surface polish starts to degrade. The etchant evaporates as the temperature rises, absorbing the surface of the workpiece and lowering $\%\Delta R_a$. The fluctuation of $\%\Delta R_a$ with the number of coatings at various levels of etchant weight and temperature is explained by Figure 6.5(c). After a certain number of coatings, a particular number of coatings were sensitive and caused oxidation, which reduced the finish. As the number of coatings increased, the finish improved because the coating filled the voids on the surface.

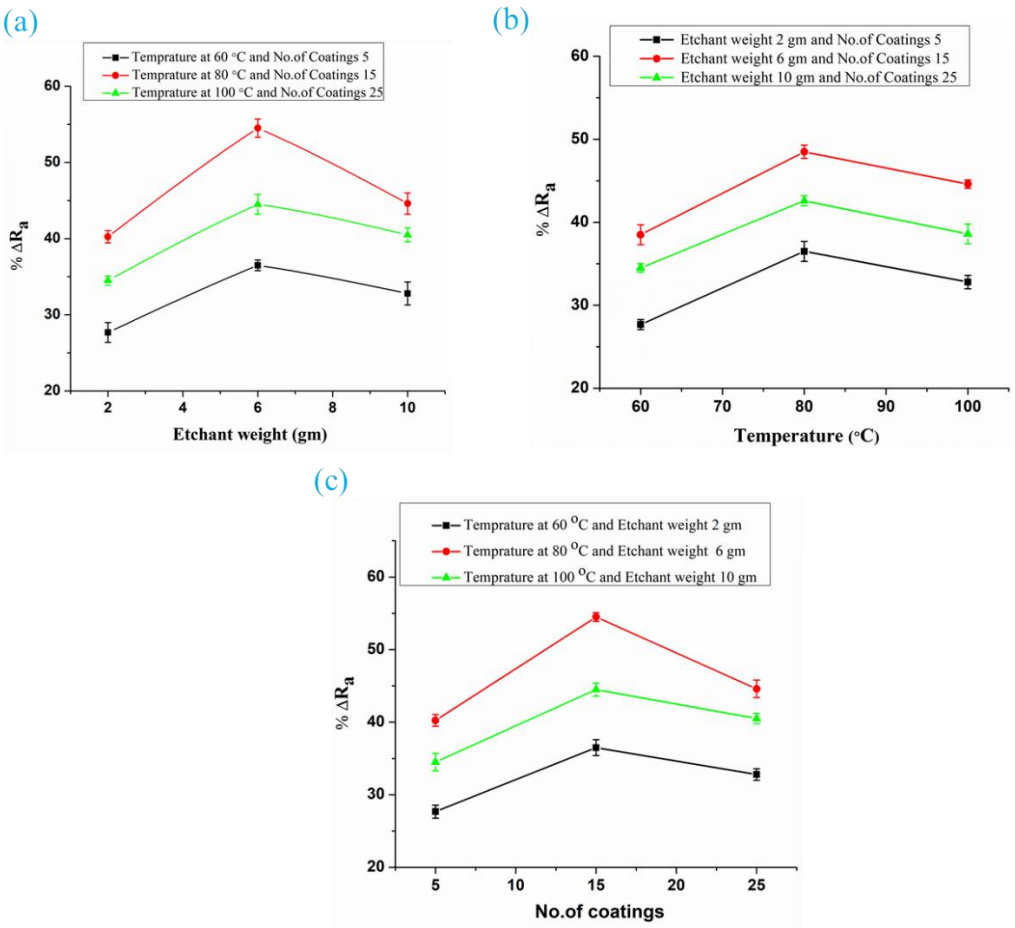

Figure 6.5: Influence of coating parameters on $\%\Delta R_a$ (a) Etchant weight (b) Temperature (c) no. of coatings

6.5 Comparison

The surface profiles of the MAF, UAMAF, Chemo UAMAF, and grinded surfaces were taken into consideration. Ra, Rq (mean square root surface finish), Rt (total profile height), and Rz (average peak to valley height) are the main surface texture parameters that were measured and are shown in Figure 6.6. The Chemo UAMAF was shown to give a better surface finish when the space between peak valleys was at its smallest.

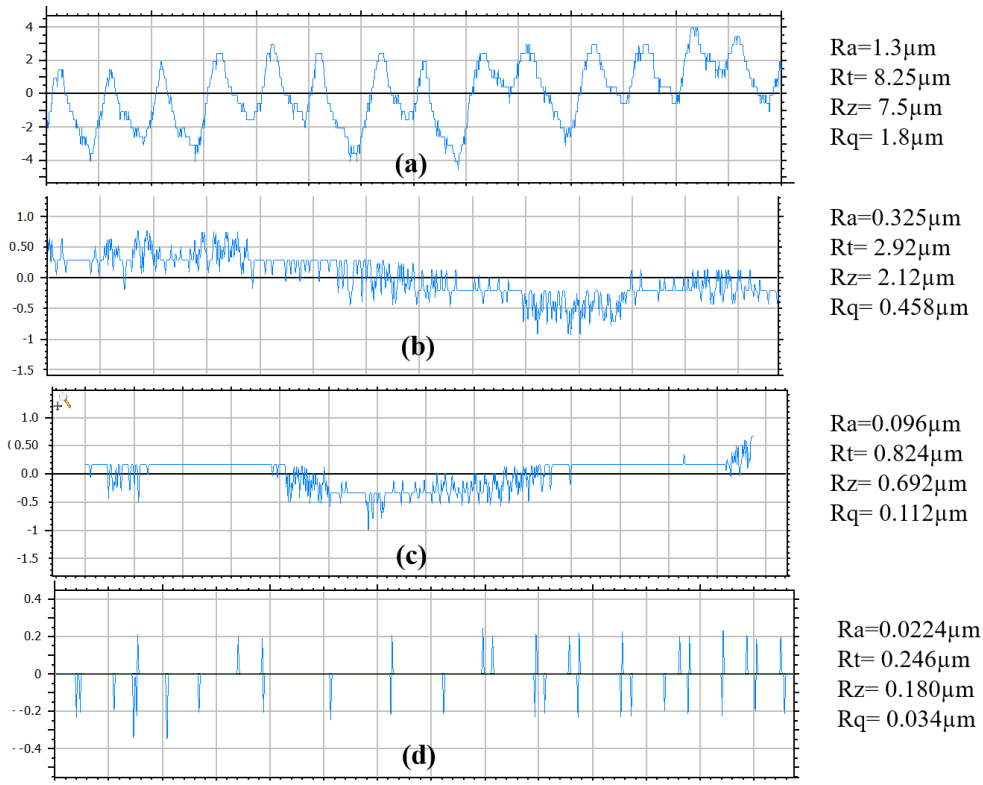

Figure 6.6: Surface profiles of Hastelloy C-276 after (a) Ground (b) MAF (c) UAMAF (d) Chemo-based UAMAF

Figure 6.7 illustrates the surface morphology analysis performed at a resolution of 50 µm using SEM on grinded, MAF, UAMAF, and Chemo-based UAMAF completed surfaces. The workpiece that has been surface ground is shown in Figure 6.7 (a). Due to high cutting forces and high-speed operation, grinding marks may be seen going in that direction. After MAF finishing, the workpiece is shown in Figure 6.7 (b). It has been observed that the rotational moment of the FMAB on the workpiece results in a better level of surface finish as compared to grinding. Despite the fact that abrasives' action on the surface left some very small spots behind. Figure 6.7 (c) depicts the UAMAF-finished workpiece, which has a smooth finish because there were fewer abrasive impacts than with MAF. Random movement of abrasives additionally offer a superior finish because of ultrasonic vibrations. The UAMAF surface with a chemical coating is shown in Figure 6.7 (d). Micro indentation marks are eliminated while etching activity covered up spots. The workpiece's surface characteristics improve as a result.

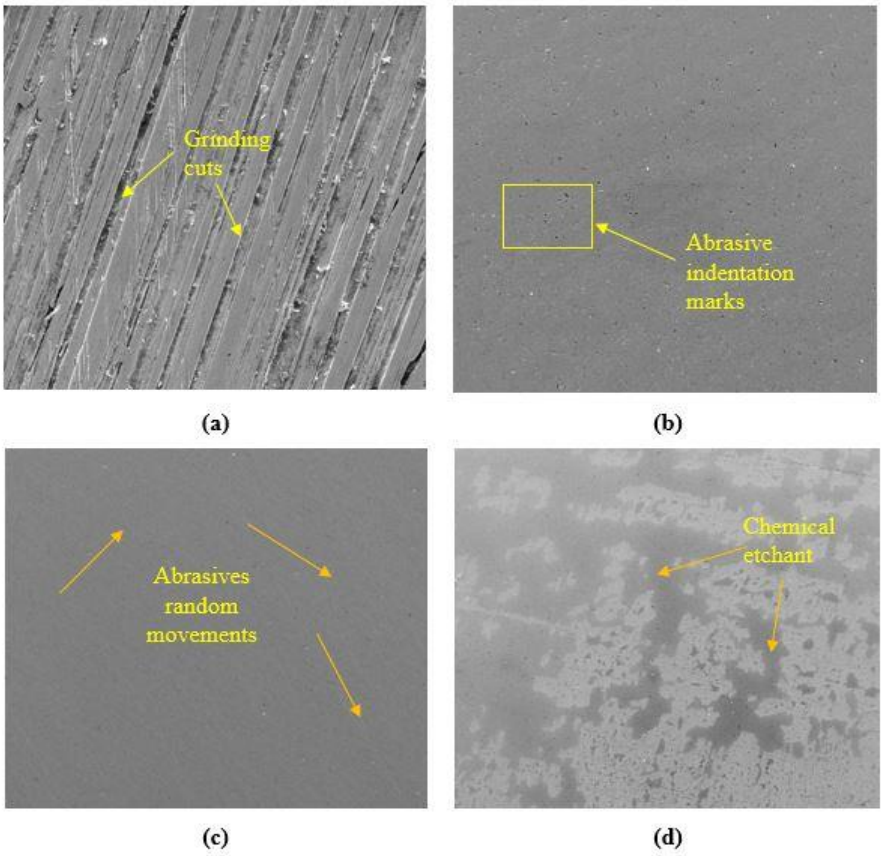

Figure 6.7: SEM images of Hastelloy C-276 after (a) Ground (b) MAF (c) UAMAF (d) Chemo UAMAF

6.6 Summary

The current chapter explains how to finish Hastelloy C-276 by an ultrasonic attachment. Process variables such as power intensity, voltage, speed, abrasive percentage, and working gap were evaluated for their effects on responses. In comparison to the traditional MAF method, the experimental findings of the UAMAF process were examined. Using the UAMAF procedure, it has been found, results in greater completing rates and other answers. Additionally, spray coating was used on the UAMAF procedure produced specimen, and this resulted in superior surface polish.

7 OPTIMIZATION OF PROCESS PARAMETERS OF MAF AND UAMAF PROCESSES

7.1 Introduction

This chapter used the RSM technique to do multi-objective optimisation for Hastelloy C-276 for both MAF and UAMAF finishing. Additionally, the confirmation experiments were run at the ideal process parameters and validated by the outcomes of the experiments and simulations. Prior to and following the UAMAF process, the surface residual stresses were assessed using the best process parameters.

7.2 Optimization of process parameters

The process of optimising cutting parameters is frequently difficult [80], necessitating the use of empirical formulae relating to tool life, force, performance, surface polish, etc. Realistic constraints, definitions of the capabilities of the machine tools, useful optimisation criteria, and familiarity with mathematical and numerical optimisation techniques are all necessary. The most crucial outcome, also known as the optimisation goal or optimisation criterion, must be identified for each optimisation process. The unique expenditures incurred by researchers are the optimisation criteria that are used in the production process the most frequently[81]. Optimization of process parameters is essential for any finishing process to reduce the finishing cost and finishing time and also to improve the finishing rate of the process. This chapter discusses the multi-objective optimization of different magnetic abrasive finishing processes (MAF, UAMAF). Because they may produce a population of solutions for generations without being characterised by the investigation of difficult research spaces and the use of genetic resources, genetic algorithms have drawn a lot of interest as an effective technique for optimising numerous targets.

The composite desirability function is an advanced multi-optimization method that can be applied to real-world issues and maintains the clashing of replies in difficult situations [82]. The calculation of the desirability function value starts the process. Based on the minimization and maximization the target goal obtained based on Equations 7.1 and 7.2, respectively) [83]:

$$d_{ir}\,(min) = \{\frac{Yir - max\,Yir}{minYir - max\,Yir}\} \quad \min y_{ir} \leq y_i \leq \max y_{ir} \qquad \textit{Equation 7-1}$$

$$d_{ir}\,(max) = \{\frac{yir - minyir}{minyir - maxyir}\} \min y_{ir} \leq y_i \leq \max y_{ir} \qquad \textit{Equation 7-2}$$

where di is the desired response quality for the i^{th} experiment and, y_{ir} is the observed value of the response after the i^{th} treatment, max y_{ir} and min y_{ir} are the highest and lowest observed values at the i^{th} response, a is the assigned weight, which is the same for all responses. On the interval between the upper and lower target and limit, this establishes the desirability function distribution.

7.2.1 Response Optimization

The computation of normalised SN ratio values using the desirability function criterion in accordance with Equations 7.1 and 7.2 for multi-optimization. The technique used to establish the relative importance (weights) for each quality attribute is largely responsible for the validity of multi-objective optimisation [84]. The composite desirability values are shown in Table 7.1 and Table 7.2.

Optimization for the responses of the MAF and UAMAF processes are performed with RSM. The optimum response was observed at 30% of abrasives, 45 V voltage, 750 rpm speed of electromagnet, working gap of 2.5 mm for MAF process. Also, the optimum responses for UAMAF process were observed at 30% of abrasives, 45 V voltage, 750 rpm speed of electromagnet, working gap of 2.5 mm along with power intensity of 90 W/m^2. The composite desirability is found to be 0.95, which is acceptable for the optimum response and the optimized values are significant.

Table 7.1: Optimum values of MAF parameters and responses by composite desirability function

Solution	C_1 (%)	C_2 (V)	C_3 (rpm)	C_4 (mm)	ΔR_a (%)	MR (mg)	F_N (N)	Ft (N)	Composite desirability
local	25	45	500	3	42.5	13.4	28.85	12.85	0.78
local	20	45	500	3	35.6	12.6	26.55	11.65	0.82
local	25	45	750	3	43.5	11.8	89.74	12.42	0.81
local	20	45	750	3	36.8	10.6	28.33	11.84	0.84
local	20	55	750	3	52.5	13.2	27.02	11.46	0.89
local	30	45	500	3	32.4	10.2	26.63	11.56	0.88
local	30	45	750	3	47.8	12.4	27.52	12.2	0.90

local	25	55	750	3	48.8	12.5	26.96	10.8	0.92
local	20	55	1000	3	39.8	10.6	27.50	11.24	0.91
global	**30**	**45**	**750**	**2.5**	**51.5**	**13.8**	**28.65**	**12.76**	**0.95**

Table 7.2: Optimum value of UAMAF parameters and responses by composite desirability function

Solution	C_1 (%)	C_2 (V)	C_3 (rpm)	C_4 (mm)	C_5 (W/m^2)	ΔR_a (%)	MR (mg)	F_N (N)	Ft (N)	Composite desirability
local	30	45	538	3	90	62.5	16.4	39.85	16.85	0.84
local	30	35	674	3	80	45.6	14.6	37.55	14.65	0.85
local	30	35	538	2	80	42.5	13.8	39.74	16.42	0.85
local	20	35	631	2	80	36.8	12.8	38.33	15.34	0.89
local	30	35	551	2.5	80	52.5	14.2	37.02	14.46	0.90
local	20	35	500	3	80	32.4	13.2	37.63	14.56	0.92
local	20	35	559	2	80	33.8	13.4	37.52	15.2	0.93
local	30	35	533	3	80	46.8	14.5	36.96	13.8	0.93
local	20	35	545	2	80	30.8	12.6	37.50	14.24	0.94
global	**30**	**45**	**750**	**2.5**	**90**	**62.5**	**16.12**	**38.65**	**15.76**	**0.95**

7.2.2 Validation of the optimized model

The response obtained from the RSM is validated with experimental results at the global process parameters are represented in Table 7.3 and 7.4. For this purpose, the experiments were conducted at optimum process parameters. The experimental values are compared with output values given by the model. The percentage error obtained for MAF and UAMAF process are less than 5% and hence the proposed model may be well predicted the results with less deviation.

Table 7.3: Responses in MAF condition and RSM technique

Output parameters	MAF condition (experimental)	RSM Technique	% of error
ΔR_a (%)	56.4	54.8	2.8%
Material removal	12.4	12.2	1.6%
Normal force (N)	29.45	28.45	3.4%
Cutting force (N)	13.15	12.8	2.7%

Table 7.4: Responses in UAMAF condition and RSM technique

Output parameters	UAMAF condition (experimental)	RSM Technique	% of error
ΔR_a (%)	64.6	62.5	3.2%
Material removal	16.8	16.12	4.0%
Normal force (N)	39.45	38.65	2.0%
Cutting force (N)	16.15	15.76	2.4%

7.3 Surface residual stress

The functionality, fatigue life, and surface integrity of the machined component are predominantly affected by surface residual stress. The principal causes of residual stresses are the cutting temperature (thermal load) and cutting force (mechanical load). These stresses could either be compressive or tensile. Regardless of the material, compression pressures prolong product life, increase corrosion resistance, prolong fatigue life, and reduce early failure [85] . Compressive stresses are produced by mechanical load, while tensile stresses are produced by heat load. The $\sin^2\Psi$ method is used to determine the specimen's surface residual stress.

The figure 7.1 represents the surface residual stress developed on the surface of as grinded which was measured by the XRD technique. It is observed that the one direction, it developed residual compressive stress whether in the remaining two directions, it developed tensile stress. In grinding the mechanical load applied by the abrasive particles developed compressive residual stress on x – direction. Anyhow there is a large amount of specific energy consumption in grinding due to multi-edge contact of the tool and workpiece and the rubbing action is also higher. There is continuous contact in-between the tool and the

workpiece. That causes ineffective removal of heat. All these lead to a high thermal load in the other two directions apart from the x- direction. The same scenario reflects in the figure that d-spacing increases with the sin2w value indicating the tensile residual stress due to the domination of thermal load.

$$\begin{bmatrix} -196 & 0 & 79.0 \\ 0 & 320.2 & 93.4 \\ 79.0 & 93.4 & 0 \end{bmatrix}$$

The figure 7.2 represents the surface residual stress developed on the surface of UAMAF specimen. It is clearly observed that d-spacing decreases with the sin2w in all three directions which indicates that residual compressive stress was developed on the surface. The prime reason was the intermittent finishing operation. By applying external vibration using an ultrasonic transducer. This removes the thermal load developed on the surface and magnifies the mechanical load which was already developed due to the initial grinding process. This causes the residual compressive stress in all directions which is very helpful in increasing the fatigue life of the component. The comparison results of residual stresses are listed in Table 7.5.

$$\begin{bmatrix} -630.5 & 0 & 45.6 \\ 0 & -486.2 & 86.1 \\ 45.6 & 86.1 & 0 \end{bmatrix}$$

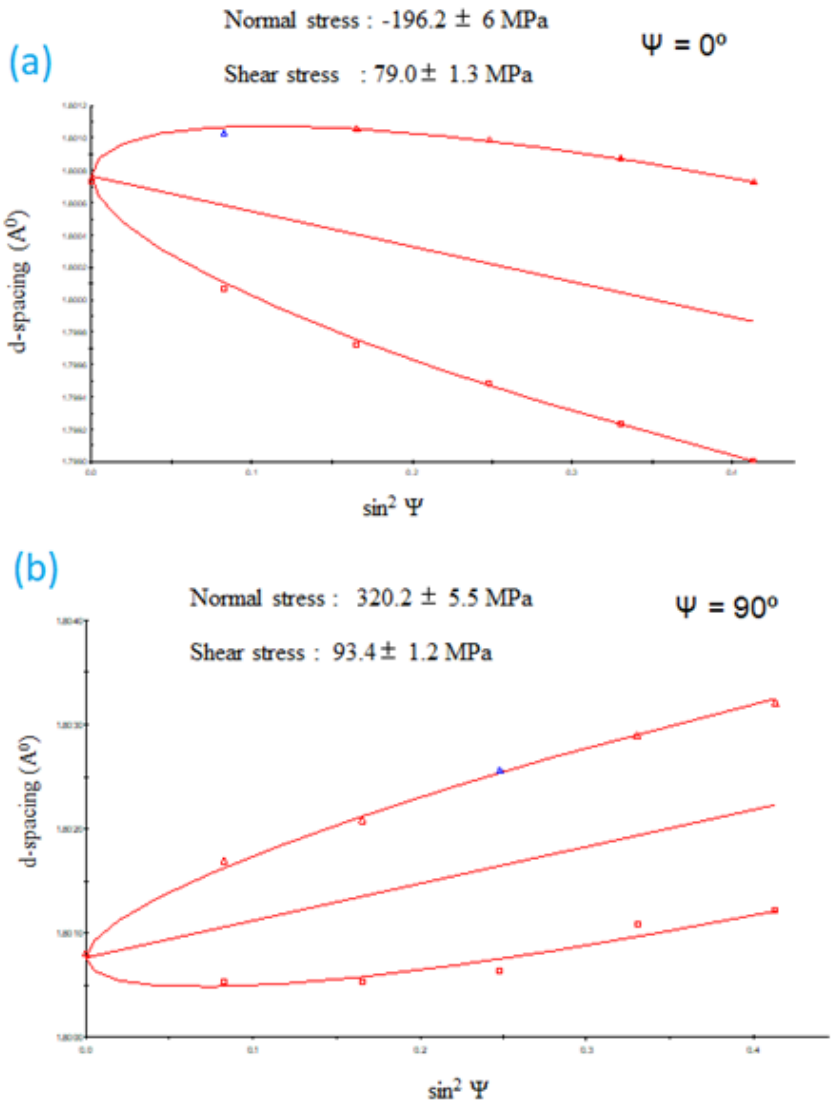

Figure 7.1: Surface residual stresses developed under surface ground condition

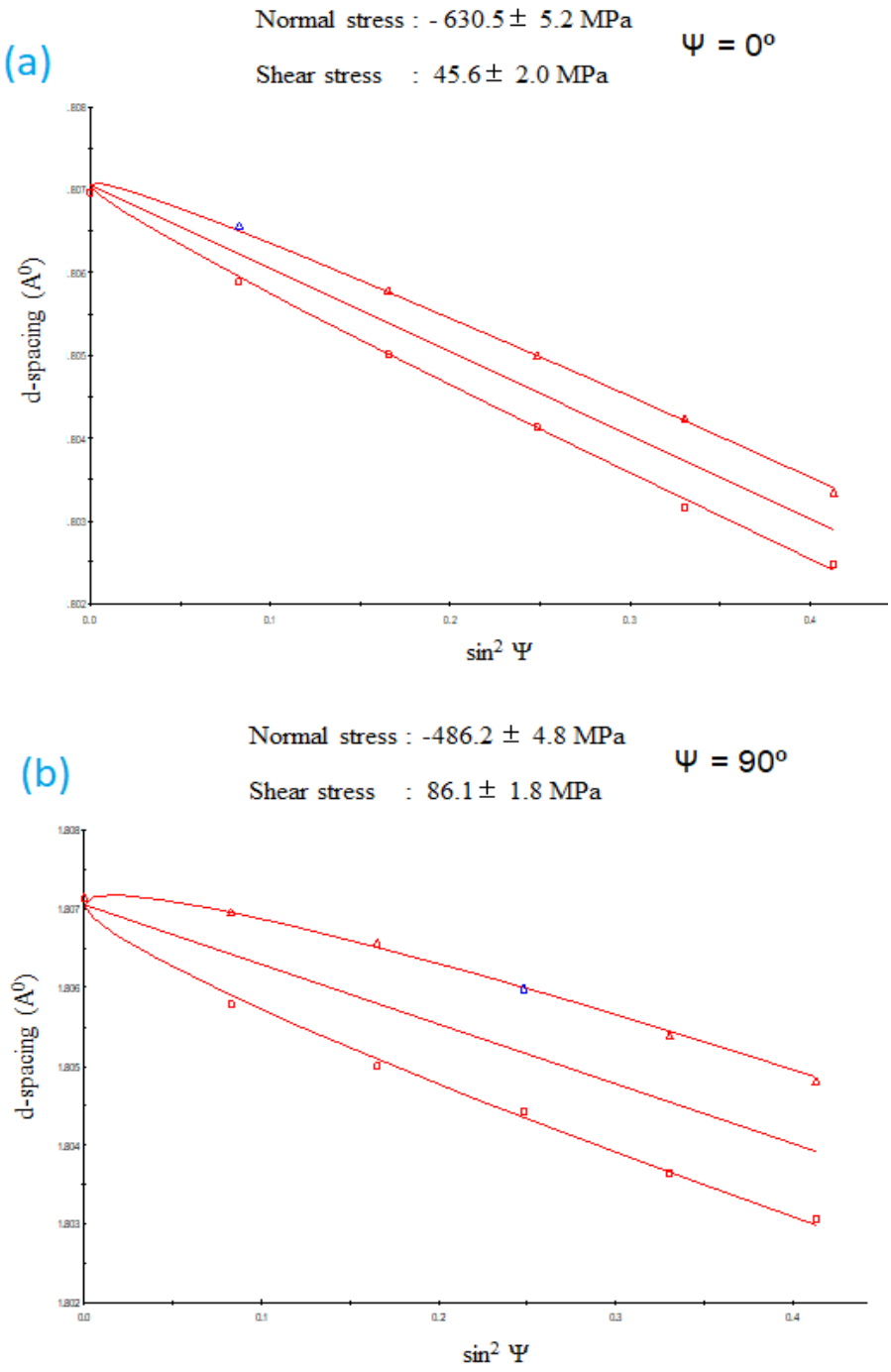

Figure 7.2: Surface residual stresses developed under UAMAF condition

Table 7.5: Principal residual stress on the machined surface

	σ_1 (MPa)	σ_2 (MPa)	σ_3 (MPa)
Surface ground	-196.2	320.2	0
UAMAF	-630.5	-486.2	0

7.4 Summary

In this chapter, the multi-objective optimization was carried out for MAF and UAMAF finishing of Hastelloy C-276 using the RSM technique. Additionally, the validation experiments were conducted with the best process parameters and supported by simulation and experiment findings. Prior to and after the UAMAF process, surface residual stresses were conducted at optimal process parameters.

8 CONCLUSIONS AND FUTURE SCOPE

8.1 Introduction

The present work is concerned with the finishing of advanced nickel-based alloy Hastelloy C-276 using MAF and UAMAF processes. Numerical and experimental analysis of the process mechanism and influence of process parameters on responses have been presented. Performance evaluation of MAF and UAMAF process has been explained with exhaustive experimental work. Further, multi-objective optimization is carried out using advanced optimization techniques. The surface residual stresses were studied at optimum process conditions. The following sections contain major conclusions on of the work, as well as an outline of potential future directions.

8.2 Conclusions

- For all experiments, the simulation shows that the magnetic flux density fluctuates between 1 and 1.5 Tesla.
- The magnetic flux density varies minimum at the ends of the workpiece and increases in the area FMAB. Also, the maximum observed at the circumference of the brush compared to the centre.
- The process parameters considered for simulation are working gap, voltage, speed and power intensity for the experimentation and the forces are measured for both normal and tangential forces based on simulation and experimentation.
- It has been determined that the electromagnet's voltage and speed have a significant impact on factors that increase the surface quality of both MS and Al 2024 alloy.
- The percentage increase in the surface finish after the MAF process is $\%\Delta R_a = 83$ for MS and $\%\Delta R_a = 65$ for Al 2024. MS showed better surface finish compared to Al 2024 because of its magnetic nature.
- From the SEM analysis, it can be seen that MS has a superior surface quality than Al. This is due to the fact that MS is a low strength material and that the high magnetic field created between the workpiece and tool and the FMAB makes this possible.
- All process parameters except working gap increase surface finish and tangential force. The working gap in the UAMAF process caused the surface finish increases as the working gap decreases.
- The percentage of abrasives, the power intensity, and the voltage all raised MR and normal force, whereas working gap and speed decreased it. The intensity of forces is

high in the case of the UAMAF process as compared to the MAF process due to additional axial movement in the UAMAF process.

- The surface finish of Hastelloy C- 276 improvement in UAMAF is 82.87% higher compared to the initial MAF operation.
- SEM micrographs show that UAMAF gave superior surface characteristics over grinding and MAF.
- The coating added to the surface finish improvement made by the UAMAF procedure. The parameters of coating method, including weight of etchant, chamber temperature, and number of coatings, were taken into consideration for improved reaction.
- The number of coatings up to a specific limit further decreases with an increase in these parameters. The coating performance improves with the weight of the etchant, the temperature of the workpiece, and the coating weight.
- The optimized process parameters for better surface finish are 6 gm weight, 80 °C temperature and 15 number of coatings.
- The addition of chemo treatment the surface finish improved by 76.6% compared to UAMAF.
- The optimum process parameters for UAMAF process while finishing Hastelloy C-276 were obtained based on composite desirability using Minitab software.
- The optimum process parameters for UAMAF process while finishing Hastelloy C-276 were obtained based on composite desirability using Minitab software and the residual stresses were measured at this condition.
- Based on surface residual stresses, it is observed that the one direction, it developed residual compressive stresses while in the remaining other two directions, it developed of tensile stresses.
- The same scenario observed based on d-spacing increases with the $\sin^2\Psi$ value that indicates the tensile residual stress due to the domination of thermal load
- It is also clearly observed that d-spacing decreases with the $\sin^2\Psi$ in all three directions, that indicates the residual compressive stress has developed in the surface

8.3 Future scope

The present work has opened up more opportunities of research in MAF field

- ✓ Future Developments on new hybrid variants for finishing of super alloys, composite materials etc.
- ✓ Full Automation of newly developed hybrid variant for better accuracy.
- ✓ Further investigation to finish soft materials and nonmetals by online monitoring strategy using Acoustic emission setup
- ✓ To develop a prediction model by applying suitable AI and ML Algorithms.

.

9 REFERENCES

[1] R. V. Rao, D. P. Rai, and J. Balic, ‘Surface grinding process optimization using Jaya algorithm’, *Advances in Intelligent Systems and Computing*, vol. 411, pp. 487–495, 2016, doi: 10.1007/978-81-322-2731-1_46.

[2] Q. Han *et al.*, ‘Effects of TiC content on microstructure and mechanical properties of nickel-based hastelloy X nanocomposites manufactured by selective laser melting’, *Materials Science and Engineering A*, vol. 796, no. August, p. 140008, 2020, doi: 10.1016/j.msea.2020.140008.

[3] Z. W. Du, Y. Chen, K. Zhou, and C. Li, ‘Research on the electrolytic-magnetic abrasive finishing of nickel-based superalloy GH4169’, *International Journal of Advanced Manufacturing Technology*, vol. 81, no. 5–8, pp. 897–903, 2015, doi: 10.1007/s00170-015-7270-4.

[4] R. S. Mulik and P. M. Pandey, ‘Mechanism of surface finishing in ultrasonic-assisted magnetic abrasive finishing process’, *Materials and Manufacturing Processes*, vol. 25, no. 12, pp. 1418–1427, 2010, doi: 10.1080/10426914.2010.499580.

[5] Y. Zou, H. Xie, and Y. Zhang, ‘Study on surface quality improvement of the plane magnetic abrasive finishing process’, *International Journal of Advanced Manufacturing Technology*, vol. 109, no. 7–8, pp. 1825–1839, 2020, doi: 10.1007/s00170-020-05759-z.

[6] M. J. Jackson, ‘Recent advances in ultraprecision abrasive machining processes’, *SN Applied Sciences*, vol. 2, no. 7. Springer Nature, Jul. 01, 2020. doi: 10.1007/s42452-020-2982-y.

[7] S. Ali, ‘FUNDAMENTALS OF MODERN MANUFACTURING: MATERIALS, PROCESSES, AND SYSTEMS Second Edition’.

[8] J. du Kim and M. S. Choi, ‘Stochastic approach to experimental analysis of cylindrical lapping process’, *Int J Mach Tools Manuf*, vol. 35, no. 1, pp. 51–59, 1995, doi: 10.1016/0890-6955(94)E0005-4.

[9] E. Saljé, M. von S.-C. annals, and undefined 1987, ‘Process-optimization in honing’, *Elsevier*, Accessed: Sep. 18, 2019.

[10] B. Varghese, S. M.-C. Annals, and undefined 1998, ‘Experimental investigation of methods to enhance stock removal for superfinishing’, *Elsevier*, Accessed: Sep. 18, 2019.

[11] J. McGeough, *Advanced methods of machining*. Springer, 1988.

[12] M. R. Sankar, V. K. Jain, and J. Ramkumar, 'Abrasive flow machining (AFM): An overview', *Department of Mechanical Engineering, Indian Institute of Technology, Kanpur, India*, no. January 2011, pp. 1–8, 2011.

[13] P. Taylor, G. Z. Kremen, E. A. Elsayed, and V. I. Rafalovich, 'Mechanism of material removal in the magnetic abrasive process and the accuracy of machining', no. February 2013, pp. 37–41, 2007.

[14] P. Y. Wu and H. Yamaguchi, 'Material Removal Mechanism of Additively Manufactured Components Finished using Magnetic Abrasive Finishing', *Procedia Manuf*, vol. 26, pp. 394–402, 2018, doi: 10.1016/j.promfg.2018.07.047.

[15] T. Shinmura, K. Takazawa, E. Hatano, M. Matsunaga, and T. Matsuo, 'Study on Magnetic Abrasive Finishing', *CIRP Ann Manuf Technol*, vol. 39, no. 1, pp. 325–328, 1990, doi: 10.1016/S0007-8506(07)61064-6.

[16] R. S. Mulik and P. M. Pandey, 'Mechanism of surface finishing in ultrasonic-assisted magnetic abrasive finishing process', *Materials and Manufacturing Processes*, vol. 25, no. 12, pp. 1418–1427, 2010, doi: 10.1080/10426914.2010.499580.

[17] R. S. Mulik and P. M. Pandey, 'Experimental investigations and optimization of ultrasonic assisted magnetic abrasive finishing process', *Proc Inst Mech Eng B J Eng Manuf*, vol. 225, no. 8, pp. 1347–1362, 2011, doi: 10.1177/09544054JEM2122.

[18] A. Misra, P. M. Pandey, and U. S. Dixit, 'Modeling of material removal in ultrasonic assisted magnetic abrasive finishing process', *Int J Mech Sci*, vol. 131–132, no. April, pp. 853–867, 2017, doi: 10.1016/j.ijmecsci.2017.07.023.

[19] S. C. Jayswal, V. K. Jain, and P. M. Dixit, 'Modeling and simulation of magnetic abrasive finishing process', *International Journal of Advanced Manufacturing Technology*, vol. 26, no. 5–6, pp. 477–490, Sep. 2005, doi: 10.1007/s00170-004-2180-x.

[20] A. M. Wani, V. Yadava, and A. Khatri, 'Simulation for the prediction of surface roughness in magnetic abrasive flow finishing (MAFF)', *J Mater Process Technol*, vol. 190, no. 1–3, pp. 282–290, Jul. 2007, doi: 10.1016/j.jmatprotec.2007.02.036.

[21] V. K. Jain, S. C. Jayswal, and P. M. Dixit, 'Modeling and simulation of surface roughness in magnetic abrasive finishing using non-uniform surface profiles', *Materials and Manufacturing Processes*, vol. 22, no. 2, pp. 256–270, Feb. 2007, doi: 10.1080/10426910601134096.

[22] Y. Gao, Y. Zhao, G. Zhang, F. Yin, and H. Zhang, ‘Modeling of material removal in magnetic abrasive finishing process with spherical magnetic abrasive powder’, *Int J Mech Sci*, vol. 177, Jul. 2020, doi: 10.1016/j.ijmecsci.2020.105601.

[23] M. Mosavat and A. Rahimi, ‘Numerical-experimental study on polishing of silicon wafer using magnetic abrasive finishing process’, *Wear*, vol. 424–425, pp. 143–150, Apr. 2019, doi: 10.1016/j.wear.2019.02.007.

[24] W. Li, X. Li, S. Yang, and W. Li, ‘A newly developed media for magnetic abrasive finishing process: Material removal behavior and finishing performance’, *J Mater Process Technol*, vol. 260, pp. 20–29, Oct. 2018, doi: 10.1016/j.jmatprotec.2018.05.007.

[25] Z. Fan, Y. Tian, Z. Liu, C. Shi, and Y. Zhao, ‘Investigation of a novel finishing tool in magnetic field assisted finishing for titanium alloy Ti-6Al-4V’, *J Manuf Process*, vol. 43, no. November 2018, pp. 74–82, 2019, doi: 10.1016/j.jmapro.2019.05.007.

[26] A. Misra, P. M. Pandey, and U. S. Dixit, ‘Modeling and simulation of surface roughness in ultrasonic assisted magnetic abrasive finishing process’, *Int J Mech Sci*, vol. 133, no. September, pp. 344–356, 2017, doi: 10.1016/j.ijmecsci.2017.08.056.

[27] R. S. Mulik, V. Srivastava, and P. M. Pandey, ‘Experimental investigations and modeling of temperature in the work-brush interface during ultrasonic assisted magnetic abrasive finishing process’, *Materials and Manufacturing Processes*, vol. 27, no. 1, pp. 1–9, Jan. 2012, doi: 10.1080/10426914.2010.515647.

[28] H. S. Farwaha, D. Deepak, and G. S. Brar, ‘Mathematical modeling and process parameters optimization of ultrasonic assisted electrochemical magnetic abrasive machining’, *Journal of Mechanical Science and Technology*, vol. 34, no. 12, pp. 5063–5073, Dec. 2020, doi: 10.1007/s12206-020-1110-7.

[29] V. C. Shukla, P. M. Pandey, U. S. Dixit, A. Roy, and V. Silberschmidt, ‘Modeling of normal force and finishing torque considering shearing and ploughing effects in ultrasonic assisted magnetic abrasive finishing process with sintered magnetic abrasive powder’, *Wear*, vol. 390–391, pp. 11–22, 2017, doi: 10.1016/j.wear.2017.06.017.

[30] F. Ma, Y. Liu, Q. Luo, and S. Chen, ‘Finite element simulation of micro cutting process of ultrasonic assisted magnetic abrasive finishing’, in *2021 IEEE International Conference on Electrical Engineering and Mechatronics Technology, ICEEMT 2021*, Institute of Electrical and Electronics Engineers Inc., 2021, pp. 507–510. doi: 10.1109/ICEEMT52412.2021.9601721.

[31] A. Misra, P. M. Pandey, U. S. Dixit, A. Roy, and V. v. Silberschmidt, ‘Modeling of finishing force and torque in ultrasonic-assisted magnetic abrasive finishing process’, *Proc Inst Mech Eng B J Eng Manuf*, vol. 233, no. 2, pp. 411–425, Jan. 2019, doi: 10.1177/0954405417737579.

[32] V. K. Jain, ‘Abrasive-based nano-finishing techniques: An overview’, *Machining Science and Technology*, vol. 12, no. 3, pp. 257–294, 2008, doi: 10.1080/10910340802278133.

[33] B. Gupta, A. Jain, R. Purohit, R. S. Rana, and B. Gupta, ‘Effects of process parameters on the surface finish of flat surfaces in magnetic assist abrasive finishing process’, *Mater Today Proc*, vol. 5, no. 9, pp. 17725–17729, 2018, doi: 10.1016/j.matpr.2018.06.095.

[34] J. Zhang, H. Wang, A. Senthil Kumar, and M. Jin, ‘Experimental and theoretical study of internal finishing by a novel magnetically driven polishing tool’, *Int J Mach Tools Manuf*, vol. 153, no. March, p. 103552, 2020, doi: 10.1016/j.ijmachtools.2020.103552.

[35] O. Khalil Alrahmani, H. Tavakoli, P. Saraeian, H. Soleimani Mehr, and B. Moradi, ‘Study of Magnetic Abrasive Finishing for AISI321 Stainless Steel’, *Materials and Manufacturing Processes*, vol. 31, no. 15, pp. 2023–2029, 2016, doi: 10.1080/10426914.2016.1140195.

[36] B. Girma, S. S. Joshi, M. V. G. S. Raghuram, and R. Balasubramaniam, ‘An experimental analysis of magnetic abrasives finishing of plane surfaces’, *Machining Science and Technology*, vol. 10, no. 3, pp. 323–340, 2006, doi: 10.1080/10910340600902140.

[37] D. K. Singh, V. K. Jain, and V. Raghuram, ‘Parametric study of magnetic abrasive finishing process’, *J Mater Process Technol*, vol. 149, no. 1–3, pp. 22–29, 2004, doi: 10.1016/j.jmatprotec.2003.10.030.

[38] J. Zhang, A. Chaudhari, and H. Wang, ‘Surface quality and material removal in magnetic abrasive finishing of selective laser melted 316L stainless steel’, *J Manuf Process*, vol. 45, no. August, pp. 710–719, 2019, doi: 10.1016/j.jmapro.2019.07.044.

[39] H. Xie, Y. Zou, C. Dong, and J. Wu, ‘Study on the magnetic abrasive finishing process using alternating magnetic field: investigation of mechanism and applied to aluminum alloy plate’, *International Journal of Advanced Manufacturing Technology*, no. January, 2019, doi: 10.1007/s00170-018-03268-8.

[40] W. Li, X. Li, S. Yang, and W. Li, ‘A newly developed media for magnetic abrasive finishing process: Material removal behavior and finishing performance’, *J Mater*

Process Technol, vol. 260, no. 79, pp. 20–29, 2018, doi: 10.1016/j.jmatprotec.2018.05.007.

[41] J. Zhang, J. Hu, H. Wang, A. S. Kumar, and A. Chaudhari, 'A novel magnetically driven polishing technique for internal surface finishing', *Precis Eng*, vol. 54, no. April, pp. 222–232, 2018, doi: 10.1016/j.precisioneng.2018.05.015.

[42] A. Babbar, P. Singh, and H. S. Farwaha, 'Regression Model and Optimization of Magnetic Abrasive Finishing of Flat Brass Plate', *Indian J Sci Technol*, vol. 10, no. 31, pp. 1–7, 2017, doi: 10.17485/ijst/2017/v10i31/113860.

[43] J. Zhang, W. G. Tai, H. Wang, A. S. Kumar, W. F. Lu, and J. Y. H. Fuh, 'Magnetic abrasive polishing of additively manufactured 316L stainless steel parts', *European Society for Precision Engineering and Nanotechnology, Conference Proceedings - 18th International Conference and Exhibition, EUSPEN 2018*, no. March 2020, pp. 401–402, 2018, doi: 10.13140/RG.2.2.35486.08002.

[44] J. Guo, Z. E. Tan, K. H. Au, and K. Liu, 'Experimental investigation into the effect of abrasive and force conditions in magnetic field-assisted finishing', *International Journal of Advanced Manufacturing Technology*, vol. 90, no. 5–8, pp. 1881–1888, 2017, doi: 10.1007/s00170-016-9491-6.

[45] V. C. Shukla and P. M. Pandey, 'Experimental investigations into sintering of magnetic abrasive powder for ultrasonic assisted magnetic abrasive finishing process', *Materials and Manufacturing Processes*, vol. 32, no. 1, pp. 108–114, 2017, doi: 10.1080/10426914.2016.1176199.

[46] R. S. Mulik and P. M. Pandey, 'Ultrasonic assisted magnetic abrasive finishing of hardened AISI 52100 steel using unbonded SiC abrasives', *Int J Refract Metals Hard Mater*, vol. 29, no. 1, pp. 68–77, 2011, doi: 10.1016/j.ijrmhm.2010.08.002.

[47] J. Wu, Y. Zou, and H. Sugiyama, 'Study on finishing characteristics of magnetic abrasive finishing process using low-frequency alternating magnetic field', *International Journal of Advanced Manufacturing Technology*, vol. 85, no. 1–4, pp. 585–594, 2016, doi: 10.1007/s00170-015-7962-9.

[48] Y. H. Lee, K. L. Wu, J. H. Jhou, Y. H. Tsai, and B. H. Yan, 'Two-dimensional vibration-assisted magnetic abrasive finishing of stainless steel SUS304', *International Journal of Advanced Manufacturing Technology*, vol. 69, no. 9–12, pp. 2723–2733, 2013, doi: 10.1007/s00170-013-5242-0.

[49] K. Zhou, Y. Chen, Z. W. Du, and F. L. Niu, 'Surface integrity of titanium part by ultrasonic magnetic abrasive finishing', *International Journal of Advanced*

Manufacturing Technology, vol. 80, no. 5–8, pp. 997–1005, 2015, doi: 10.1007/s00170-015-7028-z.

[50] N. Sihag, P. Kala, and P. M. Pandey, 'Analysis of Surface Finish Improvement during Ultrasonic Assisted Magnetic Abrasive Finishing on Chemically treated Tungsten Substrate', *Procedia Manuf*, vol. 10, pp. 136–146, 2017, doi: 10.1016/j.promfg.2017.07.040.

[51] W. Sun, A. W. Y. Tan, A. Bhowmik, F. Xue, I. Marinescu, and E. Liu, 'Evaluation of cold sprayed graphene nanoplates–Inconel 718 composite coatings', *Surf Coat Technol*, vol. 378, no. August, p. 125065, 2019, doi: 10.1016/j.surfcoat.2019.125065.

[52] N. Sihag, P. Kala, and P. M. Pandey, 'Chemo assisted magnetic abrasive finishing: Experimental investigations', *Procedia CIRP*, vol. 26, pp. 539–543, 2015, doi: 10.1016/j.procir.2014.07.067.

[53] H. S. Farwaha, D. Deepak, and G. S. Brar, 'Design and performance of ultrasonic assisted magnetic abrasive finishing combined with electrolytic process set up for machining and finishing of 316L stainless steel', *Mater Today Proc*, vol. 33, pp. 1626–1631, 2019, doi: 10.1016/j.matpr.2020.06.143.

[54] A. Jain and V. Bajpai, 'Mechanical micro-texturing and characterization on Ti6Al4V for the improvement of surface properties', *Surf Coat Technol*, vol. 380, no. July, p. 125087, 2019, doi: 10.1016/j.surfcoat.2019.125087.

[55] X. Sun, Y. Fu, W. Lu, and W. Hang, 'Investigation on the electrochemical assisted magnetic abrasive finishing for a stainless steel of SUS304', *International Journal of Advanced Manufacturing Technology*, vol. 116, no. 5–6, pp. 1509–1522, 2021, doi: 10.1007/s00170-021-07529-x.

[56] R. V. Rao, D. P. Rai, and J. Balic, 'Multi-objective optimization of abrasive waterjet machining process using Jaya algorithm and PROMETHEE Method', *J Intell Manuf*, vol. 30, no. 5, pp. 2101–2127, 2019, doi: 10.1007/s10845-017-1373-8.

[57] B. V. Dharmendra, S. P. Kodali, and B. Nageswara Rao, 'A simple and reliable Taguchi approach for multi-objective optimization to identify optimal process parameters in nano-powder-mixed electrical discharge machining of INCONEL800 with copper electrode', *Heliyon*, vol. 5, no. 8, p. e02326, 2019, doi: 10.1016/j.heliyon.2019.e02326.

[58] Y. Yang, L. Cao, C. Wang, Q. Zhou, and P. Jiang, 'Multi-objective process parameters optimization of hot-wire laser welding using ensemble of metamodels and NSGA-II',

Robot Comput Integr Manuf, vol. 53, no. April, pp. 141–152, 2018, doi: 10.1016/j.rcim.2018.03.007.

[59] M. Venkata Ramana, G. Krishna Mohan Rao, and D. Hanumantha Rao, 'Multi objective optimization of process parameters in turning of Ti-6Al-4V alloy', *Mater Today Proc*, vol. 5, no. 9, pp. 18966–18974, 2018, doi: 10.1016/j.matpr.2018.06.247.

[60] P. M. Ajith, T. M. A. F. S. A. L. Husain, P. Sathiya, and S. Aravindan, 'Multi-objective Optimization of Continuous Drive Friction Welding Process Parameters Using Response Surface Methodology with Intelligent Optimization Algorithm', *Journal of Iron and Steel Research International*, vol. 22, no. 10, pp. 954–960, 2015, doi: 10.1016/S1006-706X(15)30096-0.

[61] N. Aslan, A. A. Shahrivar, and H. Abdollahi, 'Multi-objective optimization of some process parameters of a lab-scale thickener using grey relational analysis', *Sep Purif Technol*, vol. 90, pp. 189–195, 2012, doi: 10.1016/j.seppur.2012.02.033.

[62] M. Gul *et al.*, 'Multi-objective-optimization of process parameters of industrial-gas-turbine fueled with natural gas by using Grey-Taguchi and ANN methods for better performance', *Energy Reports*, vol. 6, pp. 2394–2402, 2020, doi: 10.1016/j.egyr.2020.08.002.

[63] P. N. Huu, 'Multi-objective optimization in titanium powder mixed electrical discharge machining process parameters for die steels', *Alexandria Engineering Journal*, vol. 59, no. 6, pp. 4063–4079, 2020, doi: 10.1016/j.aej.2020.07.012.

[64] R. Quiza Sardiñas, M. Rivas Santana, and E. Alfonso Brindis, 'Genetic algorithm-based multi-objective optimization of cutting parameters in turning processes', *Eng Appl Artif Intell*, vol. 19, no. 2, pp. 127–133, 2006, doi: 10.1016/j.engappai.2005.06.007.

[65] P. Vijian and V. P. Arunachalam, 'Modelling and multi objective optimization of LM24 aluminium alloy squeeze cast process parameters using genetic algorithm', *J Mater Process Technol*, vol. 186, no. 1–3, pp. 82–86, 2007, doi: 10.1016/j.jmatprotec.2006.12.019.

[66] R. V. Rao and V. Patel, 'Multi-objective optimization of heat exchangers using a modified teaching-learning-based optimization algorithm', *Appl Math Model*, vol. 37, no. 3, pp. 1147–1162, 2013, doi: 10.1016/j.apm.2012.03.043.

[67] R. V. Rao, D. P. Rai, and J. Balic, 'Multi-objective optimization of machining and micro-machining processes using non-dominated sorting teaching–learning-based

optimization algorithm', *J Intell Manuf*, vol. 29, no. 8, pp. 1715–1737, 2018, doi: 10.1007/s10845-016-1210-5.

[68] V. Ghai, P. Ranjan, A. Batish, and H. Singh, 'Atomic-level finishing of aluminum alloy by chemo-mechanical magneto-rheological finishing (CMMRF) for optical applications', *J Manuf Process*, vol. 32, no. March, pp. 635–643, 2018, doi: 10.1016/j.jmapro.2018.03.032.

[69] K. B. Judal, V. Yadava, and D. Pathak, 'Experimental investigation of vibration assisted cylindrical-magnetic abrasive finishing of aluminum workpiece', *Materials and Manufacturing Processes*, vol. 28, no. 11, pp. 1196–1202, 2013, doi: 10.1080/10426914.2013.811725.

[70] J. I. Akhter, M. A. Shaikh, M. Ahmad, M. Iqbal, K. A. Shoaib, and W. Ahmad, 'Effect of aging on the hardness and impact properties of Hastelloy C-276', *J Mater Sci Lett*, vol. 20, no. 4, pp. 333–335, 2001, doi: 10.1023/A:1006773316488.

[71] J. C. Wen, Y. Wang, S. P. Hao, B. B. Feng, K. Shaheen, and H. L. Suo, 'Fabrication and characterization of coated Hastelloy C-276 Alloy by SDP technology', *Mater Res Express*, vol. 7, no. 1, 2020, doi: 10.1088/2053-1591/ab6ad7.

[72] S. Yin and T. Shinmura, 'A comparative study: Polishing characteristics and its mechanisms of three vibration modes in vibration-assisted magnetic abrasive polishing', *Int J Mach Tools Manuf*, vol. 44, no. 4, pp. 383–390, 2004, doi: 10.1016/j.ijmachtools.2003.10.002.

[73] R. S. Mulik and P. M. Pandey, 'Experimental Investigations and Modeling of Finishing Force and Torque in Ultrasonic Assisted Magnetic Abrasive Finishing', *J Manuf Sci Eng*, vol. 134, no. 5, p. 051008, 2012, doi: 10.1115/1.4007131.

[74] A. B. Khairy, 'Aspects of surface and edge finish by magnetoabrasive particles', *J Mater Process Technol*, vol. 116, no. 1, pp. 77–83, 2001, doi: 10.1016/S0924-0136(01)00840-8.

[75] T. Mori, K. Hirota, and Y. Kawashima, 'Clarification of magnetic abrasive finishing mechanism', *J Mater Process Technol*, vol. 143–144, no. 1, pp. 682–686, 2003, doi: 10.1016/S0924-0136(03)00410-2.

[76] S. Ahmad, S. Gangwar, P. C. Yadav, and D. K. Singh, 'Optimization of process parameters affecting surface roughness in magnetic abrasive finishing process', *Materials and Manufacturing Processes*, vol. 32, no. 15, pp. 1723–1729, 2017, doi: 10.1080/10426914.2017.1279307.

[77] A. Babbar, C. Prakash, S. Singh, M. K. Gupta, M. Mia, and C. I. Pruncu, ‘Application of hybrid nature-inspired algorithm: Single and bi-objective constrained optimization of magnetic abrasive finishing process parameters’, *Journal of Materials Research and Technology*, vol. 9, no. 4, pp. 7961–7974, 2020, doi: 10.1016/j.jmrt.2020.05.003.

[78] V. C. Shukla, P. M. Pandey, U. S. Dixit, A. Roy, and V. Silberschmidt, ‘Modeling of normal force and fi nishing torque considering shearing and ploughing e ff ects in ultrasonic assisted magnetic abrasive fi nishing process with sintered magnetic abrasive powder’, *Wear*, vol. 390–391, no. June, pp. 11–22, 2017, doi: 10.1016/j.wear.2017.06.017.

[79] N. Sihag, P. Kala, and P. M. Pandey, ‘Chemo assisted magnetic abrasive finishing: Experimental investigations’, *Procedia CIRP*, vol. 26, pp. 539–543, 2015, doi: 10.1016/j.procir.2014.07.067.

[80] M. Sushil, K. Vinod, and K. Harmesh, ‘Multi-objective optimization of process parameters involved in micro-finishing of Al/SiC MMCs by abrasive flow machining process’, *Proceedings of the Institution of Mechanical Engineers, Part L: Journal of Materials: Design and Applications*, vol. 232, no. 4, pp. 319–332, 2018, doi: 10.1177/1464420715627292.

[81] M. N. Pervez, F. Shafiq, Z. Sarwar, M. M. Jilani, and Y. Cai, ‘Multi-response optimization of resin finishing by using a taguchi-based grey relational analysis’, *Materials*, vol. 11, no. 3, 2018, doi: 10.3390/ma11030426.

[82] N. R. Costa, J. Lourenço, and Z. L. Pereira, ‘Desirability function approach: A review and performance evaluation in adverse conditions’, *Chemometrics and Intelligent Laboratory Systems*, vol. 107, no. 2, pp. 234–244, Jul. 2011, doi: 10.1016/j.chemolab.2011.04.004.

[83] M. Abas, L. Sayd, R. Akhtar, Q. S. Khalid, A. M. Khan, and C. I. Pruncu, ‘Optimization of machining parameters of aluminum alloy 6026-T9 under MQL-assisted turning process’, *Journal of Materials Research and Technology*, vol. 9, no. 5, pp. 10916–10940, 2020, doi: 10.1016/j.jmrt.2020.07.071.

[84] J. C. Outeiro, J. C. Pina, R. M’Saoubi, F. Pusavec, and I. S. Jawahir, ‘Analysis of residual stresses induced by dry turning of difficult-to-machine materials’, *CIRP Ann Manuf Technol*, vol. 57, no. 1, pp. 77–80, 2008, doi: 10.1016/j.cirp.2008.03.076.

Visible output

*SCI Journals

Sl. No.	Title of the paper, Authors (in the order as it appears on the paper), Name of the Journal, Volume, Page No. & year of publication
1.	Kamepalli Anjaneyulu, Gudipadu Venkatesh, "Surface texture improvement of magnetic and non-magnetic materials using magnetic abrasive finishing process ", Proceedings of the Institution of Mechanical Engineers, Part C: Journal of Mechanical Engineering Science, Vol – 235, 4084-4096 pages -2021 (SCI), https://doi.org/10.1177/0954406220970590
2	Kamepalli Anjaneyulu, Gudipadu Venkatesh**,** "On surface integrity of Hastelloy C -276 using Chemo Based Ultrasonic-Assisted Magnetic Abrasive Finishing Process", Sadhana 47, Article number: 190 (2022), (SCI), https://doi.org/10.1007

*Scopus / SCIE Indexed Journals

Sl. No.	Title of the paper, Authors (in the order as it appears on the paper), Name of the Journal, Volume, Page No. & year of publication
1.	Kamepalli Anjaneyulu, Gudipadu Venkatesh, "Optimization of Process Parameters of Magnetic Abrasive Finishing Using Jaya Algorithm", International conference, ICAM^{5}-2019, Materials Today Proceedings, Vol-41, 1035-1040 pages -2021 (Scopus), https://doi.org/10.1016/j.matpr.2020.06.568
2.	Kamepalli Anjaneyulu, Gudipadu Venkatesh, "Experimental investigation of finishing forces on Hastelloy C-276 using UAMAF process", International Journal on Interactive design and manufacturing (*IJIDeM*), https://doi.org/10.1007/s12008-022-01113-7 (ESCI)
3	Kamepalli Anjaneyulu, Gyan Prakash, Gudipadu Venkatesh, "Modelling of Finishing Forces on Hastelloy C-276 using Ultrasonic Assisted Magnetic Abrasive Finishing process", International Journal on Interactive design and manufacturing (*IJIDeM*), https://doi.org/10.1007/s12008-023-01210-1 (ESCI)
4	Kamepalli Anjaneyulu, Gudipadu Venkatesh, "Experimental investigation of Aluminium 2024 using cylindrical magnetic abrasive finishing process**",** Materials Today Proceedings**,** https://doi.org/10.1016/j.matpr.2023.03.036